DISSERTATION

APPLICATION OF SEMI-ANALYTICAL MULTIPHASE FLOW MODELS FOR THE SIMULATION AND OPTIMIZATION OF GEOLOGICAL CARBON SEQUESTRATION

Submitted by

Brent M. Cody

Department of Civil and Environmental Engineering

In partial fulfillment of the requirements

For the Degree of Doctor of Philosophy

Colorado State University

Fort Collins, Colorado

Spring 2014

Doctoral Committee:

Advisor: Domenico Bau

John Labadie
Tom Sale
Edwin Chong

ABSTRACT

APPLICATION OF SEMI-ANALYTICAL MULTIPHASE FLOW MODELS
FOR THE SIMULATION AND OPTIMIZATION OF
GEOLOGICAL CARBON SEQUESTRATION

Geological carbon sequestration (GCS) has been identified as having the potential to reduce increasing atmospheric concentrations of carbon dioxide (CO_2). However, a global impact will only be achieved if GCS is cost effectively and safely implemented on a massive scale. This work presents a computationally efficient methodology for identifying optimal injection strategies at candidate GCS sites having caprock permeability uncertainty. A multi-objective evolutionary algorithm is used to heuristically determine non-dominated solutions between the following two competing objectives: 1) maximize mass of CO_2 sequestered and 2) minimize project cost. A semi-analytical algorithm is used to estimate CO_2 leakage mass rather than a numerical model, enabling the study of GCS sites having vastly different domain characteristics. The stochastic optimization framework presented herein is applied to a case study of a brine filled aquifer in the Michigan Basin (MB). Twelve optimization test cases are performed to investigate the impact of decision maker (DM) preferences on heuristically determined Pareto-optimal objective function values and decision variable selection. Risk adversity to CO_2 leakage is found to have the largest effect on optimization results, followed by degree of caprock permeability uncertainty. This analysis shows that the feasible of GCS at MB test site is highly dependent upon DM risk adversity. Also, large gains in computational efficiency achieved using parallel processing and archiving are discussed.

Because the risk assessment and optimization tools used in this effort require large numbers of simulation calls, it important to choose the appropriate level of complexity when selecting the type of simulation model. An additional premise of this work is that an existing multiphase semi-analytical algorithm used

to estimate key system attributes (i.e. pressure distribution, CO_2 plume extent, and fluid migration) may be further improved in both accuracy and computational efficiency. Herein, three modifications to this algorithm are presented and explored including 1) solving for temporally averaged flow rates at each passive well at each time step, 2) using separate pressure response functions depending on fluid type, and 3) applying a fixed point type iterative global pressure solution to eliminate the need to solve large sets of linear equations. The first two modifications are aimed at improving accuracy while the third focuses upon computational efficiency. Results show that, while one modification may adversely impact the original algorithm, significant gains in leakage estimation accuracy and computational efficiency are obtained by implementing two of these modifications.

Finally, in an effort to further enhance the GCS optimization framework, this work presents a performance comparison between a recently proposed multi-objective gravitational search algorithm (MOGSA) and the well-established fast non-dominated sorting genetic algorithm (NSGA-II). Both techniques are used to heuristically determine Pareto-optimal solutions by minimizing project cost and maximizing the mass of CO_2 sequestered for nine test cases in the Michigan Basin (MB). Two performance measures are explored for each algorithm, including 1) objective solution diversity and 2) objective solution convergence rate. Faster convergence rates by the MOGSA are observed early in the majority of test optimization runs, while the NSGA-II is found to consistently provide a better search of objective function space and lower average cost per kg sequestered solutions.

ACKNOWLEDGEMENTS

I greatly appreciate the help and support of my academic advisor, Dr. Domenico Bau. This dissertation would not have been possible if not for his guidance and encouragement over the past four years. I would like to thank the U.S. Department of Energy-NETL Office for their funding of this project. The constructive advice and comments provided by my academic committee consisting of Dr. John Labadie, Dr. Tom Sale, and Dr. Edwin Chong greatly added to the quality of this dissertation. My family has been incredible throughout my academic career. I especially would like to thank my beautiful wife, Julie, for keeping me on track and being so supportive, as well as my children, Gavin, Bryce, and the third on the way, for providing wonderful distractions.

TABLE OF CONTENTS

CHAPTER I: INTRODUCTION

1 Problem Statement

The steady increase in atmospheric concentrations of CO_2 is referred to as the "carbon problem". Historical ice core data have indicated that the atmospheric concentration of CO_2 has ranged between about 170 ppm and 300 ppm over the past 650,000 years. The current value of 390 ppm is a third higher than the highest value seen in the past 650 millennia. The mass of annual anthropogenic carbon emissions has been recently estimated to be between 8 and 9 gigitonnes (Gt). Reference [47] reports that global emissions are composed of the following: Electricity and Heat (41%), Transport (22%), Industry (20%), Other (10%), and Residential (7%). This distribution reflects the reality that both the United States and China have an abundance of cheap coal making coal fired power generation likely for at least the next few decades [47]. This heavy dependence upon fossil fuels requires the evaluation of a portfolio of carbon emission reduction technologies [55].

Carbon capture and storage (CCS) has been proposed as a method of reducing CO_2 emissions while our society continues to utilize fossil fuels. Capture, as it pertains to CCS, involves the separation of CO_2 from fossil fuel emissions. Isolated CO_2 is then stored at some location other than the atmosphere. Geological carbon sequestration (GCS) refers to long term storage by injection into in deep geological formations. Due to favorable phase dependent properties such as high density and low buoyancy drive, it is advantageous to inject CO_2 at depths where both temperature and pressure are in excess the critical point of CO_2 (i.e. 31.1°C and 7.4 MPa, respectively). Supercritical conditions exist at depths below 800m for typical geothermal gradients [47].

There are several advantages associated with this method. The technology needed for GCS already exists as the deep geological injection of CO_2 has been used for enhanced oil recovery (EOR) for decades and

there are multiple large scale GCS projects currently active. Also, GCS allows the continued use of fossils fuel energy sources while reducing global greenhouse gas emissions. The combination these two advantages suggest that GCS could be used as a temporary solution to the carbon problem while more sustainable methods of reducing CO_2 emissions are developed.

There are, however, several disadvantages associated with the implementation of GCS. Capture, transport, and injection of CO_2 require additional energy and water resources, where the generation of addition energy resources is likely to produce additional CO_2 emissions. In addition, injection wells must be properly designed and operated to maintain the long-term injectivity into the formation. Perhaps the largest disadvantage of GCS is the potential for the leakage of CO_2 or brine to overlying aquifers or the surface. Although due to natural conditions caused by volcanic activity, the Lake Nyos disaster, in which 1,700 people died of asphyxiation from a release of approximately one cubic kilometer of build-up of CO_2, shows an extreme example of the risk associated with CO_2 leakage [25]. Due to storage into porous media rather than subterraneous voids, leakage from sequestered CO_2 deposits is likely to occur slowly over several decades. While a slow release of sequestered CO_2 does not pose asphyxiation hazards, it may seep into overlying drinking water aquifers and create conditions which release immobilized pollutants or change pH values. Therefore, the risk of CO_2 leakage need to be fully understood and minimized before implementation of GCS.

Although GCS has been identified as a prominent technology to manage increasing atmospheric concentrations of carbon dioxide (CO_2) [47,55], the effective application of GCS will require a global implementation of large numbers of carbon injection projects. While an individual large coal-fired power plant may emit up to 5-10 megatonnes (Mt) of CO_2 per year [6], total annual global anthropogenic carbon emissions measured in mass of CO_2 are approximately 30,000 Mt [47]. Results from [23] suggest that specific regions of a small number of candidate aquifers will provide the majority of low cost geological CO_2 storage. Thus, as the selection of the appropriate subsurface reservoir is crucial to the success of a

GCS project [7], many potential injection sites will need to be assessed world-wide for GCS suitability. The efficient preliminary characterization of candidate GCS injection sites has the potential to create massive resource savings to society. In addition, a comprehensive pre-screening effort will increase GCS storage reliability by eliminating "bad" and identifying "good" GCS reservoirs.

Conjunctive preliminary project planning will involve the characterization, optimization, and risk assessment of potential GCS sites. There are, however, several difficulties associated with these tasks. The first is that the large-scale, multiphase numerical modeling of several potential injection sites for the purpose of initial assessment is infeasible due to the effort involved in model construction and calibration. Data characterizing the subsurface domain are typically scarce, which introduces parameter uncertainty and adds to the complexity of modeling GCS. Also, because of their propensity to be computationally expensive [24], the direct use of large-scale, multiphase numerical models would be unrealistic in simulating the high volume of realizations needed for risk assessment and optimization. The high computational cost associated with numerical models may be overcome by the use of data-based response surface methods (e.g. [8]). However, it is the authors' intent for the resulting framework to ultimately be used to optimize and compare large numbers of potential injection sites having vastly different domain characteristics. Creating and calibrating each potential injection site's numerical model, as well as training the resulting response surface would require user expertise and large investments of computational time. Therefore, this work has chosen to simulate multiphase subsurface flow using a semi-analytical model presented by [53] and modified by [16]. This semi-analytical leakage algorithm is very general and can be applied to simplified computational models of the vast majority of potential injection sites.

An additional difficulty associated with preliminary GCS project planning is that potential storage reservoirs typically exhibit a high degree of uncertainty associated with physical parameters. Reference [10] identified abandoned (herein referred to as "passive") well permeabilities as the most dominant

uncertainty parameter when estimating fluid leakage due to GCS. In North America, significant numbers of passive wells may perforate the caprock in formations suitable for GCS [9,45,47]. Most likely, very little information exists on the location and/or sealing properties of these wells. However, several efforts have been made to investigate and account for the uncertainty associated with passive well permeability. References [67,68] developed a passive well integrity scoring index based upon typically available information (e.g. completion date, regulatory requirements, etc.). Reference [17] physically sampled and analyzed segments of a 30 year old passive well that had been continuously exposed to 96% CO_2 finding that cement interfaces are more important than the cement matrix when quantifying migration pathways.

Multiphase subsurface optimization problems are typically highly non-linear due to the irregular spatial location of preferential flow pathways and the multiphase flow (i.e. CO_2 and brine) equations governing pressure response and CO_2 plume migration. Therefore, a robust global optimization tool is needed to find best performing injection strategies that maximize the mass of CO_2 sequestered and minimize project cost by selecting optimal injection well locations and injection rates. In multi-objective problems, a Pareto-optimal, or non-dominated, solution outperforms all other solutions with respect to all objectives [58]. Multi-objective evolutionary algorithms (MOEAs) have been shown to be effective in providing Pareto-optimal solutions for a large number of subsurface flow applications possessing several decision variables [1,5,12,28,37,41,44,56,59,61,62,63,64,70]. In particular, [58] presents a comprehensive review of state-of-the-art MOEAs highlighting key algorithm advances which may be used to identify critical tradeoffs in water resources problems. A fast non-dominated sorting genetic algorithm (NSGA-II) [19] with ε-dominance [39] has been selected as a computational optimization tool because it is among the best performing multi-objective optimization evolutionary algorithms available [13].

If computationally feasible, stochastic methods should be applied in cases where parameter uncertainty is of significant concern. A popular approach for accomplishing this is to apply a Monte Carlo (MC) method where simulation is performed for an ensemble of uncertain parameter sets to estimate the

statistics of optimization objectives and constraints. There are several examples in the literature where MOEAs are coupled with MC techniques to optimize groundwater problems having parameter uncertainty. A multi-objective groundwater flow optimization problem with aquifer hydraulic conductivity uncertainty is solved by [5] using an NPGA. Reference [1] used a MC-based Bayesian update scheme to approximate posterior uncertainty in hydraulic conductivity and head when using an NSGA-II to perform multi-objective design of aquifer monitoring networks. A MC approach was also used by [41] when determining optimal remediation methods for groundwater aquifers having hydraulic conductivity uncertainty. MC techniques are also used to investigate parameter uncertainty associated with GCS [27,54,66,69]. In particular, Reference [10] applied a stochastic Monte Carlo approach to estimate leakage risk associated with passive well permeability uncertainty. Reference [45] used a large-scale Monte Carlo method to explore the effects of caprock permeability uncertainty on fluid leakage estimation, determining that the amount of CO_2 leakage from GCS is typically acceptable for climate change mitigation.

Herein, several computational tools have been integrated into a stochastic multi-objective optimization framework for the purpose of performing large-scale candidate GCS site feasibility studies. These tools include 1) a semi-analytical leakage algorithm to rank the performance of trial injection strategies; 2) a Monte Carlo procedure to quantify risk resulting from parameter uncertainty; and 3) an NSGA-II with ε-dominance to heuristically determine Pareto-optimal solutions between competing objectives. Three fundamental goals are investigated by applying this framework to a test site in the Michigan Basin (MB): 1) quantify the impact of decision maker (DM) preferences on heuristically determined Pareto-optimal objective values (i.e. mass sequestered and project cost); 2) quantify the impact of DM preferences on heuristically chosen decision variables (i.e. injection well flow rates and locations), and; 3) preliminarily assess the suitability of the MB test site for GCS.

Stochastic techniques for preliminary GCS site assessment (e.g. injection strategy optimization, risk analysis, and sensitivity analysis, etc.) require large numbers of simulations. Therefore, it is important to continually develop the accuracy and efficiency of simulation tools. Several attempts have been made to analytically quantify the hydraulic communication between aquifers separated by leaky aquitard layers [29,30,31,43]. In addition, several other authors have presented analytical or semi-analytical solutions used to estimate subsurface pressure distributions and fluid flux across layer boundaries resulting from leaky wells [33,34]. For example, [42] introduced fluid and matrix compressibility to the similarity solutions governing single-well CO_2 injection presented in [51], while [71] presented a single-phase semi-analytical solution for large scale injection-induced pressure perturbation and leakage in a laterally bounded aquifer-aquitard system. Also, a semi-analytical model estimating multiphase fluid flux through a single caprock perforation was developed by [36] to determine optimal injection intervals based upon trapping effects for secure CO_2 storage in saline aquifers and [6,15,14] presented and applied a single-phase semi-analytical model for both forced and diffuse leakage in a multi-layer system. Finally, [4] combined solutions presented by [29], [49], and [65] to create a semi-analytical solution for approximating the area of potential impact from a single CO_2 injection well.

However, while other semi-analytical algorithms provide insight regarding specific processes (e.g. diffuse leakage [14]), the work presented herein focuses upon the multiphase subsurface flow model proposed by [53] and further developed by [10] because it is the only semi-analytical model able to simulate multiphase flow in domains having multiple injection wells and multiple aquifer and aquitard (i.e. caprock) layers. An analytical algorithm was first developed by [49] for estimating the pressure distribution and leakage resulting from single-phase injection (e.g. injection of brine into a brine filled domain of aquifer) into a domain having multiple passive wells and multiple aquifer-aquitard layers. This algorithm creates a set of linear equations describing the pressure distribution throughout the domain by superimposing pressure changes caused by each source or sink in each aquifer. The general algorithm presented in [49] in conjunction with the development of a multiphase pressure response function

[50,51,52,49] led to the semi-analytical CO_2 leakage algorithm, presented in [53] and expounded upon in [10], which estimates both brine and CO_2 flux across confining layers resulting from GCS. While there are multiple pathways for the leakage of sequestered CO_2 from subsurface storage reservoirs (e.g. geological discontinuities, caprock permeability, etc.), [53] assumes that hydrocarbon exploration and production boreholes created preferential flow paths in the domain [2,3,18,20,26,38,46]. This assumption appears reasonable, as the existing caprock had successfully held the recently produced hydrocarbons for many millennia prior to production [48].

Herein, three modifications to this semi-analytical leakage algorithm are presented and explored. These include 1) solving for temporally averaged flow rates at each passive well at each time step, 2) using separate pressure response functions depending on fluid type [65], and 3) applying a fixed point type iterative global pressure solution to eliminate the need to solve large sets of linear equations.

In addition, due to the complexity of the optimization problem, it is also important to select the best performing optimization algorithm. Reference [57] recently proposed a novel heuristic optimization method inspired by Newtonian laws of gravity. While the gravitational search algorithm (GSA) had not yet been applied to the field of subsurface hydrology, several other studies report favorable results when comparing the GSA to other heuristic search algorithms for optimizing a number of non-linear engineering applications. Reference [57] compared the GSA to particle swarm optimization (PSO), a real genetic algorithm (RGA), and central force optimization (CFO), finding that the GSA provided superior results in most cases and comparable results in all other cases. Reference [11] found the GSA to exhibit better performance in terms of final fitness values and computational efficiency when compared against a modified PSO algorithm. Reference [40] studied parameter identification of a hydraulic turbine governing system finding their improved GSA to be more accurate and efficient than both genetic and particle swarm algorithms. References [21] and [22] used the GSA to solve large scale electrical power control problems while a slope stability analysis was performed using a modified GSA by [35].

Several versions of multi-objective GSAs (MOGSA) have also been presented. Reference [32] proposed and compared a MOGSA with a multi-objective genetic algorithm (MOGA), Pareto-archived evolution strategy (PAES), and multi-objective particle swarm optimization (MOPSO) finding the MOGSA to outperform all the other methods. A MOGSA has also been proposed and tested by [60]. This MOGSA was found to outperform almost 20 other heuristic algorithms when optimizing a Routing and Wavelength Assignment problem.

Also in this work, a performance comparison is made between the MOGSA and the NSGA-II to determine the best algorithm for the preliminary optimization of potential GCS sites. In order to accomplish this, a total of 360 optimization runs are processed where each of 9 test cases at the MB test site are optimized 20 times using each algorithm.

2 Major Findings

A stochastic methodology is presented herein where a semi-analytical CO_2 leakage algorithm and a Monte Carlo procedure are integrated into a NSGA-II with ε-dominance to determine optimal GCS injection strategies. In an effort to show how this method may be applied to real world candidate injection sites, the stochastic optimization framework is applied to a hypothetical GCS project at a MB test site in northern Michigan, USA. Three fundamental goals are investigated using the stochastic optimization framework: 1) quantify the impact of DM preferences on heuristically determined Pareto-optimal objective values (i.e. mass sequestered and project cost); 2) quantify the impact of DM preferences on heuristically chosen decision variables (i.e. injection well flow rates and locations), and; 3) preliminarily assess the suitability of the MB test site for GCS. To accomplish this twelve stochastic optimization cases, each having differing DM preferences, are performed using MB test site data where the risk adversity factor, r_A, is set to either 1.0 or 1.2 while the stochastic non-exceedance cost probability, z, is set to either 50% or 95% for each of three passive well uncertainty scenarios. Uncertainty scenarios tested and compared include 1) data supporting an abundance of intact passive well segments (U1); 2) no

available passive well permeability data (U2); and 3) data supporting an abundance of degraded passive well segments (U3).

In cases where the estimated mass of CO_2 leakage is high, DM risk adversity, r_A, is found to have a profound effect on project cost. While all optimization cases assigned a U1 uncertainty scenario (i.e. 90% of passive well segments assigned as intact) exhibit very little CO_2 leakage, substantial CO_2 leakage masses are estimated for test cases assigned U2 (i.e. 50% of passive well segments assigned as intact) and U3 (i.e. 10% of passive well segments assigned as intact) uncertainty scenarios, resulting in very large leakage costs when $r_A = 1.2$. Test cases assigned uncertainty scenarios with a greater percentage of intact well segments are found to exhibit less CO_2 leakage. All optimization cases having a U1 uncertainty scenario exhibit minimal CO_2 leakage costs resulting in total project costs being very similar to capital, operation, and maintenance (CO&M) costs. Cases assigned U3 uncertainty scenarios are found to have much more leakage cost than corresponding cases with U2 uncertainty scenarios, especially when $r_A = 1.2$. Also, while estimated project costs increase when a greater value of z is used, the value chosen for z is found to have only a minor impact on resulting Pareto-optimal objective function values.

Two quantitative analyses are performed to study how DM preferences ultimately influence the heuristic selection of carbon injection strategies. First, the relative insensitivity of carbon injection strategy selection in relation to each DM parameter (i.e. r_A, z, and uncertainty scenario) is quantified as the percentage of injection well rate/location combinations that remain constant when varying each DM preference. The percentage of injection strategies that remain constant in both location and injection rate when varying values of r_A, uncertainty scenario, and values of z is quantified as 72.2%, 75.5%, and 87.9%, respectively. Secondly, a categorical distribution analysis is used to identify general injection strategy trends associated with DM preferences. The number of times each candidate location is selected for injection well placement is counted for all cases having each given DM preference value. This analysis shows that the southwest corner of the candidate injection well field is heavily favored by the

optimization algorithm, regardless of parameter choice, with 94.2% of all injection well placements being made at the three furthest candidate injection well locations. Also, the furthest southwest candidate injection well location is found to have a substantially greater number of selections than all other individual locations.

DM risk adversity is found to have the greatest effect on injection strategy selection. Increasing r_A from 1.0 to 1.2 is found to increase the total number of candidate well location selections from 138 to 154. This increased number in total candidate well location selections is caused by the optimization algorithm attempting to alleviate incurred CO_2 leakage cost by using additional injection wells to spread out and reduce the injection induced pressure distribution. This finding suggests that the leakage penalty savings from diversifying the injection well field are greater in certain cases than the additional CO&M costs incurred from installing, operating, and maintaining more injection wells. Passive well uncertainty scenario selection is also found to significant affect injection strategy. The total number of candidate well location selections is found to increase from 92 for uncertainty scenario U1 to 100 for the more "leaky" uncertainty scenario U2, further validating the trend found when studying risk adversity. Also, greater estimated CO_2 leakage, as in the case of uncertainty scenarios U2 and U3, is clearly observed to drive candidate injection well location selections further southwest. The likelihood of selecting the three furthest southwest candidate locations increases from 83.7% in cases assigned uncertainty scenario U1 to 99.0% in cases assigned either uncertainty scenario U2 or U3. While stochastic non-exceedance cost probability, z, is found to have the least effect on injection strategy selection, trends are still observed when examining results from this analysis. As with uncertainty scenario selection, increases in estimated CO_2 leakage (e.g. increasing z from 50% to 95%) are also found to drive candidate injection well location selections further southwest when studying the stochastic non-exceedance cost probability. The likelihood of selecting the three furthest candidate injection well locations increased from 89.7% in cases assigned z = 50% to 98.6% in cases assigned z = 95%.

The final decision of whether or not to proceed with GCS project planning will be made by the DM. This choice will ultimately be made by assessing a large number of political and financial indicators. However, the preliminary stochastic cost assessment presented herein suggests that GCS feasibility at the MB test site is highly dependent upon the DM's risk adversity preference. All three uncertainty scenarios are shown to produce feasible project cost results if the DM selects r_A = 1.0, although a U3 uncertainty scenario is predicted to be about twice as expensive as the U1 uncertainty scenario. If the DM decides to select r_A = 1.2, U1 is the only uncertainty scenario providing feasible project cost results due to high CO_2 leakage costs resulting from the exponential leakage cost term, r_A.

Because of the iterative nature of the evolutionary search and Monte Carlo processes, large numbers of model simulations are needed for each stochastic optimization run. Assuming that a numerical model would require two hours per simulation, complete enumeration of each MB optimization problem would take approximately 4,068 years to complete. However, a semi-analytical algorithm and a NSGA-II optimization approach is used for this problem. Without using simulation archiving, when applying a NSGA-II the total number of model calls required for each stochastic optimization run is equal to the product of number of Monte Carlo realizations, N_{MC}, the population size, N_{pop}, and the number of generations, N_{gens}. To improve computational efficiency, this work also utilizes parallel computing and simulation archiving. The theoretical evaluation time to process CO_2 leakage evaluations may be reduced by 96% using parallel processing. The actual CPU time required for a single optimization run with N_{MC} = 400, N_{pop} = 25, and N_{gens} = 200 using 12 processor cores is approximately 1.04 days, or about six orders of magnitude less than the theoretical time required for the complete enumeration of this problem using a numerical model.

Because of the large set of assumptions made by the semi-analytical CO_2 leakage algorithm, the stochastic optimization framework may only be used for initial site planning and characterization. After 'coarse scale' project planning has been completed using this stochastic optimization framework, more

rigorous, although slower, numerical models should be used for final project development of individual potential injection sites. However, this tool has potential for initial carbon sequestration project planning and performing initial screening and ranking of large sets of potential carbon sequestration sites.

In addition, this work leads to important modifications of the semi-analytical CO_2 leakage algorithm presented by [39]. Three proposed modifications to a semi-analytical leakage algorithm are proposed and tested. A modification involving the use of temporally averaged flux rates (TAFR) to estimate aquifer fluid pressure changes throughout the domain is found to address an underestimation of fluid leakage by the original algorithm. Results show that the ELSA-TAFR algorithm estimates leakage to be 11.2% higher on average that the original algorithm with an insignificant increase in computational expense. It is important that the TAFR modification be implemented in all cases as the original algorithm may significantly underestimate leakage.

The use of separate pressure response functions (SPRF) for fluid types was found to provide no change in accuracy while greatly decreasing computational efficiency. It is therefore suggested that this modification not be applied to this semi-analytical algorithm.

The final modification to the semi-analytical algorithm proposes the use of a fixed point type iterative global pressure solution (IGPS) as opposed to solving large linear sets of equations to determine the global pressure solution. This method is found to significantly increase computational efficiency. The average difference in fractional leakage between the two algorithms is found to be very small with the computational cost decreasing on average by approximately one order of magnitude. From the results obtained, the simulation of domains having large quantities of passive wells and aquifer layers would greatly benefit by using the IGPS modification. In addition, this modification would be extremely beneficial when large numbers or simulations need to be performed such as in the cases of stochastic

analysis or optimization. It should be noted that the TAFR modification does not need to be applied when using the IGPS modification as there is no need to linearize the pressure solution.

In addition, a performance comparison is made between the MOGSA and the NSGA-II to determine the best algorithm for injection strategy optimization at candidate GCS sites. It is important that multi-objective optimization algorithms perform the following: 1) fully explore the objective space providing diverse Pareto-optimal tradeoff sets and 2) find the best or close-to-best Pareto-optimal solutions with minimal computational expense. To explore how well each algorithm accomplishes these tasks, a total of 360 deterministic optimization runs are processed where 20 different random seed optimization runs are performed for each of nine MB test cases using each algorithm. Two performance measures are explored for each algorithm, including 1) objective solution diversity and 2) objective solution convergence rate.

The results show the NSGA-II to outperform the MOGSA when evaluating objective solution diversity where an average of 94% and 78% of full solutions sets are found using the NSGA-II and the MOGSA, respectively. However, when comparing the rate at which each algorithm converges (i.e. progresses) toward Pareto-optimal solutions, the MOGSA tends to display large but less frequent reductions in average project cost per unit mass sequestered while the NSGA-II is found to have a more gradual improvement pattern. Also related to the previous observation, in 78% of cases studied, the MOGSA finds better average project cost per unit mass sequestered values early in the optimization run only to be overtaken by the NSGA-II. These trends are caused by a fundamental methodology difference between the two optimization algorithms. The MOGSA takes a significantly more direct approach when generating new sets of trial injection strategies compared to the NSGA-II. With the MOGSA, new trial injection strategies are directly driven toward well-performing trial injection strategy positions in decision space where the NSGA-II uses a much more complex method to generate each new trial population member.

Both algorithms are shown to arrive at relatively similar final objective function tradeoff solutions in all trial cases. At first glance, the NSGA-II is found to outperform the MOGSA when comparing solution accuracy. However, a further investigation of the results data shows that the relative differences in final solution accuracy are fairly small. Although the MOGSA provides less accurate solutions in seven out of nine of the test cases, the average relative difference in solution accuracy is found to be only 3.1%. In test cases having only two or three injection wells the average relative difference between the two algorithms is much less, at approximately 1.0%. The largest relative differences are found in test cases having four injection wells, where the average relative difference is found to be approximately 7.2%. Even with slightly less accurate final objective solutions, the MOGSA may still be preferable over the NSGA-II due to its fast early convergence rates. When optimizing a particular test case, the MOGSA found a comparable tradeoff solution using only about one-quarter of the computational cost spent by the NSGA-II.

The decision of whether or not to pursue GCS is complex. The answer to this question lies in the comparison between two unknown, yet imminent, potential costs to society. Significantly addressing the carbon problem through a global GCS effort would be immensely costly and extremely difficult to politically coordinate. In addition, physical parameter uncertainties inherent in subsurface domain result in a level of CO_2 and brine leakage risk that is difficult to quantify. Upon initial inspection, it is easy to conclude the futility of pursuing this technology. However, global climate change has the potential to incur a massive cumulative cost upon society. For example, what will the cost be of replacing or improving our existing marine infrastructure should ocean levels drastically change? Is the carbon problem influencing the frequency, severity, and spatial distribution of extreme weather events? How significantly will global hydrological patterns change and thereby affect the existing structure of agriculture and water distribution? These questions need to be thoroughly investigated and continually monitored before firmly determining the viability of GCS.

3 Research Accomplishments

The following is a list of the accomplishments presented by this dissertation:

- An improved the state of semi-analytical multi-layer, multiphase flow modeling
- The development a computationally efficient stochastic GCS optimization framework
- A demonstration of a real-world case study using the stochastic GCS optimization framework
- An analysis of the sensitivity of decision maker preference parameters upon optimal objective solutions and injection strategies
- A performance comparison between a MOGSA and a NSGA-II for the purposes of GCS optimization

4 Future Research

It is the authors' intent for the stochastic optimization framework to ultimately be used to optimize and compare large numbers of real-world GCS sites. There are several tasks which would be beneficial in realizing this future goal. The effects associated with each assumption of the semi-analytical leakage algorithm will need to be exhaustively investigated. If computationally feasible, important leakage model complexities should be incorporated. These may be made possible through the additional parallelization of trial injection strategy processing. Substantial additional gains in computational efficiency may be obtained by processing each trial injection strategy's MC ensemble in parallel using large processor core clusters. Increased computational efficiency will also lead to the ability to increase the number of model calls per optimization run or to process greater quantities of potential injection sites.

There are also several possible variations of the optimization framework which may be explored. For example, the injection duration may be included as a third decision variable in addition to location and flow rate of each injection well. Also, the minimization of risk of cost exceedance may be included as a third objective function in addition to maximizing the mass of CO_2 sequestered and minimizing the

project cost. A multi-criteria decision analysis (MCDA) may also be performed upon the resulting Pareto-optimal sets of equations to quantify the importance of conflicting objectives and aid in the final selection of injection strategy selection. Finally, if additional accuracy is required for a particular candidate injection site, the semi-analytical algorithm may be replaced by an artificial neural network (ANN) trained by a site specific numerical model.

It will be important to use the best optimization algorithm when processing large numbers of potential injection sites. While the NSGA-II outperformed the MOGSA in both the objective solution diversity and solution accuracy performance measures, it may be possible to exploit the MOGSA's trend of faster early convergence rates by creating a multi-stage hybrid method between the two algorithms where the MOGSA is first used to quickly perform an initial optimization then the NSGA-II is used complete the final stage of decision variable selection.

This framework may be applied to multi-layer single-phase stochastic optimization problems (e.g. aquifer storage and recovery). It would also be interesting to research the applicability of the semi-analytical model to surface-ground water interactions.

5 Organization

This dissertation is organized in the following three sections:

- Chapter 2 is entitled *Improved Semi-Analytical Simulation of Geological Carbon Sequestration* and includes an article by Cody, Baù, and González-Nicolás [2014a] currently under review for "Computational Geosciences".
- Chapter 3 is entitled *Stochastic Injection strategy Optimization for the Preliminary Assessment of Candidate Geological Storage Sites* and includes an article by Cody, Baù, and González-Nicolás [2014b] being submitted to "Hydrology Journal".

- Chapter 4 is entitled *Performance Comparison between a Multi-objective Gravitational Search Algorithm and NSGA-II for Injection strategy Optimization of Geological CO_2 Sequestration* and includes an article by Cody, Baù, and González-Nicolás [2014c] being submitted to "Swarm and Evolutionary Computation".

REFERENCES

1. Alzraiee, A.H., Bau, D.A., Garcia, L.A.: Multiobjective design of aquifer monitoring networks for optimal spatial prediction and geostatistical parameter estimation. Water Resour. Res. 49, 3670–3684 (2013).
2. Avci, C.: Evaluation of flow leakage through abandoned wells and boreholes. Water Resour Res 30:2565–2578 (1994)
3. Bachu, S., Bennion, D.B.: Experimental assessment of brine and/or CO2 leakage through well cements at reservoir conditions. Int J Greenh Gas Control 3:494–501 (2009)
4. Bandilla, K.W., Kraemer, S.R., Birkholzer, J.T.: Using semi-analytic solutions to approximate the area of potential impact for carbon dioxide injection. Int J Greenh Gas Control 8:196–204 (2012)
5. Baú, D.A.: Planning of Groundwater Supply Systems Subject to Uncertainty Using Stochastic Flow Reduced Models and Multi-Objective Evolutionary Optimization. Water Resour. Manag. 26, 2513–2536 (2012).
6. Birkholzer, J.T., Cihan, A., Zhou, Q.: Impact-driven pressure management via targeted brine extraction—Conceptual studies of CO2 storage in saline formations. Int. J. Greenh. Gas Control. 7, 168–180 (2012).
7. Bossie-Codreanu, D., Le Gallo, Y.: A simulation method for the rapid screening of potential depleted oil reservoirs for CO2 sequestration. Energy. 29, 1347–1359 (2004).
8. Box, G., Draper, N.: Response surfaces, mixtures, and ridge analyses. (2007).
9. Celia, M.A., Nordbotten, J.M., Bachu, S., Dobossy, M., Court, B.: Risk of Leakage versus Depth of Injection in Geological Storage. Energy Procedia. 1, 2573–2580 (2009).
10. Celia, M.A., Nordbotten, J.M., Court, B., Dobossy, M., Bachu, S.: Field-scale application of a semi-analytical model for estimation of CO2 and brine leakage along old wells. Int. J. Greenh. Gas Control. 5, 257–269 (2011).
11. Chatterjee, A., Mahanti, G., Pathak, N.: Comparative performance of gravitational search algorithm and modified particle swarm optimization algorithm for synthesis of thinned scanned concentric ring array. Prog. Electromagn. Res. B. 25, 331–348 (2010).
12. Chen, L., McPhee, J., Yeh, W.W.-G.: A diversified multiobjective GA for optimizing reservoir rule curves. Adv. Water Resour. 30, 1082–1093 (2007).
13. Cheng, Y., Jin, Y., Hu, J.: Adaptive epsilon non-dominated sorting multi-objective evolutionary optimization and its application in shortest path problem. ICCAS-SICE, 2009. 2545–2549 (2009).

14. Cihan A., Zhou Q., Birkholzer J.T.: Analytical solutions for pressure perturbation and fluid leakage through aquitards and wells in multilayered-aquifer systems. Water Resour Res (2011) doi: 10.1029/2011WR010721
15. Cihan, A., Birkholzer, J.T., Zhou, Q.: Pressure buildup and brine migration during CO2 storage in multilayered aquifers. Ground Water 51:252–67 (2013)
16. Cody, B.M., Baú, D.A., González-Nicolás, A.: Improved Semi-Analytical Simulation of Geological Carbon Sequestration. In press (2014)
17. Crow, W., Brian Williams, D., William Carey, J., Celia, M., Gasda, S.: Wellbore integrity analysis of a natural CO2 producer. Energy Procedia. 1, 3561–3569 (2009).
18. Crow, W., Carey, J.W., Gasda, S., et al.: Wellbore integrity analysis of a natural CO2 producer. Int J Greenh Gas Control 4:186–197 (2010)
19. Deb, K., Agrawal, S.: A fast elitist non-dominated sorting genetic algorithm for multi-objective optimization: NSGA-II. Proc. Parallel Probl. Solving from Nat. VI. 849–858 (2000).
20. Duguid, A., Butsch, R.J., Loizzo, M., Stamp, V.: Collection of baseline wellbore cement data in multiple wells in the same field. Energy Procedia 4:5130–5137 (2011)
21. Duman, S., Güvenç, U., Sönmez, Y., Yörükeren, N.: Optimal power flow using gravitational search algorithm. Energy Convers. Manag. 59, 86–95 (2012).
22. Duman, S., Guvenc, U., Yorkukeren, N.: Gravitational search algorithm for economic dispatch with valve-point effects. Int. J. Electr. Eng. 5, 2890–2895 (2010).
23. Eccles, J.K., Pratson, L., Newell, R.G., Jackson, R.B.: The impact of geologic variability on capacity and cost estimates for storing CO2 in deep-saline aquifers. Energy Econ. 34, 1569–1579 (2012).
24. Espinet, A.J., Shoemaker, C.A.: Comparison of optimization algorithms for parameter estimation of multi-phase flow models with application to geological carbon sequestration. Adv. Water Resour. 54, 133–148 (2013).
25. Evans, W., Kling, G., Tuttle, M.: Gas buildup in Lake Nyos, Cameroon: The recharge process and its consequences. Appl. Geochemistry. 8, 207–221 (1993).
26. Gasda, S.E., Nordbotten, J.M., Celia, M.A.: Determining effective wellbore permeability from a field pressure test: a numerical analysis of detection limits. Environ Geol 54:1207–1215. doi: 10.1007/s00254-007-0903-7 (2007)

27. Goda, T., Sato, K.: Optimization of well placement for geological sequestration of carbon dioxide using adaptive evolutionary Monte Carlo algorithm. Energy Procedia. 4, 4275–4282 (2011).
28. Hansen, A.K., Hendricks Franssen, H.-J., Bauer-Gottwein, P., Madsen, H., Rosbjerg, D., Kaiser, H.-P.: Well Field Management Using Multi-Objective Optimization. Water Resour. Manag. 27, 629–648 (2013).
29. Hantush, M.S., and Jacob C.E.: Nonsteady radial flow in an infinite leaky aquifer, Am. Geophys. Union Trans., 36: 95-100 (1955)
30. Hantush, M.S.: Modification of the theory of leaky aquifers. J Geophys Res 65:11:3717-3725 (1960)
31. Hantush, M.S.: Nonsteady flow to flowing wells in leaky aquifers. J Geophys Res 64:1043–1052 (1959)
32. Hassanzadeh, H.R., Rouhani, M.: A Multi-objective Gravitational Search Algorithm. 2010 2nd Int. Conf. Comput. Intell. Commun. Syst. Networks. 1, 7–12 (2010).
33. Hunt, B.: Flow to a well in a multiaquifer system. Water Resour Res 21:1637–1641 (1985)
34. Javandel, I., Witherspoon, P.: A semianalytical solution for partial penetration in two-layer aquifers. Water Resour Res 16:1099–1106 (1980)
35. Khajehzadeh, M., Taha, M.R., El-Shafie, A., Eslami, M.: A modified gravitational search algorithm for slope stability analysis. Eng. Appl. Artif. Intell. 25, 1589–1597 (2012).
36. Kumar, N., Bryant, S.L.: Semi-analytical model to determine perforation interval for secure CO2 storage in saline aquifers. Energy Procedia 1:3071–3078 (2009)
37. Kumphon, B.: Genetic Algorithms for Multi-objective Optimization: Application to a Multi-reservoir System in the Chi River Basin, Thailand. Water Resour. Manag. 27, 4369–4378 (2013).
38. Lacombe, S., Sudicky, E.: Influence of Leaky Boreholes on Cross-Formational Groundwater Flow and Contaminant Transport. Water Resour (1995)
39. Laumanns, M., Thiele, L., Deb, K., Zitzler, E.: Combining convergence and diversity in evolutionary multiobjective optimization. Evol. Comput. 10, 263–82 (2002).
40. Li, C., Zhou, J.: Parameters identification of hydraulic turbine governing system using improved gravitational search algorithm. Energy Convers. Manag. 52, 374–381 (2011).
41. Mantoglou, A., Kourakos, G.: Optimal Groundwater Remediation Under Uncertainty Using Multi-objective Optimization. Water Resour. Manag. 21, 835–847 (2006).

42. Mathias, SA, Hardisty, P.E., Trudell M.R., Zimmerman R.W.: Approximate Solutions for Pressure Buildup During CO2 Injection in Brine Aquifers. Transp Porous Media 79:265–284 (2008)

43. Neuman, S., Witherspoon, P.: Applicability of current theories of flow in leaky aquifers. Water Resour. Res. 5: 817-829 (1969)

44. Nicklow, J., Reed, P., Savic, D.: State of the art for genetic algorithms and beyond in water resources planning and management. J. Water Resour. Plan. Manag. 412–432 (2010).

45. Nogues, J., Dobossy, M.: A methodology to estimate maximum probable leakage along old wells in a geological sequestration operation. Int. J. Greenh. Gas Control. 7, 39–47 (2012).

46. Nogues, J., Nordbotten, J., Celia, M.: Detecting leakage of brine or CO2 through abandoned wells in a geological sequestration operation using pressure monitoring wells. Energy Procedia 4:3620–3627 (2011)

47. Nordbotten, J., Celia M., Geological Storage of CO2, Wiley, 2012.

48. Nordbotten, J., Celia, M., Bachu S.: Analytical solutions for leakage rates through abandoned wells. Water Resour Res 40:1–10. (2004)

49. Nordbotten, J., Celia, M., Bachu S.: Injection and storage of CO2 in deep saline aquifers: Analytical solution for CO2 plume evolution during injection. Transp Porous media 58:339–360 (2005)

50. Nordbotten, J., Celia, M.: An improved analytical solution for interface upconing around a well. Water Resour Res 42:1–10. (2006a)

51. Nordbotten, J., Celia, M.: Semianalytical solution for CO2 leakage through an abandoned well. Environ Sci Technol 39:602–611 (2005)

52. Nordbotten, J., Celia, M.: Similarity solutions for fluid injection into confined aquifers. J Fluid Mech 561:307–327. (2006b)

53. Nordbotten, J., Kavetski, D., Celia, M., Bachu, S.: Model for CO2 leakage including multiple geological layers and multiple leaky wells. Environ. Sci. Technol. 43, 743–749 (2009).

54. Oladyshkin, S., Class, H., Helmig, R., Nowak, W.: An integrative approach to robust design and probabilistic risk assessment for CO2 storage in geological formations. Comput. Geosci. 15, 565–577 (2011).

55. Pacala, S., Socolow, R.: Stabilization wedges: solving the climate problem for the next 50 years with current technologies. Science. 305, 968–972 (2004).

56. Peralta, R.C., Forghani, A., Fayad, H.: Multiobjective genetic algorithm conjunctive use optimization for production, cost, and energy with dynamic return flow. J. Hydrol. (2014).

57. Rashedi, E., Nezamabadi-Pour, H., Saryazdi, S.: GSA: a gravitational search algorithm. Inf. Sci. (Ny). 179, 2232–2248 (2009).

58. Reed, P.M., Hadka, D., Herman, J.D., Kasprzyk, J.R., Kollat, J.B.: Evolutionary multiobjective optimization in water resources: The past, present, and future. Adv. Water Resour. 51, 438–456 (2013).

59. Reed, P.M., Kollat, J.B.: Visual analytics clarify the scalability and effectiveness of massively parallel many-objective optimization: A groundwater monitoring design example. Adv. Water Resour. 56, 1–13 (2013).

60. Rubio-Largo, A., Vega-Rodriquez, M.., Gomez-Pulido, J.A., Sanchez-Perez, J.M.: A Multiobjective Gravitational Search Algorithm Applied to the Static Routing and. Appl. Evol. Comput. Lect. Notes Comput. Sci. 6625, 41–50 (2011).

61. Singh, A.: Simulation and optimization modeling for the management of groundwater resources. I: Distinct applications. J. Irrig. Drain. Eng. 1–10 (2013).

62. Singh, A.: Simulation and Optimization Modeling for the Management of Groundwater Resources. II: Combined Applications. J. Irrig. Drain. Eng. 1–9 (2014).

63. Singh, T.S., Chakrabarty, D.: Multi-objective optimization for optimal groundwater remediation design and management systems. Geosci. J. 14, 87–97 (2010).

64. Tabari, M.M.R., Soltani, J.: Multi-Objective Optimal Model for Conjunctive Use Management Using SGAs and NSGA-II Models. Water Resour. Manag. 27, 37–53 (2012).

65. Theis, C.V.: The relation between the lowering of the piezometric surface and the rate and duration of discharge of a well using groundwater storage, Am. Geophys. Union Trans., 16: 519-524 (1935)

66. Walter, L., Binning, P., Oladyshkin, S.: Brine migration resulting from CO2 injection into saline aquifers–An approach to risk estimation including various levels of uncertainty. Int. J. Greenh. Gas Control. 9, 495–506 (2012).

67. Watson, T., Bachu, S.: Evaluation of the potential for gas and CO2 leakage along wellbores. SPE Drill. Complet. SPE, (2009).

68. Watson, T., Bachu, S.: Identification of wells with high CO2-leakage potential in mature oil fields developed for CO2-enhanced oil recovery. SPE Symp. Improv. Oil Recover. SPE, (2008).

69. Wriedt, J., Deo, M., Han, W.S., Lepinski, J.: A methodology for quantifying risk and likelihood of failure for carbon dioxide injection into deep saline reservoirs. Int. J. Greenh. Gas Control. 20, 196–211 (2014).

70. Zheng, F., Zecchin, A.: An efficient decomposition and dual-stage multi-objective optimization method for water distribution systems with multiple supply sources. Environ. Model. Softw. 55, 143–155 (2014).

71. Zhou, Q., Birkholzer, J., Tsang, C.: A semi-analytical solution for large-scale injection-induced pressure perturbation and leakage in a laterally bounded aquifer–aquitard system. Transp Porous Media 78:127–148 (2009)

CHAPTER II: IMPROVED SEMI-ANALYTICAL SIMULATION OF GEOLOGICAL CARBON SEQUESTRATION

Summary Successful large-scale implementation of geological CO_2 sequestration (GCS) will require the preliminary assessment of multiple potential injection sites. Risk assessment and optimization tools used in this effort typically require large numbers of simulations. This makes it important to choose the appropriate level of complexity when selecting the type of simulation model. A promising multiphase semi-analytical method proposed by [39] to estimate key system attributes (i.e. pressure distribution, CO_2 plume extent, and fluid migration) has been found to reduce computational run times by three orders of magnitude when compared to other standard numerical techniques. The premise of this work is that the existing semi-analytical leakage algorithm proposed by [39] may be further improved in both accuracy and computational efficiency. Herein, three modifications to this algorithm are presented and explored including 1) solving for temporally averaged flow rates at each passive well at each time step, 2) using separate pressure response functions depending on fluid type [41], and 3) applying a fixed point type iterative global pressure solution to eliminate the need to solve large sets of linear equations. The first two modifications are aimed at improving accuracy while the third focuses upon computational efficiency. Results show that, while one modification may adversely impact the original algorithm, significant gains in leakage estimation accuracy and computational efficiency are obtained by implementing two of these modifications. In addition, these two beneficial modifications provide the same enhancements to similar semi-analytical algorithms that simulate singe-phase injection into multi-layer domains.

1 Introduction

Geological CO_2 sequestration (GCS) has the potential to greatly reduce greenhouse gas loading to the atmosphere while cleaner, more sustainable energy solutions are developed. However, displaced brine or sequestered CO_2 may intrude into and adversely affect shallow groundwater resources. Brine leakage would increase aquifer salinity, while CO_2 intrusion may cause secondary effects, such as the mobilization of hazardous inorganic constituents present in aquifer minerals and changes in pH values. These risks must be fully understood and minimized before project implementation.

It is thus often beneficial to use faster, though less accurate, leakage estimation models to perform the large quantities of model simulations required for preliminary GCS planning, site selection, optimization, and sensitivity analysis. In addition, inherent subsurface uncertainties often necessitate the need for stochastic methods, further increasing the quantity of simulations needed. The direct use of other multiphase multi-layer numerical methods in the initial planning stage is typically prohibited by both the high computational cost per simulation and the significant effort involved in building and calibrating a custom model for each potential injection site. In response to these obstacles, analytical and semi-analytical methods have been developed which greatly reduce simulation complexity and computational run times.

Several attempts have been made to analytically quantify the hydraulic communication between aquifers separated by leaky aquitard layers [19,20,21,30]. In addition, several other authors have presented analytical or semi-analytical solutions used to estimate subsurface pressure distributions and fluid flux across layer boundaries resulting from leaky wells [24,25]. For example, [29] introduced fluid and matrix compressibility to the similarity solutions governing single-well CO_2 injection presented in [33], while [42] presented a single-phase semi-analytical solution for large scale injection-induced pressure perturbation and leakage in a laterally bounded aquifer-aquitard system. Also, a semi-analytical model estimating multiphase fluid flux through a single caprock perforation was developed by [27] to determine optimal injection intervals based upon trapping effects for secure CO_2 storage in saline aquifers and [5,9,10] presented and applied a single-phase semi-analytical model for both forced and diffuse leakage in a multi-layer system. Finally, [4] combined solutions presented by [21], [37], and [41] to create a semi-analytical solution for approximating the area of potential impact from a single CO_2 injection well.

However, while other semi-analytical algorithms provide insight regarding specific processes (e.g. diffuse leakage[10]), this work focuses upon the multiphase subsurface flow model proposed by [39] and further

developed by [7] because it is the only semi-analytical model able to simulate multiphase flow in domains having multiple injection wells and multiple aquifer and aquitard (i.e. caprock) layers.

An analytical algorithm was developed by [37] for estimating the pressure distribution and leakage for single-phase injection (e.g. injection of brine into a brine filled domain of aquifer) into a domain having multiple passive wells and multiple aquifer-aquitard layers. This algorithm creates a set of linear equations describing the pressure distribution throughout the domain by superimposing pressure changes caused by each source or sink in each aquifer. The general algorithm presented in [37] in conjunction with the development of a multiphase pressure response function [33,34,35,37] has led to a semi-analytical CO_2 leakage algorithm, presented in [39] and expounded upon in [7], which estimates both brine and CO_2 flux across confining layers resulting from the injection of CO_2. While there are multiple pathways for the leakage of sequestered CO_2 from subsurface storage reservoirs (e.g. geological discontinuities, caprock permeability, etc.), [39] assumes that hydrocarbon exploration and production boreholes created preferential flow paths in the domain [2,3,12,14,18,28,32]. This assumption appears reasonable as the existing caprock had successfully held the recently produced hydrocarbons for many millennia prior to production [36].

Stochastic techniques for preliminary GCS site assessment (e.g. injection strategy optimization, risk analysis, and sensitivity analysis, etc.) require large numbers of simulations. Therefore, it is important to be continually developing the accuracy and efficiency of simulation tools. Three modifications to this semi-analytical CO_2 leakage algorithm are presented and explored. These include 1) solving for temporally averaged flow rates at each passive well at each time step, 2) using separate pressure response functions depending on fluid type [41], and 3) applying a fixed point type iterative global pressure solution to eliminate the need to solve large sets of linear equations.

This work first includes a detailed description of the original semi-analytical leakage algorithm then presents the methodology for applying the three proposed modifications. Following this is a description of hypothetical test cases, then a discussion regarding the accuracy and computational efficiency results for each proposed method. Finally, we conclude with suggestions of cases when usage of these modifications would be essential.

2 Methodology

A thorough understanding of the existing semi-analytical leakage algorithm's methodology is needed before describing potential modifications. Therefore, the first part of this section provides a detailed description of work presented in [39] and [7].

2.1 The Estimating Leakage Semi-analytically (ELSA) Algorithm

Referred to as Estimating Leakage Semi-analytically (ELSA) when used by [31] to estimate the maximum probable leakage along abandoned oil wells, this semi-analytical algorithm estimates both brine and CO_2 flux through permeable caprock locations resulting from GCS. Permeable caprock locations are conceptualized as segments of abandoned wells and represent cylindrical portions of the aquitard layers having non-negligible permeability values. These are referred to as 'passive wells' and are assumed to be the only pathways for fluid flux between aquifer layers. Users of this model are able to specify the number of injection wells (M), passive wells (N), and aquifer/aquitard layers (L), as well as their respective spatial locations and hydrogeological parameters when characterizing the domain.

The domain is structured as a stack of aquifer/aquitard layers perforated by injection and passive wells. Aquifers are assumed to be horizontally level, homogenous, and isotropic. Aquitards are assumed to be impermeable, except where perforated by passive wells. Injection wells are able to inject into any layer. Initially, fluid is not flowing through any of the passive wells because the entire domain is assumed to be

saturated with brine at hydrostatic pressure. Additional assumptions made by this model include: 1) Aquifers exhibit horizontal flow; 2) Capillary pressure is negligible resulting in a sharp fluid interface; 3) CO_2 plume thickness at any given location is assumed to be the maximum plume thickness from all sources in the aquifer; 4) Pressure response from sources and sinks are superimposed in each aquifer; and 5) the injectivity of the formation remains constant. Several of these processes are important [9,11,13,15,17,22,26] and should be included [6,16,23,38] when model accuracy is more important that efficiency (e.g. during final project design).

At the start of injection, aquifer fluid pressures throughout the domain begin to change resulting in pressure differentials across aquitards and fluid flux through passive wells. It is therefore very important to understand aquifer fluid pressure response resulting from changes in the mass storage of CO_2 and brine. A pressure response function for the injection of CO_2 into a brine filled confined aquifer was derived in [33]. Reference [7] expresses this radial overpressure response, Δp, at the bottom of a confined aquifer for a single well injecting CO_2 as:

$$\Delta p = p - p_0 = \Delta p'(\rho_b - \rho_c)gH \tag{1}$$

where p_0 and p are the initial and resulting fluid pressures at the bottom of the aquifer, ρ is fluid density, g is gravitational acceleration, H is aquifer thickness, and subscripts b and c denote phase types brine and CO_2, respectively. In addition, $\Delta p'$ is a dimensionless function defined as:

$$\Delta p'(\chi) = \begin{cases} 0, & \chi \geq \psi \\ -\frac{1}{2\Gamma}\ln\left(\frac{\chi}{\psi}\right) + \Delta p'(\psi), & \psi > \chi \geq 2\lambda \\ \frac{1}{\Gamma} - \frac{\sqrt{\chi}}{\Gamma\sqrt{2\lambda}} + \Delta p'(2\lambda) + F(h'), & 2\lambda > \chi \geq \frac{2}{\lambda} \\ -\frac{1}{2\lambda\Gamma}\ln\left(\frac{\chi\lambda}{2}\right) + \Delta p'\left(\frac{2}{\lambda}\right), & \frac{2}{\lambda} > \chi \end{cases} \tag{2}$$

where,

$$\chi = \frac{2\pi H\varphi(1 - S_b^{res})r^2}{Q \cdot t} \tag{3}$$

$$\Gamma = \frac{2\pi(\rho_b - \rho_c)gkH^2}{\mu_b Q} \tag{4}$$

$$\psi = \frac{4.5\pi H\varphi k(1 - S_b^{res})}{\mu_b c_{eff} Q} \tag{5}$$

$$h' = \frac{h(\chi)}{H} = \frac{1}{\lambda - 1}\left(\frac{\sqrt{2\lambda}}{\sqrt{\chi}} - 1\right) \tag{6}$$

$$F(h') = \frac{-\lambda}{\lambda - 1}\left[\mathrm{h}' - \frac{ln[(\lambda - 1)h' + 1]}{\lambda - 1}\right] \tag{7}$$

In Equations (2-7), B is aquitard thickness, h is CO_2 plume thickness, h' is the ratio of CO_2 plume thickness to aquifer thickness, S_b^{res} is the residual saturation of the brine, t is the injection duration, k is the aquifer permeability, μ is the dynamic viscosity, φ is the aquifer porosity, Q is the total volumetric well flux, c_{eff} is the effective compressibility of the fluid and solid matrix, and r is the radial distance from the CO_2 source or sink. Also, $F(h')$ is an offset term related to the vertical pressure distribution [7] and the mobility ratio is defined as $\lambda = \lambda_c/\lambda_b$, where $\lambda_\alpha = k_{r,\alpha}/\mu_\alpha$ and $k_{r,\alpha}$ is the relative permeability of phase α ($\alpha = b$ for brine or $\alpha = c$ for CO_2).

ELSA uses Equation (1) to determine the pressure distribution throughout the aquifer, then applies a multiphase version of Darcy's law to determine each flow rate, $Q_{\alpha\, j,l}$, for each phase α across each confining layer l (l=1,2,..,L) for each passive well j (j=1,2,..,N):

$$Q_{\alpha\,j,l} = \pi r_{pw\,j,l}^2 \frac{k_{r,\alpha\,j,l} k_{pw\,j,l}}{\mu_\alpha B_l} \left(p_{j,l-1} - \rho_\alpha g B_l - g\rho_\alpha H_{l-1} - p_{j,l}\right) \quad (8)$$

In Equation (8), $r_{pw\,j,l}$ is the passive well radius and $k_{pw\,j,l}$ is the permeability for passive well j (j=1,2,..,N) and aquitard layer l.

Equation (1) differs significantly from the solution derived by [41] for single phase flow in that estimated pressure responses are non-linear with respect to the injection flow rate. Also, unlike single phase flow, CO_2 plume locations and thicknesses must be known when determining fluid saturations and relative permeabilities found in passive well pathways. ELSA overcomes these problems by linearizing Equation (1) using Green's functions and applying time stepping to approximate the changing pressure distribution, passive well fluxes, and CO_2 plume locations and thicknesses over the injection duration. For each time step, the following linear equation is written for each passive well in each aquifer.

$$p_{i,l} = p_{0_l} + \sum_{iw=1}^{M} G_{i,iw,l} Q_{iw,l} + \sum_{j=1}^{N} G_{i,j,l}\{Q_{j,l} - Q_{j,l+1}\} + F(h'_{max})(\rho_b - \rho_c)gH \quad (9)$$

where i (i=1,2,..,N) denotes the passive well at which pressure is being solved, l (l=1,2,..,L) denotes aquifer layer, and iw (iw=1,2,..,M) and j (j=1,2,..,N) denote the injection and passive well, respectively, whose flux is causing pressure change at well i. Green's functions are defined by the partial derivatives:

$$G_{i,j,l} = \frac{\partial(\Delta p_{i,l})}{\partial Q_{avg\,j,l}} \quad (10)$$

Reference [39] describes the Green's functions defined by Equation (10) as representations of "the sensitivity of the pressure field for a given source or sink". These are obtained analytically by calculating

the partial derivative of Equation (1) with respect to the average flux, $Q_{avg}{}_{j,l}$, of a given injection or passive well. For each time step, Green's function coefficients, $G_{i,j,l}$, are evaluated using the previous time step's flow rates. As shown by the denominator of Equation (3), for each time step, ELSA estimates the total pressure change from the start of simulation, rather than the incremental pressure change over the time step, at well i (i=1,2,..,N) resulting from fluid flux at well j (j=1,2,..,N), by multiplying the current time step's passive well flow rate by a Green's function constant calculated using the average flow rate over all previous time steps:

$$\Delta p_{i,j,l} = G_{i,j,l} \cdot Q_{j,l}^{(t)} \tag{11}$$

Substituting Equation (8) into Equation (9) yields the following:

$$\begin{aligned} p_{i,l} = p_{0_l} + \sum_{iw=1}^{M} G_{i,iw,l} Q_{iw,l} \\ + \sum_{j=1}^{N} G_{i,j,l} \Bigg\{ \pi r_{pw}^2{}_{j,l} \frac{k_{r,eff}{}_{j,l} k_{pw}{}_{j,l}}{\mu_{eff} B_l} \big(p_{j,l-1} - \rho_b g B_l - g H_{l-1} (\rho_b - \rho_b h'_{i,l-1} \\ + \rho_c h'_{i,l-1}) - p_{j,l} \big) \\ - \pi r_{pw}^2{}_{j,l+1} \frac{k_{r,eff}{}_{j,l+1} k_{pw}{}_{j,l+1}}{\mu_{eff} B_{l+1}} \big(p_{j,l} - \rho_b g B_{l+1} - g H_l \big(\rho_b - \rho_b h'_{i,l} + \rho_c h'_{i,l} \big) \\ - p_{j,l+1} \big) \Bigg\} + F(h'_{max})(\rho_b - \rho_c) g H \end{aligned} \tag{12}$$

where the subscript *eff* denotes 'effective'. Effective phase dependent parameters are needed because total volumetric flow rates may be composed of both CO_2 and brine. It is now possible to isolate unknown pressure terms $p_{i,l}$, $p_{j,l-1}$, $p_{j,l}$, and $p_{j,l+1}$ in Equation (12):

$$p_{i,l} + \sum_{j=1}^{N} \left(A_{i,j,l} \cdot p_{j,l-1} + B_{i,j,l} \cdot p_{j,l} + C_{i,j,l} \cdot p_{j,l+1} \right) = D_{i,l} \tag{13}$$

where $A_{i,j,l}$, $B_{i,j,l}$, $C_{i,j,l}$, and $D_{i,l}$, are constants for the current time step and defined as:

$$A_{i,j,l} = -G_{i,j,l} \pi {r_{pw}}^2_{j,l} \frac{{k_{r,eff}}_{j,l} {k_{pw}}_{j,l}}{\mu_{eff} B_l} \tag{14}$$

$$B_{i,j,l} = G_{i,j,l} \pi {r_{pw}}^2_{j,l} \frac{{k_{r,eff}}_{j,l} {k_{pw}}_{j,l}}{\mu_{eff} B_l} + G_{i,j,l} \pi {r_{pw}}^2_{j,l+1} \frac{{k_{r,eff}}_{j,l+1} {k_{pw}}_{j,l+1}}{\mu_{eff} B_{l+1}} \tag{15}$$

$$C_{i,j,l} = -G_{i,j,l} \pi {r_{pw}}^2_{j,l+1} \frac{{k_{r,eff}}_{j,l+1} {k_{pw}}_{j,l+1}}{\mu_{eff} B_{l+1}} \tag{16}$$

$$\begin{aligned} D_{i,l} = {} & p_{0_l} + \sum_{iw=1}^{M} \left[G_{i,iw,l} Q_{iw,l} \right] \\ & + \sum_{j=1}^{N} \left[G_{i,j,l} \left\{ \pi {r_{pw}}^2_{j,l} \frac{{k_{r,eff}}_{j,l} {k_{pw}}_{j,l}}{\mu_{eff} B_l} \left(-\rho_b g B_l - g H_{l-1} (\rho_b - \rho_b h'_{i,l-1} \right. \right. \right. \\ & \left. + \rho_c h'_{i,l-1} \right) \Big) \\ & \left. \left. \left. - \pi {r_{pw}}^2_{j,l+1} \frac{{k_{r,eff}}_{j,l+1} {k_{pw}}_{j,l+1}}{\mu_{eff} B_{l+1}} \left(-\rho_b g B_{l+1} - g H_l \left(\rho_b - \rho_b h'_{i,l} + \rho_c h'_{i,l} \right) \right) \right\} \right] \\ & + F(h'_{max}) (\rho_b - \rho_c) g H \end{aligned} \tag{17}$$

Equation (13) is written for each passive well i (i=1,2,..,N) at the bottom of each aquifer l (l=1,2,..,L) resulting in a linear system of N*L equations and unknowns. Solving this set of linear equations provides fluid pressures, $p_{i,l}$, at each passive well at each layer.

Once pressures are known throughout the domain, Equation (8) is used to explicitly calculate passive well segment fluxes for the current time step. The time step is then advanced and the process is repeated until the full simulation duration is reached. Mass storage changes in each layer, $\Delta M_{\alpha,l}$, may be determined for both CO_2 ($\alpha = c$) and brine ($\alpha = b$) by calculating the product of fluid density, ρ_α, injection duration, t_{inj}, and the sum of average passive well segment flow rates, $Q_{\alpha,avg}$:

$$\Delta M_{\alpha,l} = \rho_\alpha t_{inj} \sum_{iw=1}^{M} Q_{avg}{}_{iw,l} + \rho_\alpha t_{inj} \sum_{j=1}^{M+N} \left[Q_{\alpha,avg}{}_{j,l} - Q_{\alpha,avg}{}_{j,l+1} \right] \tag{18}$$

2.2 Temporally Averaged Flow Rate (TAFR) Modification

In [37], the CO_2 pressure response function is derived for sources or sinks having a constant flow rate. However, passive well fluxes occur as a response to pressure differentials across caprock layers and therefore change over the injection duration. This work proposes the estimation of pressure change by multiplying the average passive well flow rate by its corresponding Green's function constant. Therefore, Equation (11) is changed as follows:

$$\Delta p_{i,j,l} = G_{i,j,l} \cdot Q_{avg}^{(t)}{}_{j,l} \tag{19}$$

Figure 2.1 shows the rate of CO_2 leakage through a passive well over an injection period of 180 days. In this example, the CO_2 plume encounters the passive well at 56 days (point A in Figure 2.1). Following this, there is a dramatic increase in the CO_2 flow rate due to the rapidly increasing saturation of CO_2 in the passive well. At 147 days (point B in Figure 2.1), the slope of the passive well's flow rate abruptly reduces upon reaching the maximum CO_2 saturation in the passive well segment.

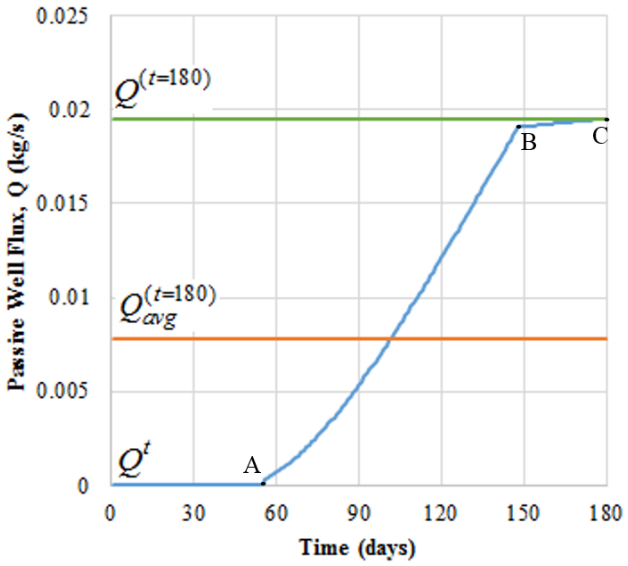

Figure 2.1: Rate of CO_2 leakage through a passive well segment over 180 days of injection

In this case, the leakage rate at 180 days (point C in Figure 2.1), $Q^{(t=180)}$, is much greater than the average leakage rate over the 180 day injection period, $Q_{avg}^{(t=180)}$. Accordingly, multiplying $Q^{(t=180)}$ by the injection duration in Equation (3) overestimates both the mass of fluid transferred and the resulting pressure changes.

To apply this modification, Equation (9) is rewritten with respect to Q_{avg}.

$$p_{i,l} = p_{0_l} + \sum_{iw=1}^{M} G_{i,iw,l} Q_{avg}{}_{iw,l} + \sum_{j=1}^{N} G_{i,j,l} \left\{ Q_{avg}{}_{j,l} - Q_{avg}{}_{j,l+1} \right\} + F(h'_{max})(\rho_b - \rho_c) g H \qquad (20)$$

Next, unknown passive well flow rates are defined. Average volumetric flow rate is equal to total fluid mass transferred through passive well segment, $M_{j,l}^{(t)}$, divided by the effective fluid density, ρ_{eff}, divided by the time, t.

$$Q_{avg}{}_{j,l}^{(t)} = M_{j,l}^{(t)}/\rho_{eff}t \tag{21}$$

Effective fluid densities are needed in this case because $M_{j,l}^{(t)}$ may be composed of both CO_2 and brine. The total fluid mass transferred from the start of injection through the current time step between aquifers by a passive well segment may be defined as:

$$M_{j,l}^{(t)} = M_{j,l}^{(t-\Delta t)} + \Delta t \cdot 0.5\left(Q_{j,l}^{(t-\Delta t)} + Q_{j,l}^{(t)}\right)\rho_{eff} \tag{22}$$

where $M_{j,l}^{(t-\Delta t)}$ is total fluid mass transferred by the well segment during all previous time steps, Δt is the time step duration, and $0.5\left(Q_{j,l}^{(t-\Delta t)} + Q_{j,l}^{(t)}\right)\rho_{eff}$ is the average mass flux over the current time step. Substituting Equation (22) into Equation (21) gives:

$$Q_{avg}{}_{j,l}^{(t)} = \left[M_{j,l}^{(t-\Delta t)} + 0.5\Delta t\left(Q_{j,l}^{(t-\Delta t)} + Q_{j,l}^{(t)}\right)\rho_{eff}\right]/\rho_{eff}t \tag{23}$$

Subtracting the bottom layer's average flow rate by the top layer's average flow rate gives:

$$Q_{avg}{}_{j,l} - Q_{avg}{}_{j,l+1} = c_2\left(Q_{j,l} - Q_{j,l+1}\right) + c_1 \tag{24}$$

where c_1 and c_2 are defined as:

$$c_1 = \frac{M_{j,l}^{(t-\Delta t)} - M_{j,l+1}^{(t-\Delta t)} + 0.5\Delta t\left(Q_{j,l}^{(t-\Delta t)} - Q_{j,l+1}^{(t-\Delta t)}\right)\rho_{eff}}{\rho_{eff}t} \tag{25}$$

$$c_2 = \frac{0.5\Delta t}{t} \tag{26}$$

Finally, substituting Equation (24) into Equation (20) gives the pressure equation for the modified method:

$$\begin{aligned} p_{i,l} = p_{0,l} + \sum_{iw=1}^{M} \left[G_{i,iw,l} Q_{iw,l}\right] \\ + \sum_{j=1}^{N} \Bigg[c_2 G_{i,j,l} \Bigg\{ \pi {r_{pw}}_{j,l}^2 k_{j,l} \frac{k_{r,eff,j,l}}{\mu_{eff} B_l} \big(p_{j,l-1} - \rho_b g B_l - g H_{l-1}(\rho_b - \rho_b h'_{i,l-1} \\ + \rho_c h'_{i,l-1}) - p_{j,l}\big) \\ - \pi {r_{pw}}_{j,l+1}^2 k_{j,l+1} \frac{k_{r,eff,j,l+1}}{\mu_{eff} B_{l+1}} \big(p_{j,l} - \rho_b g B_{l+1} - g H_l(\rho_b - \rho_b h'_{i,l} + \rho_c h'_{i,l}) \\ - p_{j,l+1}\big) \Bigg\} + c_1 G_{i,j,l} \Bigg] + F(h'_{max})(\rho_b - \rho_c) g H \end{aligned} \tag{27}$$

2.3 Separate Pressure Response Function (SPRF) Modification

ELSA uses the sum of CO_2 and brine fluxes to calculate the total volumetric source or sink when determining *Q* for Equation (1). Since the fundamental pressure response equation was derived for a single well injecting only CO_2, the use of a separate pressure response equations for each fluid type is proposed as a potential accuracy improvement.

This modification is applied by continuing to estimate pressure changes from CO_2 leakage with Equation (1) while determining pressures changes from brine leakage using the Theis equation [41]:

$$p_{i,l} - p_{0_l} = \frac{\rho_b g}{4\pi T_l} W\big(u_{i,j,l}\big) Q_{b\,j,l} \tag{28}$$

where,

$$u_{i,j,l} = \frac{r_{i,j}^2 S_l}{4T_l t} \tag{29}$$

In Equations (28) and (29) T_l is the layer transmissivity, $W(u)$ is the Well function [41], S_l is the layer storativity, and $r_{i,j}$ is the horizontal distance between passive well i (i=1,2,..,N) and passive well j (j=1,2,..,N). ELSA assumes c_{eff} in Equation (5) to be equal to the compressibility of brine [7]. Therefore, in order to maintain consistency between the original and modified algorithms, S is assumed to be the storativity resulting solely from the compressibility of brine, c_b:

$$S_l = \rho_b c_b g H_l \tag{30}$$

Pressure changes from each source or sink are superimposed at each passive well location i (i=1,2,..,N) in each aquifer:

$$\begin{aligned} p_{i,l} = p_{0\,l} + \sum_{iw=1}^{M} \left[G_{i,iw,l} Q_{c\,iw,l} + \frac{\rho_b g}{4\pi T_l} W\left(u_{i,iw,l}\right) Q_{b\,iw,l} \right] \\ + \sum_{j=1}^{N} \left[G_{i,j,l} \left\{ Q_{c\,j,l} - Q_{c\,j,l+1} \right\} \right] + \frac{\rho_b g}{4\pi T_l} \sum_{j=1}^{N} \left[W\left(u_{i,j,l}\right) \left\{ Q_{b\,j,l} - Q_{b\,j,l+1} \right\} \right] \end{aligned} \tag{31}$$

2.4 Iterative Global Pressure Solution (IGPS) Modification

The number of unknown variables, hence the number of linear equations, is equal to the product of the number of passive wells and the number of aquifer layers (N*L). Domains having large numbers of passive wells and/or layers produce very large sets of linear equations and resulting in significantly higher

simulation run times. An iterative fixed point [40] approach is proposed here to increase computational efficiency by solving the global pressure solution. In addition, this method is able to solve nonlinear sets of equations, therefore eliminating the need to linearize the pressure response equation. In the following methodology, *iter* denotes iteration index, $\mathbf{Q_{avg}}$ and $\mathbf{Q}$ are vectors of average and current time step passive well flow rates with a size of [*N***L*], $\mathbf{p}$ is a vector of fluid pressures at the bottom of each aquifer at each passive well with a size of [*N***L*], and $\mathbf{\Omega_1}$ and $\mathbf{\Omega_2}$ are sets of parameters and independent variables, other than $\mathbf{Q}$ and $\mathbf{p}$, for Equation (1) and Equation (8), respectively:

$$\mathbf{\Omega}_1 \equiv \left\{ \rho_c, \rho_b, g, \mathbf{H}, \lambda, \pi, \boldsymbol{\varphi}, S_b^{res}, \mathbf{r}, t, \mathbf{k}, \mu_b, c_{eff} \right\} \tag{32}$$

$$\mathbf{\Omega}_2 \equiv \left\{ \pi, \mathbf{r}_{pw}, \mathbf{k}_{r,c}, \mathbf{k}_{r,b}, \mathbf{k}_{pw}, \mu_c, \mu_b, \mathbf{B}, \rho_c, \rho_b, g, \mathbf{H} \right\} \tag{33}$$

where $\mathbf{H}$, $\boldsymbol{\varphi}$, and $\mathbf{k}$ are vectors of aquifer thicknesses, porosities, and permeabilities, respectively, with size [*L*], $\mathbf{B}$ is a vector of aquitard thicknesses with size [*L*+1], $\mathbf{r}$ is an array of radial distances with size [*M*+*N*] *x* [*M*+*N*], and $\mathbf{r}_{pw}$, $\mathbf{k}_{pw}$, $\mathbf{k}_{r,c}$, and $\mathbf{k}_{r,b}$ are arrays of passive well radii, permeabilities, and relative permeabilities of the CO_2 and brine phases, respectively, with size [*N*] *x* [*L*+1]. The following is the procedure for the IGPS modification.

1. Use the initial assumption that passive well flow rates for the current time step remain constant from the previous time step:

$$\mathbf{Q}(\mathrm{t})^{(iter=0)} = \mathbf{Q}(\mathrm{t} - \Delta t) \tag{34}$$

2. Use Equation (21) to determine average passive well flux rates then apply the non-linear Equation (1) to calculate the global pressure distribution by superimposing pressure changes from both assumed passive well flow rates and known injection well flow rates at each passive well in each aquifer:

$$\mathbf{p}(\mathrm{t})^{(iter)} = \mathbf{p}\left(\boldsymbol{\Omega_1}, \mathbf{Q}_{\mathrm{avg}}(\mathrm{t})^{(iter-1)}\right) \tag{35}$$

3. Calculate new passive well flow rates using this new pressure distribution and Equation (8):

$$\mathbf{Q}(\mathrm{t})^{(iter)} = \mathbf{Q}\left(\boldsymbol{\Omega_2}, \mathbf{p}(\mathrm{t})^{(iter)}\right) \tag{36}$$

4. Repeat steps 2 and 3 until the maximum relative error, ε, between the preceding and current iteration's flow rate becomes smaller than a prescribed tolerance coefficient, ε_{max}:

$$\varepsilon = max\left\{\begin{matrix}\left|\frac{{Q_{1,1}}^{(iter+1)} - {Q_{1,1}}^{(iter)}}{{Q_{1,1}}^{(iter+1)}}\right|, \cdots, \left|\frac{{Q_{j,l}}^{(iter+1)} - {Q_{j,l}}^{(iter)}}{{Q_{j,l}}^{(iter+1)}}\right| \\ , \cdots, \left|\frac{{Q_{N,L}}^{(iter+1)} - {Q_{N,L}}^{(iter)}}{{Q_{N,L}}^{(iter+1)}}\right|\end{matrix}\right\} \leq \varepsilon_{max} \tag{37}$$

Two additional parameters are implemented when applying this modification to ensure time step convergence stability. First, a maximum passive well flow rate, $Q_{pw,max}$, is specified to dampen artificially high-magnitude pressure differentials calculated when using either large time step intervals or closely-spaced passive well positions. Secondly, a relaxation factor, ω, between preceding and current iterative passive well flow rates is specified to reduce the likelihood of divergent oscillations:

$$\mathbf{Q}^{(iter)} = \omega\mathbf{Q}^{(iter)} + (1-\omega)\mathbf{Q}^{(iter-1)} \tag{38}$$

This work has found that setting $Q_{pw,max}$ equal to one tenth the volumetric injection rate and ω equal to 0.1 has resulted in algorithm stability for all cases tested.

3 Results and Discussion

CO_2 leakage estimation and simulation run times are compared for the three proposed modifications. The following information is constant for all analyses presented herein. A continuous CO_2 injection rate of 50 kg/s is simulated through one injection well (M = 1) into the lower of two 20 m thick aquifers (L = 2) separated by one 20 m thick aquitard. All aquifers have k = 100 mD, λ = 5, S_b^{res} = 30%, c_{eff} = 4.6 x 10^{-10} m^2/N, and φ = 10%. The bottom of the lower aquifer is set to a depth of 2000 m. Parameter values for the domain include g = 9.81 m/s^2, ρ_b = 1000 kg/m^3, ρ_c = 600 kg/m^3, μ_b = 0.5 mPa s, and μ_c = 0.05 mPa s. All passive wells have a radius, r_{pw}, equal to 0.2 m.

All sets of linear equations are solved by LU decomposition with partial pivoting using the DGESV solver available in the optimized linear algebra package LAPACK [1]. This general solver is needed because the matrix characterizing our linear set of equations is non-sparse and non-symmetrical. Verified by converge testing, all injection durations are discretized into 150 time steps. A computer having a 2.4 GHz Intel® Core™ i7 processor with 8 GB of installed memory is used for all simulations. Multiple identical runs are performed to ensure computational run time consistency.

Time saving measures (e.g. neglecting far or low mass flux sources) should be included when practically implementing this semi-analytical leakage model. However, these are not used in the following comparisons to maintain run time consistency.

This work makes the assumption that Equation (1) accurately estimates pressure changes resulting from a single well injecting CO_2 into a confining aquifer and accepts the numerical validation presented by [33].

While the modifications presented above alter the implementation of the pressure solution, its fundamental form, defined by Equation (1), remains the same. Also, the upconing solution [34] and *F'* offset term defined above with Equation (7) are neglected for the purpose of simplifying the following analyses.

3.1 Application of the Temporally Averaged Flux Rate (TAFR) Modification

While the mathematical justification for using a temporally averaged flux rate (TAFR) has been provided in Section 2.2, the two analyses presented in this section provide additional support to this modification. The first analysis explores a worst case scenario for the original algorithm where large changes in passive well leakage flux occur near the end of simulation. This may occur when a highly permeable passive well encounters the CO_2 plume later in simulation, causing leakage rates for late time steps to be drastically greater than corresponding average leakage rates.

Both ELSA and the TAFR modified algorithm (herein referred to as ELSA-TAFR) are used to simulate CO_2 leakage through a passive well (N = 1) with k_{pw} = 10,000 mD located 5,000 m away from one injection well (M = 1). Fractional leakage is defined herein as the mass of CO_2 leakage into the upper aquifer divided by the mass injected. Figure 2.2 shows fractional leakage versus time estimated by the original and modified algorithms over the 50 year injection duration. In this case, ELSA-TAFR calculates a 25.6% higher fractional leakage at the end of the injection duration.

The underlying cause for the original semi-analytical algorithm's underestimation of leakage is due to the linearization of the pressure response function. Recall from Equation (11) that the change in aquifer fluid pressure is equal to the product of the Green's function and the source or sink flow rate ($\Delta p = G*Q$). Passive well flow rates typically increase over time when a constant or increasing rate of injection is occurring, causing flow rates determined for each time step (Q) to be greater than corresponding average

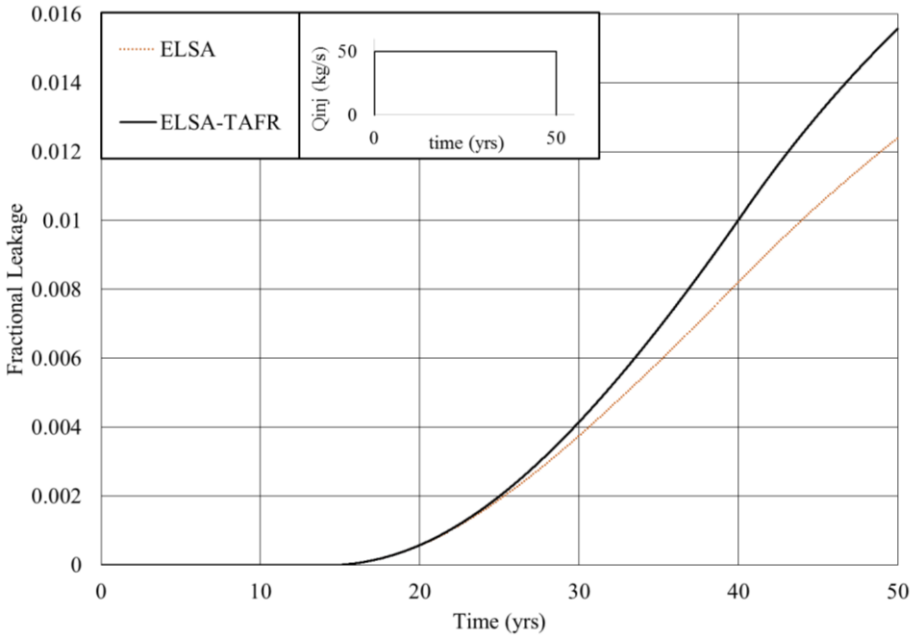

Figure 2.2: Fractional leakage vs. time for a 50 year simulation using both the ELSA and ELSA-TAFR algorithms

flow rates (Q_{avg}). In this case, the original method estimates greater pressure changes ($\Delta p_{ELSA} = G*Q$) than the modified method ($\Delta p_{ELSA\text{-}TAFR} = G*Q_{avg}$) resulting in the equalization of the pressure differential between the two aquifers with less cumulative leakage mass.

Passive well flow rates typically increase over time when a constant or increasing rate of injection is occurring, causing flow rates determined for each time step (Q) to be greater than corresponding average flow rates (Q_{avg}). In this case, the original method estimates greater pressure changes ($\Delta p_{ELSA} = G*Q$) than the modified method ($\Delta p_{ELSA\text{-}TAFR} = G*Q_{avg}$) resulting in the equalization of the pressure differential between the two aquifers with less cumulative leakage mass.

Let us now compare fluid leakage estimation between the existing and modified semi-analytical algorithms for more typical injection strategies and domain characteristics. Figure 2.3 shows the plan and elevation views of a hypothetical injection domain created for all following analyses. Passive well

Cartesian coordinates were uniformly randomly generated to be within a 50 km by 50 km domain centered with respect to the injection well.

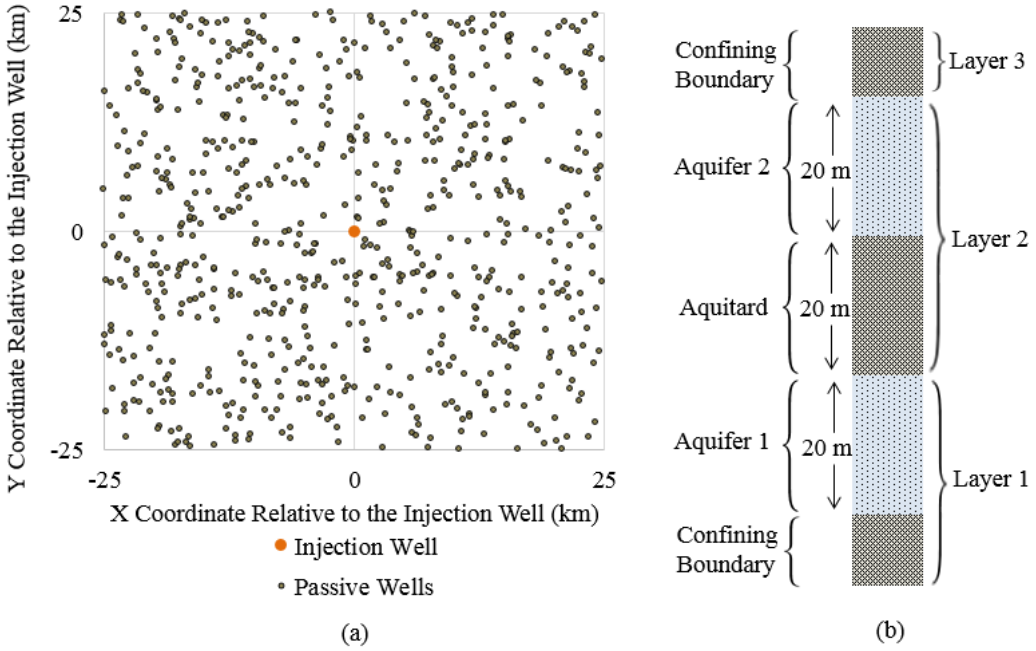

Figure 2.3: (a) Plan view of the domain showing locations of all 700 passive wells. (b) Elevation view of the domain showing layer locations and thicknesses.

All passive wells permeabilities, k_{pw}, were randomly generated having a 50% chance of being either "intact" or "degraded" [31]. Passive well permeabilities were assumed to be 0.1 mD for "intact" passive wells and 1000 mD for "degraded" passive wells. For this test, the only changing variable is the number of passive wells simulated, ranging between 50 and 700 in increments of 50.

ELSA and the TAFR modified algorithm were used to estimate CO_2 leakage at the end of the 50 year injection period for the set of domains described above. Figure 2.4 shows a comparison of simulation run times and fractional leakage at the end of the 50 year injection period versus the number of passive wells between the original and modified algorithms. A small increase of 1.7% in average CPU time was observed when applying the TAFR modification. However, differences in leakage estimation were found

to be significant. The TAFR modified algorithm's leakage estimates ranged between 2.6% and 15.6% higher than the original algorithm.

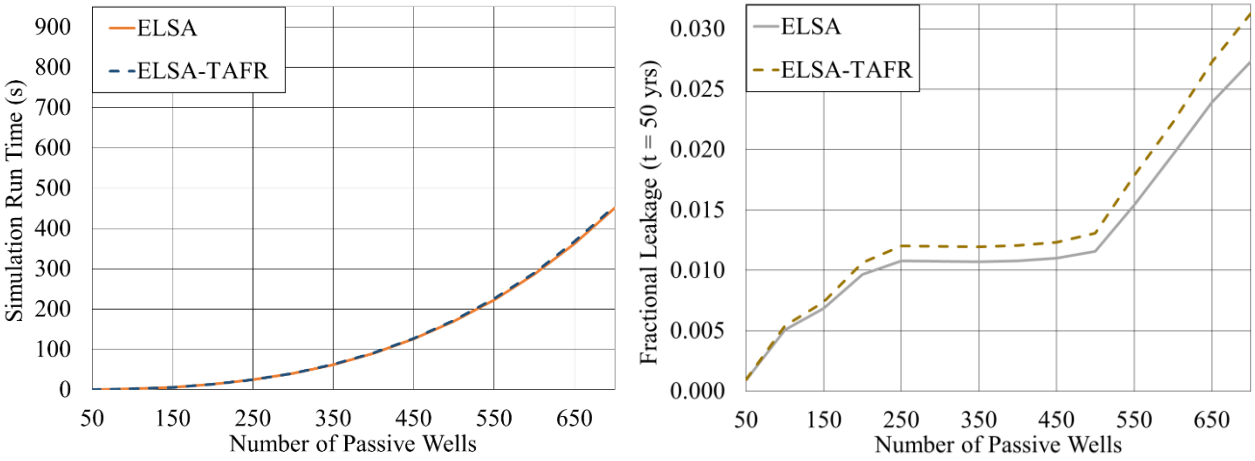

(a) (b)

Figure 2.4: Comparison of (a) simulation run time and (b) fractional leakage at the end of the 50 year injection period versus the number of passive wells between the original and TAFR modified algorithms

These results show that the original algorithm underestimates leakage for multiple randomly generated domains in addition to single passive well testing. Therefore, the TAFR modification is deemed important and is included in all following test cases.

3.2 Application of the Separate Pressure Response Equations for Fluid Type (SPRF) Modification

The use of separate pressure response functions (SPRF) for brine and CO_2 was explored as a potential modification to the existing algorithm. The TAFR and TAFR/SPRF modified algorithms were used to estimate CO_2 leakage at the end of the 50 year injection period for an identical set of domains used in the preceding analysis. Figure 2.5 shows a comparison of simulation run times and fractional leakage at the end of the 50 year injection period versus the number of passive wells between the TAFR and TAFR/SPRF modified algorithms. Results from these simulations show that TAFR/SPRF modification

produces negligible differences in CO_2 leakage estimation while greatly increasing computational expense. The average difference in fractional leakage decreased by 0.7% with the average computational cost increasing by 209%.

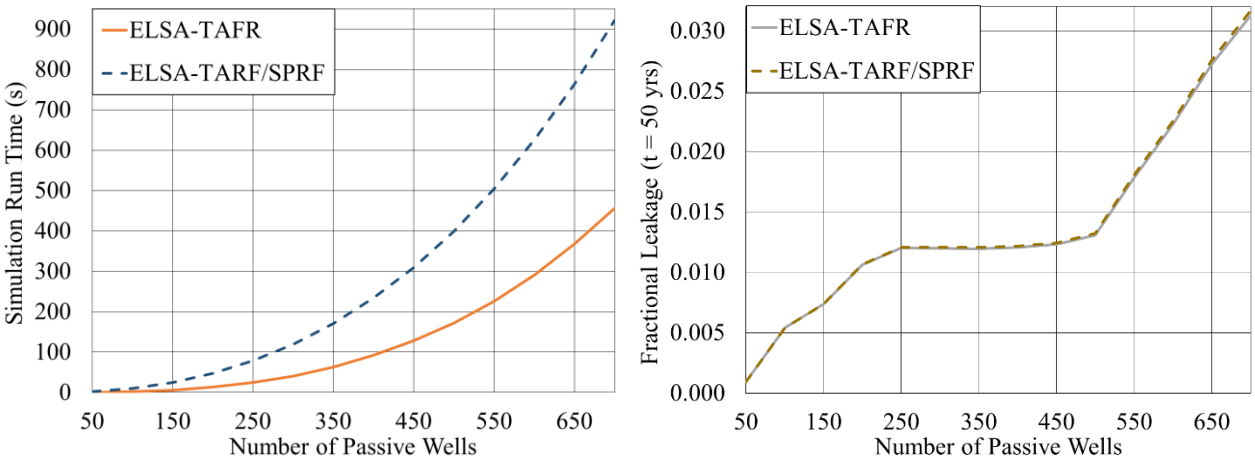

(a) (b)

Figure 2.5: Comparison of (a) simulation run time and (b) fractional leakage at the end of the 50 year injection period versus the number of passive wells between the TAFR and TAFR/SPRF modified algorithms

Computational expense is greatly increased by the SPRF modification due to the additional need to compute *W(u)* in Equation (28) for each source or sink. Leakage mass estimation is very similar between the two methods because Equation (1) and Equation (28) provide very similar estimations of pressure change. Figure 2.6 shows the aquifer fluid pressure response versus radial distance calculated by these two equations. A volumetric flux rate of 1.667 x 10^{-4} m^3/s over 50 years was used for both fluids.

The SPRF modification is found to adversely affect model efficiency with no significant difference in model accuracy and thus will not be included in the following comparisons.

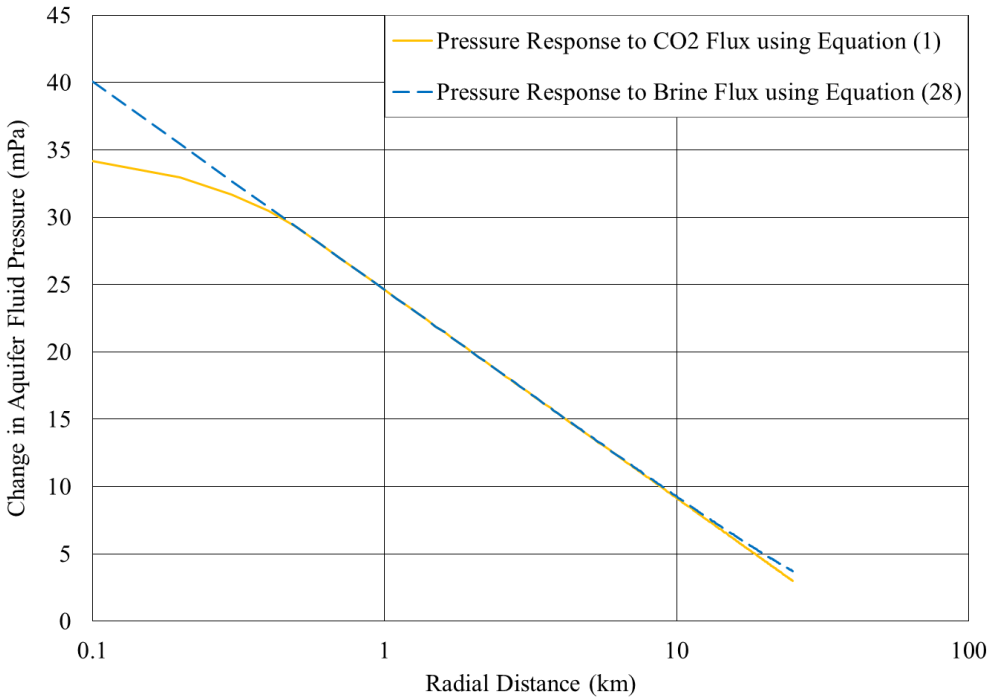

Figure 2.6: Comparison of aquifer fluid pressure response versus radial distance calculated using Equation (1) and Equation (28)

3.3 Application of the Iterative Global Pressure Solution (IGPS) Modification

The randomly generated domains presented in Section 3.1 were also used to quantify the accuracy and efficiency of the iterative global pressure solution (IGPS) modification. As seen in Equation (35), the IGPS modification uses average flux rates when calculating pressure changes. However, because it does not require the linearization of the pressure solution, Equations (22-27) are not used in conjunction with the IGPS modification. Figure 2.7 shows a comparison of simulation run times and fractional leakage at the end of the 50 year injection period versus the number of passive wells for the TAFR and IGPS modified algorithms. These results show that there are negligible differences in CO_2 leakage estimation between the TAFR and IGPS modified algorithms while the IGPS modification greatly decreases computational expense. The average observed difference in fractional leakage between the two algorithms is infinitesimal while computational cost is reduced by approximately one order of magnitude.

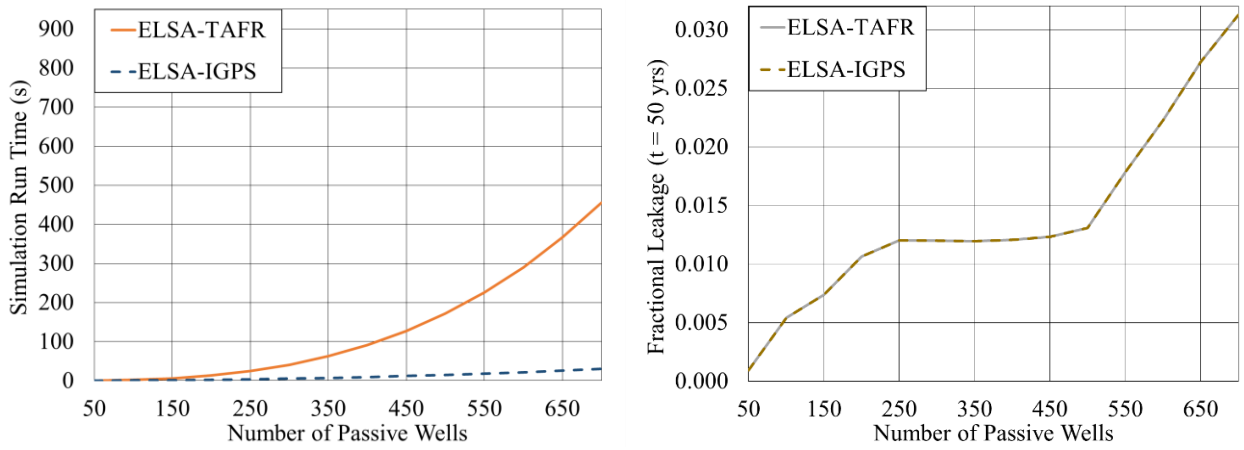

Figure 2.7: Comparison of (a) simulation run time and (b) fractional leakage at the end of the 50 year injection period versus the number of passive wells between the TAFR and IGPS modified algorithms

Leakage mass estimation is very similar between the two methods because both use the same pressure response equation and average passive well flux to estimate the pressure distributions throughout the domain. Simulations run times are drastically reduced using the IGPS modification because the problem is solved explicitly within each iteration and typically very few iterations (~1-3) are required for convergence. This provides greatly reduced simulation times. In addition, computational efficiency savings increase with the number of passive wells modeled. Figure 2.8 shows the ratio of simulation run time between the TAFR and IGPS modified algorithms versus the number of passive wells included in the domain.

4 Conclusions

This work has led to important modifications of the semi-analytical CO_2 leakage algorithm presented by [39]. Three proposed modifications to a semi-analytical leakage algorithm were proposed and tested. A modification involving the use of temporally averaged flux rates (TAFR) to estimate aquifer fluid pressure changes throughout the domain was found to address an underestimation of fluid leakage by the

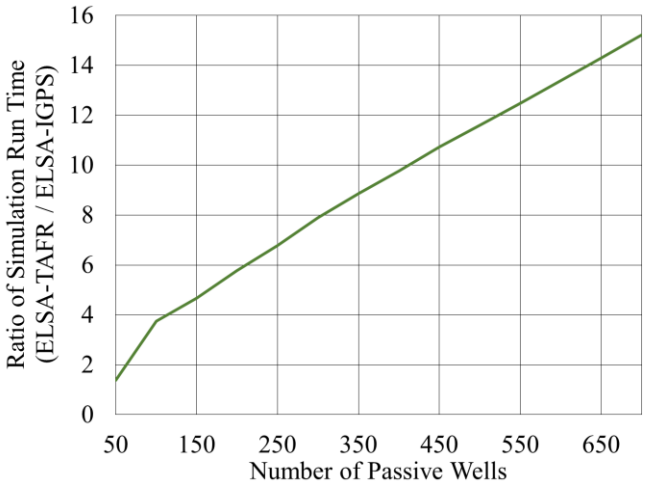

Figure 2.8: Ratio of ELSA-TAFR to ELSA-IGPS simulation run time versus the number of passive wells

original algorithm. Results showed that the ELSA-TAFR algorithm estimated leakage to be 11.2% higher on average that the original algorithm with an insignificant increase in computational expense. It is important that the TAFR modification be implemented in all cases as the original algorithm may significantly underestimate leakage.

The use of separate pressure response functions (SPRF) for fluid types was found to provide no change in accuracy while greatly decreasing computational efficiency. It is therefore suggested that this modification not be applied to this semi-analytical algorithm.

The final modification proposed the use of a fixed point type iterative global pressure solution (IGPS) as opposed to solving large linear sets of equations to determine the global pressure solution. This method was found to significantly increase computational efficiency. The average difference in fractional leakage between the two algorithms was found to be very small with the computational cost decreasing on average by approximately one order of magnitude. From the results obtained, the simulation of domains having large quantities of passive wells and aquifer layers would greatly benefit by using the IGPS

modification. In addition, this modification would be extremely beneficial when large numbers or simulations need to be performed such as in the cases of stochastic analysis or optimization.

REFERENCES

1. Anderson E., Bai Z., Bischof C., et al.: LAPACK Users Guide: Third Edition. Society for Industrial and Applied Mathematics, Philadelphia. (1999)
2. Avci C.: Evaluation of flow leakage through abandoned wells and boreholes. Water Resour Res 30:2565–2578 (1994)
3. Bachu S., Bennion D.B.: Experimental assessment of brine and/or CO_2 leakage through well cements at reservoir conditions. Int J Greenh Gas Control 3:494–501 (2009)
4. Bandilla K.W., Kraemer S.R., Birkholzer J.T.: Using semi-analytic solutions to approximate the area of potential impact for carbon dioxide injection. Int J Greenh Gas Control 8:196–204 (2012)
5. Birkholzer J.T., Cihan A., Zhou Q.: Impact-driven pressure management via targeted brine extraction—Conceptual studies of CO_2 storage in saline formations. Int J Greenh Gas Control 7:168–18 (2012)
6. Buscheck T.A., Sun Y., Chen M., et al.: Active CO_2 reservoir management for carbon storage: Analysis of operational strategies to relieve pressure buildup and improve injectivity. Int J Greenh Gas Control 6:230–245 (2012)
7. Celia M.A., Nordbotten J.M., Court B., et al.: Field-scale application of a semi-analytical model for estimation of CO_2 and brine leakage along old wells. Int J Greenh Gas Control 5:257–269 (2011)
8. Chen Z., Huan G., Ma Y.: Computational methods for multiphase flows in porous media. Society for Industrial and Applied Mathematics, Philadelphia. (2006)
9. Cihan A., Birkholzer J.T., Zhou Q.: Pressure buildup and brine migration during CO_2 storage in multilayered aquifers. Ground Water 51:252–67 (2013)
10. Cihan A., Zhou Q., Birkholzer J.T.: Analytical solutions for pressure perturbation and fluid leakage through aquitards and wells in multilayered-aquifer systems. Water Resour Res (2011) doi: 10.1029/2011WR010721
11. Court B., Bandilla K.W., Celia M.A., et al.: Applicability of vertical-equilibrium and sharp-interface assumptions in CO_2 sequestration modeling. Int J Greenh Gas Control 10:134–147 (2012)
12. Crow W., Carey J.W., Gasda S., et al.: Wellbore integrity analysis of a natural CO_2 producer. Int J Greenh Gas Control 4:186–197 (2010)
13. Doster F., Nordbotten J.M., Celia M.A.: Impact of capillary hysteresis and trapping on vertically integrated models for CO_2 storage. Adv Water Resour 62:465–474 (2013)

14. Duguid A., Butsch R.J., Loizzo M., Stamp V.: Collection of baseline wellbore cement data in multiple wells in the same field. Energy Procedia 4:5130–5137 (2011)
15. Gasda S., Nordbotten J.M., Celia M.A.: The impact of local-scale processes on large-scale CO_2 migration and immobilization. Energy Procedia 4:3896–3903 (2011)
16. Gasda S.E., Nordbotten J.M., Celia M.A.: Vertical equilibrium with sub-scale analytical methods for geological CO_2 sequestration. Comput Geosci 13:469–481 (2009)
17. Gasda S.E., Nordbotten J.M., Celia M.A.: Application of simplified models to CO_2 migration and immobilization in large-scale geological systems. Int J Greenh Gas Control 9:72–84 (2012)
18. Gasda S.E., Nordbotten J.M., Celia M.A.: Determining effective wellbore permeability from a field pressure test: a numerical analysis of detection limits. Environ Geol 54:1207–1215. doi: 10.1007/s00254-007-0903-7 (2007)
19. Hantush M.S.: Modification of the theory of leaky aquifers. J Geophys Res 65:11:3717-3725 (1960)
20. Hantush M.S.: Nonsteady flow to flowing wells in leaky aquifers. J Geophys Res 64:1043–1052 (1959)
21. Hantush M.S., and Jacob C.E.: Nonsteady radial flow in an infinite leaky aquifer, Am. Geophys. Union Trans., 36: 95-100 (1955)
22. Heße F., Prykhodko V., Attinger S.: Assessing the validity of a lower-dimensional representation of fractures for numerical and analytical investigations. Adv Water Resour 56:35–48 (2013)
23. Huang X, Bandilla K.W., Celia M.A., Bachu S.: Basin-scale modeling of CO_2 storage using models of varying complexity. Int J Greenh Gas Control 20:73–86 (2014)
24. Hunt B.: Flow to a well in a multiaquifer system. Water Resour Res 21:1637–1641 (1985)
25. Javandel I., Witherspoon P.: A semianalytical solution for partial penetration in two-layer aquifers. Water Resour Res 16:1099–1106 (1980)
26. Juanes R., MacMinn C.W., Szulczewski M.L.: The Footprint of the CO_2 Plume during Carbon Dioxide Storage in Saline Aquifers: Storage Efficiency for Capillary Trapping at the Basin Scale. Transp Porous Media 82:19–30 (2009)
27. Kumar N., Bryant S.L.: Semi-analytical model to determine perforation interval for secure CO_2 storage in saline aquifers. Energy Procedia 1:3071–3078 (2009)

28. Lacombe S., Sudicky E.: Influence of Leaky Boreholes on Cross-Formational Groundwater Flow and Contaminant Transport. Water Resour (1995)

29. Mathias SA, Hardisty P.E., Trudell M.R., Zimmerman R.W.: Approximate Solutions for Pressure Buildup During CO_2 Injection in Brine Aquifers. Transp Porous Media 79:265–284 (2008)

30. Neuman S., Witherspoon P.: Applicability of current theories of flow in leaky aquifers. Water Resour. Res. 5: 817-829 (1969)

31. Nogues J., Court B., Dobossy M., et al.: A methodology to estimate maximum probable leakage along old wells in a geological sequestration operation. Int J Greenh Gas Control 7:39–47 (2012)

32. Nogues J., Nordbotten J., Celia M.: Detecting leakage of brine or CO_2 through abandoned wells in a geological sequestration operation using pressure monitoring wells. Energy Procedia 4:3620–3627 (2011)

33. Nordbotten J., Celia M.: Semianalytical solution for CO_2 leakage through an abandoned well. Environ Sci Technol 39:602–611 (2005)

34. Nordbotten J., Celia M.: An improved analytical solution for interface upconing around a well. Water Resour Res 42:1–10. (2006a)

35. Nordbotten J., Celia M.: Similarity solutions for fluid injection into confined aquifers. J Fluid Mech 561:307–327. (2006b)

36. Nordbotten J., Celia M., Bachu S.: Analytical solutions for leakage rates through abandoned wells. Water Resour Res 40:1–10. (2004)

37. Nordbotten J., Celia M., Bachu S.: Injection and storage of CO_2 in deep saline aquifers: Analytical solution for CO_2 plume evolution during injection. Transp Porous media 58:339–360 (2005)

38. Nordbotten J., Flemisch B.: Uncertainties in practical simulation of CO_2 storage. Int J Greenh Gas Control 9:234–242 (2012)

39. Nordbotten J., Kavetski D., Celia M., Bachu S.: Model for CO_2 leakage including multiple geological layers and multiple leaky wells. Environ Sci Technol 43:743–749 (2009)

40. Takahashi W.: Nonlinear Functional Analysis: Fixed Point Theory and Its Applications, Yokohama Publishers, Yokohama (2000)

41. Theis C.V.: The relation between the lowering of the piezometric surface and the rate and duration of discharge of a well using groundwater storage, Am. Geophys. Union Trans., 16: 519-524 (1935)

42. Zhou Q., Birkholzer J., Tsang C.: A semi-analytical solution for large-scale injection-induced pressure perturbation and leakage in a laterally bounded aquifer–aquitard system. Transp Porous Media 78:127–148 (2009)

CHAPTER III: STOCHASTIC INJECTION STRATEGY OPTIMIZATION FOR THE PRELIMINARY ASSESSMENT OF CANDIDATE GEOLOGICAL STORAGE SITES

Summary Geological carbon sequestration (GCS) has been identified as having the potential to reduce increasing atmospheric concentrations of carbon dioxide (CO_2). However, a global impact will only be achieved if GCS is cost effectively and safely implemented on a massive scale. This work presents a computationally efficient methodology for identifying optimal injection strategies at candidate GCS sites having caprock permeability uncertainty. A multi-objective evolutionary optimization algorithm is used to heuristically determine non-dominated solutions between the following two competing objectives: 1) maximize mass of CO_2 sequestered and 2) minimize project cost. A semi-analytical algorithm is used to estimate CO_2 leakage mass rather than a numerical model, enabling the study of GCS sites having vastly different domain characteristics. The stochastic optimization framework presented herein is applied to a study of a brine filled aquifer in the Michigan Basin (MB). Twelve optimization test cases are performed to investigate the impact of decision maker (DM) preferences on Pareto-optimal objective function values and carbon injection strategies. Risk adversity to CO_2 leakage is found to have the largest effect on optimization results, followed by degree of caprock permeability uncertainty. This analysis shows that the feasibility of GCS at the MB test site is highly dependent upon the DM's risk adversity selection. Finally, large gains in computational efficiency achieved using parallel processing and archiving are discussed.

1 Introduction

Geological carbon sequestration (GCS) has been identified as a prominent technology to manage increasing atmospheric concentrations of carbon dioxide (CO_2) [37,44], however, the effective application of GCS will require a global implementation of large numbers of carbon injection projects. While an individual large coal-fired power plant may emit up to 5-10 megatonnes (Mt) of CO_2 per year [3], total annual global anthropogenic carbon emissions measured in mass of CO_2 are approximately 30,000 Mt [37]. Results from [17] suggest that specific regions of a small number of candidate aquifers will provide the majority of low cost geological CO_2 storage. As the selection of the appropriate reservoir is crucial to the success of a GCS project [4], many potential injection sites will need to be assessed world-wide for

GCS suitability. Therefore, the efficient preliminary characterization of candidate GCS injection sites has the potential for massive resource savings. In addition, a comprehensive pre-screening effort will increase GCS storage reliability by eliminating "bad" and identifying "good" GCS reservoirs.

Large-scale conjunctive preliminary project planning will involve the characterization, optimization, and risk assessment of several potential GCS sites. There are, however, several difficulties associated with these tasks. The first is that the large-scale, multiphase numerical modeling of several potential injection sites for the purpose of initial assessment is infeasible due to the effort involved in model construction and calibration. Data characterizing the subsurface domain are typically scarce, which introduces parameter uncertainty and adds to the complexity of modeling GCS. Also, because of their propensity to be computationally expensive [18], the direct use of large-scale, multiphase numerical models would be unrealistic in simulating the high volume of realizations needed for risk assessment and optimization.

The high computational cost associated with numerical models may be overcome by the use of data-based response surface methods (e.g. [5]). However, it is the authors' intent for the resulting framework to ultimately be used to optimize and compare large numbers of potential injection sites having vastly different domain characteristics. Creating and calibrating each potential injection site's numerical model, as well as training the resulting response surface would require user expertise and large investments of computational time. This work has therefore chosen to use a semi-analytical multiphase flow model presented by [41] and modified by [12] for multiphase subsurface flow simulation. The semi-analytical leakage algorithm is very general and can be applied to simplified computational models of the vast majority of potential injection sites.

An additional difficulty associated with preliminary GCS project planning is that potential storage reservoirs typically exhibit a high degree of uncertainty associated with physical parameters. Reference [8] identified abandoned (herein referred to as "passive") well permeabilities as the most dominant

uncertainty parameter when estimating fluid leakage due to GCS. In North America, significant numbers of passive wells may perforate the caprock in formations suitable for GCS [7,36,37]. Most likely, very little information exists on the location and/or sealing properties of these wells. However, several efforts have been made to investigate and account for the uncertainty associated with passive well permeability. References [56,57] developed a passive well integrity scoring index based upon typically available information (e.g. completion date, regulatory requirements, etc.). Reference [14] physically sampled and analyzed segments of a 30 yr. old passive well that had been continuously exposed to 96% CO_2 finding that cement interfaces are more important than the cement matrix when quantifying migration pathways.

Multiphase subsurface optimization problems are typically highly non-linear due to the irregular spatial location of preferential flow pathways and the multiphase flow (i.e. CO_2 and brine) equations governing pressure response and CO_2 plume migration. Therefore, a robust global optimization tool is needed to find best performing injection strategies that maximize the mass of CO_2 sequestered while minimizing project cost by selecting optimal injection well locations and injection rates. In multi-objective problems, a Pareto-optimal, or non-dominated, solution outperforms all other solutions with respect to all objectives [46] Multi-objective evolutionary algorithms (MOEAs) have been shown to be effective in providing Pareto-optimal solutions for a large number of subsurface flow applications possessing several decision variables [1,2,9,24,28,31,35,45,47,48,49,50,51,59]. In particular, [46] presents a comprehensive review of state-of-the-art MOEAs highlighting key algorithm advances which may be used to identify critical tradeoffs in water resources problems. A non-dominated sorting genetic algorithm (NSGA-II) [15] with ε-dominance [29] has been selected as the computational optimization tool because it is among the best performing multi-objective optimization evolutionary algorithms [10].

If computationally feasible, stochastic methods should be applied in cases where parameter uncertainty is of significant concern. A popular approach for accomplishing this is to apply a Monte Carlo (MC) method where simulation is performed for an ensemble of uncertain parameter sets to estimate the

statistics of optimization objectives and constraints. There are several examples in the literature where MOEAs are coupled with MC techniques to optimize groundwater problems having parameter uncertainty. A multi-objective groundwater flow optimization problem with aquifer hydraulic conductivity uncertainty is solved by [2] using an NPGA. Reference [1] used a MC-based Bayesian update scheme to approximate posterior uncertainty in hydraulic conductivity and head using an NSGA-II when performing multi-objective design of aquifer monitoring networks. A MC approach was also used by [31] when determining optimal remediation methods for groundwater aquifers having hydraulic conductivity uncertainty. MC techniques are also used to investigate parameter uncertainty associated with GCS [22,42,54,58]. In particular, reference [8] applied a stochastic Monte Carlo approach to estimate leakage risk associated with passive well permeability uncertainty. Reference [36] used a large-scale Monte Carlo method to explore the effects of caprock permeability uncertainty on fluid leakage estimation, finding that the amount of CO_2 leakage from GCS is typically acceptable for climate change mitigation.

Herein, several computational tools are integrated into a stochastic multi-objective optimization framework for the purpose of performing large-scale GCS site feasibility studies. These tools include 1) a semi-analytical leakage algorithm to rank the performance of trial injection strategies; 2) a Monte Carlo procedure to quantify risk resulting from parameter uncertainty; and 3) an NSGA-II with ε-dominance to heuristically determine Pareto-optimal solutions between competing objectives. We begin with a detailed description of the stochastic optimization methodology including an overview of both the semi-analytical CO_2 leakage algorithm and the NSGA-II with ε-dominance. Next, a general description and GCS-specific characterization of a saline aquifer situated within the Michigan Basin (MB) is presented. Following this is the formulation of the optimization case study at a MB test site The framework is then used to investigate the following three goals regarding the stochastic optimization of the MB site: 1) quantify the impact of decision maker (DM) preferences on heuristically determined Pareto-optimal

objective values (i.e. mass sequestered and project cost); 2) quantify the impact of DM preferences on carbon injection strategy (i.e. the selection of injection well flow rate and location), and; 3) assess the suitability of the MB test site for GCS. Finally, gains in computational efficiency using parallel processing and simulation archiving are discussed.

2 Methodology

2.1 Semi-Analytical CO_2 Leakage Estimation

While other semi-analytical algorithms provide insight regarding specific processes, this work has chosen to use a modified version of the ELSA (Estimating Leakage Semi-analytically) multiphase subsurface flow model [8, 12,41] because it is the only semi-analytical model able to simulate multiphase flow in domains having multiple injection wells, geological layers, and passive wells (i.e. weak caprock areas).

Figure 3.1 shows a schematic of the semi-analytical leakage model's computational domain. This domain is structured as a stack of L+1 caprock layers separated by L aquifers layers, perforated by M carbon injection wells and N passive wells. Aquifers are assumed to be horizontally level, homogenous, and isotropic. Caprock layers are assumed to be impermeable, except where perforated by passive wells. Injection wells are able to inject into any layer. Initially, fluid is not flowing through any of the passive wells because the entire domain is assumed to be saturated with brine at hydrostatic pressure. Additional assumptions made by this model include: a) aquifers exhibit horizontal flow; b) capillary pressure is negligible, resulting in a sharp CO_2-brine interface; c) CO_2 plume thickness at any given location is assumed to be the maximum plume thickness from all sources and sinks in the aquifer; d) pressure response from sources and sinks can be superimposed in each aquifer; and e) the injectivity of the formation remains constant. Several of these processes are important [11,13,16,20,21,25,27] and should be included [6,19,26,40] when accurate is more important that efficiency (e.g. final project design).

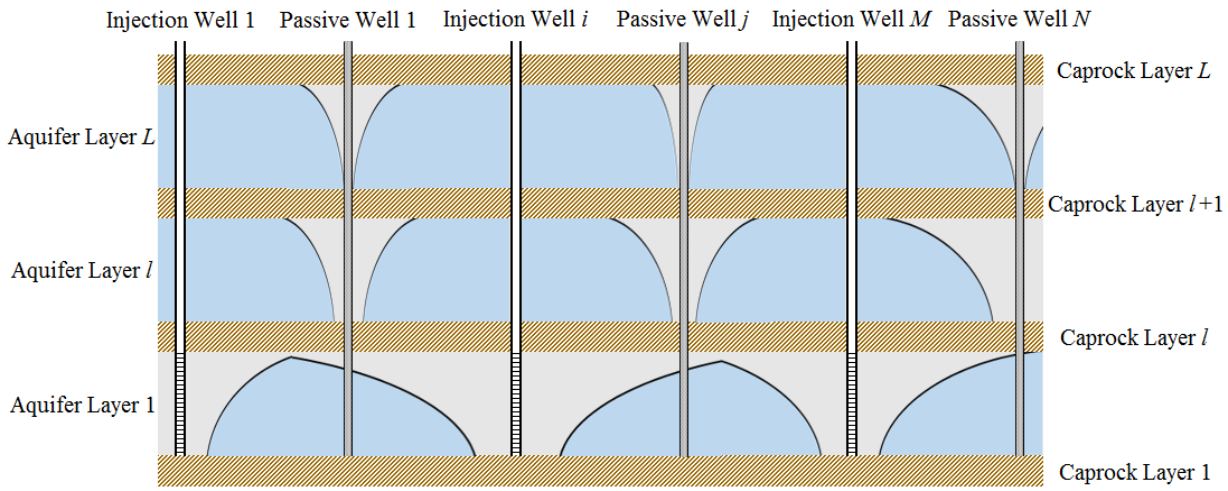

Figure 3.1. Schematic of the semi-analytical leakage model's computational domain

At the start of injection, aquifer fluid pressures throughout the domain begin to change resulting in pressure differentials across caprock layers and fluid flux through passive wells. It is therefore very important to understand aquifer fluid pressure response resulting from changes in the mass storage of CO_2 and brine. A pressure response function for the injection of CO_2 into a brine-filled confined aquifer was derived in [38]. Reference [8] expresses this radial pressure response p [$ML^{-1}T^{-2}$] at the bottom of the aquifer where a single well injects CO_2 as:

$$p = p_0 + (\rho_b - \rho_c) \cdot g \cdot H \cdot \Delta p' \tag{1}$$

where p_0 is the initial fluid pressures at the bottom of the aquifer, ρ_α is fluid density [ML^{-3}] (α denotes the phase type, b for brine and c for CO_2), g is gravitational acceleration [LT^{-2}] and H is aquifer thickness [T]. In Equation (1), $\Delta p'$ (/) is defined by:

$$\Delta p'(\chi) = \begin{cases} 0 & \text{for } \chi \geq \psi \\ -\frac{1}{2\Gamma}\ln\left(\frac{\chi}{\psi}\right) + \Delta p'(\psi) & \text{for } \psi > \chi \geq 2\lambda \\ \frac{1}{\Gamma} - \frac{\sqrt{\chi}}{\Gamma\sqrt{2\lambda}} + \Delta p'(2\lambda) + F(h') & \text{for } 2\lambda > \chi \geq \frac{2}{\lambda} \\ -\frac{1}{2\lambda\Gamma}\ln\left(\frac{\chi\lambda}{2}\right) + \Delta p'\left(\frac{2}{\lambda}\right) & \text{for } \frac{2}{\lambda} > \chi \end{cases} \quad (2)$$

where,

$$\chi = \frac{2\pi H\phi(1 - S_b^{res})r^2}{Q \cdot t} \quad (3)$$

$$\Gamma = \frac{2\pi(\rho_b - \rho_c)gkH^2}{\mu_b Q} \quad (4)$$

$$\psi = \frac{4.5\pi H\phi k(1 - S_b^{res})}{\mu_b c_{eff} Q} \quad (5)$$

$$h' = \frac{h(\chi)}{H} = \frac{1}{\lambda - 1}\left(\frac{\sqrt{2\lambda}}{\sqrt{\chi}} - 1\right) \quad (6)$$

$$F(h') = \frac{-\lambda}{\lambda - 1}\left[\mathrm{h}' - \frac{ln[(\lambda - 1)h' + 1]}{\lambda - 1}\right] \quad (7)$$

In Equations (2-7): B is aquitard thickness [/]; h is CO_2 plume thickness [L]; h' [/] is the CO_2 plume thickness relative to the aquifer thickness H; S_b^{res} is the residual saturation of the brine [/]; t is time [T]; k is the aquifer permeability [L^2]; μ is the dynamic viscosity [$ML^{-1}T^{-1}$]; ϕ is the aquifer porosity [/]; Q is the total volumetric well flux [L^3T^{-1}]; c_{eff} is the effective compressibility of the fluid and solid matrix [$M^{-1}LT^2$]; and r is the radial distance [L]. Also, $F(h')$ is an offset term related to the vertical pressure

distribution [8] and the mobility ratio is defined as $\lambda = \lambda_c/\lambda_b$, where $\lambda_\alpha = k_{r,\alpha}/\mu_\alpha$ and $k_{r,\alpha}$ is the relative permeability of phase α ($\alpha = b$ for brine or $\alpha = c$ for CO_2).

To determine the fluid overpressure at any given time throughout the aquifer system, [36] applies superposition of effects derived from the application of Equation (1) for all the volumetric sources and sinks corresponding to CO_2 injection wells and passive wells. Consequently, the fluid pressure at any given time t, at the bottom of the generic aquifer l (l=1,2,..,L) and for each passive well j (j=1,2,..,N) can be expressed as:

$$p_{j,l} = p_{0_l} + (\rho_b - \rho_c) \cdot g \cdot H_l \cdot \left[\sum_{iw=1}^{M} \Delta p'(\chi_{iw,j,l}) + \sum_{i=1}^{N} \Delta p'(\chi_{i,j,l}) \right] \quad (8)$$

where $\chi_{iw,j,l} = 2\pi H_l \phi_l \left(1 - S_{b,l}^{res}\right) r_{iw,j}^2 / \left(Q_{iw,l} \cdot t\right)$ and $\chi_{i,j,l} = 2\pi H_l \phi_l \left(1 - S_{b,l}^{res}\right) r_{i,j}^2 / \int_o^t \left(Q_{j,l} - Q_{j,l+1}\right) \cdot d\tau$ (see Equation (3)). By following this approach, the fluid pressures at the bottom of each aquifer and at each passive well can be grouped into the $N \times L$ vector $\mathbf{p}$:

$$\mathbf{p}(\mathrm{t}) = \mathbf{p}[\mathbf{P_1}, \mathbf{M}(\mathrm{t})] \quad (9)$$

Equation (9) shows that $\mathbf{p}(\mathrm{t})$ is a function of the array

$$\mathbf{P}_1 \equiv \left[\mathbf{H}, \boldsymbol{\phi}, \mathbf{k}, \boldsymbol{S}_b^{res}, \mathbf{r}, \mathbf{Q}_{iw}, \rho_c, \rho_b, g, \lambda, \pi, \mu_b, c_{eff}\right] \quad (10)$$

In Equation (10): the $L \times 1$ vectors $\mathbf{H}$, $\boldsymbol{\phi}$, $\boldsymbol{S}_b^{res}$ and $\mathbf{k}$ include the thicknesses, porosities, brine residual saturations and permeabilities of all aquifers; $\mathbf{Q}_{iw}$ is $M \times L$ vector including the CO_2 inflow rates for each

aquifer l (l=1,2,..,L) for injection well iw (iw=1,2,..,M); and the (M+N)×(M+N) **r** matrix includes the relative distances between injection and passive wells.

In addition, **p**(t) (Equation 9) is a function of the N×L vector **M**(t), whose generic component $M_{j,l}(t)$ represents the net cumulative fluid mass transferred into aquifer l through passive well j. This mass is calculated as:

$$M_{j,l}(t) = \int_0^t \rho_{eff,j,l}(\tau) \cdot \left[Q_{j,l}(\tau) - Q_{j,l+1}(\tau)\right] \cdot d\tau \tag{11}$$

where $\rho_{eff,j,l}(\tau)$ is the effective fluid density in aquifer l, at passive well j which is time-dependent since the leaking fluid composition is a function of the phase saturations of CO_2 and brine, which vary based on the CO_2 plume location. The effective fluid density is estimated as $\rho_{eff,j,l} = \rho_c \cdot S_{c\,j,l} + \rho_b \cdot \left(1 - S_{c\,j,l}\right)$.

Since application of Equation (9) requires knowing the temporal evolution of leakage rates through passive wells $Q_{j,l}$, [36] propose to use the sum of the flow rates, $Q_{\alpha\,j,l}$, for each phase α, calculated using the multiphase version of Darcy's law across each confining layer l for each passive well j:

$$Q_{j,l} = \sum_{\alpha=b,c} \left[\pi r_{pw\,j,l}^2 \frac{k_{r,\alpha\,j,l} k_{pw\,j,l}}{\mu_\alpha B_l} \left(p_{j,l-1} - \rho_\alpha g B_l - g\rho_\alpha H_{l-1} - p_{j,l}\right) \right] \tag{12}$$

In Equation (12), $r_{pw\,j,l}$ is the passive well radius and $k_{pw\,j,l}$ is the single phase passive well permeability for passive well j (j=1,2,..,N) and aquitard layer l. Note that in order to apply Equation (12), fluid pressures $p_{j,l}$ as well as CO_2 relative thicknesses in passive well pathways must be known to estimate

pressure gradients, fluid saturations and relative permeability values. Given Equation (12), the flow rates across each aquitard l (l=1,2,..,L) for each passive well j (j=1,2,..,N) can be can be grouped into the $N\times L$ vector $\mathbf{Q}$:

$$\mathbf{Q}(\mathrm{t}) = \mathbf{Q}[\mathbf{P_2}, \mathbf{p}(\mathrm{t})] \tag{13}$$

where the array $\mathbf{P}_2$ is given by:

$$\mathbf{P}_2 \equiv \left[\mathbf{B}, \mathbf{H}, \mathbf{r}_{pw}, \mathbf{k}_{pw}, \mathbf{k}_{r,c}, \mathbf{k}_{r,b}, \rho_c, \rho_b, \mu_c, \mu_b, g\right] \tag{14}$$

In Equation (14), the $(L+1)\times 1$ vector $\mathbf{B}$ includes the aquitard thicknesses, the $N\times(L+1)$ matrices $\mathbf{r}_{pw}$ and $\mathbf{k}_{pw}$ contain the passive well radii and permeabilities, and the $N\times(L+1)$ matrices $\mathbf{k}_{r,c}$ and $\mathbf{k}_{r,b}$ include the relative permeabilities of CO_2 and brine at passive wells.

By combining Equations (9) and (13), a set of $N\cdot L$ non-linear equations in $N\cdot L$ unknowns is obtained. These unknowns are the fluid pressures at the bottom of each aquifer and at each passive well (Equation 8), and the flow rates (Equation 12) across each aquitard for each passive well.

In an effort to increase computational efficiency, this work has chosen to neglect effects from upconing and apply the IGPS modification from [12] where a fixed point iteration scheme is applied to solve the system of non-linear equations introduced above at a generic time t given the solution at time t-Δt obtained at the previous time step. The resulting CO_2 leakage simulator is highly efficient, capable of simulating 50 years of injection into a domain with 100 passive wells and 4 aquifer/aquitard layers in less than 1 second on a standard laptop. Additional information regarding the implementation of the leakage

model, as well as modifications made to the original work presented by [8,39,41], are discussed in detail in [12].

2.2 Stochastic Multi-objective GCS Problem

For any given potential GCS reservoir, a set of Pareto-optimal injection scenarios exist which (a) maximize the deterministic mass of CO_2 injected, $Mass_{inj}$, and (b) minimize the stochastic project cost, C,:

$$\begin{aligned} objective\ (a): &\quad \max\{Mass_{inj}(\mathbf{Q})\} \\ objective\ (b): &\quad \min\{C(\mathbf{x}, \mathbf{Q}, \tilde{\mathbf{s}})\} \end{aligned} \tag{15}$$

In Equation (15), spatial position, **x**, and flow rate, **Q**, are the two decision variables comprising each injection strategy and $\tilde{\mathbf{s}}$ is the stochastic set of state variables (i.e. aquifer pressure distribution and CO_2 plume locations and thicknesses) dependent on each simulation's injection strategy and stochastically generated parameter set. $Mass_{inj}$ is simply the total mass of CO_2 injected into the domain during simulation, and is calculated by multiplying the sum of injection well flow rates by the injection duration, t_{inj}:

$$Mass_{inj} = \sum_{iw=1}^{M} Q_{c_{iw}} * t_{inj} \tag{16}$$

where M is the number of injection wells, and $Q_{c_{iw}}$ is the CO_2 mass injection rate for injection well iw.

In order to quantify the risk associated with passive well permeability uncertainty, an ensemble of N_{MC} parameter set realizations ($\mathbf{k}_{pw}^{(1)}$, $\mathbf{k}_{pw}^{(2)}$, … , $\mathbf{k}_{pw}^{(N_{MC})}$), with each having an equal probability of occurrence, is generated for each trial injection strategy. For each Monte Carlo (MC) realization, each passive well

segment is assigned either an "intact" (low) or "degraded" (high) [8,36] permeability value. This is accomplished using a simple bi-value probability distribution function (PDF). Passive well segments have a P_{intact} chance of being assigned an "intact" permeability value and a (1 - P_{intact}) chance of being assigned a "degraded" permeability value. The cost, $Cost_i$, associated with each MC realization, i (i = 1,2,…,N_{MC}), consists of the summation of each injection well's (iw) capital cost, *Cap*, operational cost, *OP*, surface maintenance cost, *SurM*, subsurface maintenance cost, *SubM*, and variable cost, *Var*, added to the cost associated with CO_2 leakage, *LC*:

$$Cost_i(\mathbf{Q}, Mass_{leak}) = \sum_{iw=1}^{M} \left[Cap_{iw} + OP_{iw}(t_{inj}) + SurM_{iw}(t_{inj}) + SubM_{iw}(t_{inj}) + Var_{iw}(Q_{iw}, t_{inj}) \right] + LC[Mass_{leak}(\mathbf{Q}, \mathbf{s}_i)] \quad (17)$$

where $\mathbf{s}_i$ is the set of state variables for each MC realization including the CO_2 saturation and total flow rate in each passive well segment. *LC* is estimated as:

$$LC[Mass_{leak}(\mathbf{Q}, \mathbf{s}_i)] = c_L \cdot Mass_{leak}(\mathbf{Q}, \mathbf{s}_i)^{r_A} \quad (18)$$

In Equation (18), c_L is the coefficient representing penalty cost per unit of CO_2 leakage ($/kg) and r_A is a risk adversity factor reflecting the preferences of the DM by exponentially increasing *LC* in relation to the mass of CO_2 leakage. The mass of CO_2 leakage (kg), $Mass_{leak}$, is quantified numerically using the semi-analytical leakage algorithm described in Section 2.1 as:

$$Mass_{leak}(\mathbf{Q}, \mathbf{s}_i) = \sum_{j=1}^{N} \int_0^{t_{inj}} \rho_c \cdot S_{c_{j,L}}^{(i)}(t) \cdot Q_{j,L}^{(i)}(t) \cdot dt \quad (19)$$

Empirical cumulative distribution functions (CDFs) of each injection strategy's MC **Cost** ($Cost_1$, $Cost_2$, … , $Cost_{N_{MC}}$) are then compiled by first sorting the **Cost** vector in ascending order from $i = 1 \ldots N_{MC}$, then assigning the non-exceedance probability of $Cost_i$ as $(i - 0.5)/N_{MC}$ [23]. The stochastic cost objective, $\tilde{C}$, is finally assigned as the z^{th} percentile value, P_z, of the sorted **Cost** vector:

$$C(\mathbf{x}, \mathbf{Q}, \tilde{\mathbf{s}}) = P_z(\mathbf{Cost}) \tag{20}$$

As discussed later in Section 4.1, larger N_{MC} values are needed to accurately quantify $\tilde{C}$ as z becomes farther from 50%. Several constraints are included in this problem. First, the number of injection wells is limited to a maximum integer value by constraining M to a value between 0 and M_{max}:

$$0 \leq M \leq M_{max} \tag{21}$$

All candidate injection wells must be located horizontally within prescribed minimum and maximum spatial bounds representing the areal extent selected for the construction of GCS faculties:

$$x_{min} \leq x_{iw} \leq x_{max} \; ; \; y_{min} \leq y_{iw} \leq y_{max} \; ; \; iw = 1, 2, .., M \tag{22}$$

Also, each injection well's flow rate must be between prescribed minimum and maximum flow rates Q_{min} and Q_{max}:

$$Q_{min} \leq Q_{iw} \leq Q_{max} \; ; \; iw = 1, 2, .., M \tag{23}$$

In Equation (23), Q_{min} and Q_{max} are physical constraints related to the technical capacity of injection pumps and wells. Finally, fluid pressures at each injection well in each layer, $p_{iw,l}$, must not exceed each layer's fracture pressure, p_{frac_l}.

$$p_{iw,l}(\mathbf{Q}, \tilde{\mathbf{s}}) < p_{frac_l}\ ;\ iw = 1, 2, .., M\ ; l = 1, 2, .., L \tag{24}$$

where p_{frac_l} is calculated by multiplying a specified fracture gradient [8,] by layer depth and $p_{iw,l}$ is estimated for each injection well *iw* at the end of the injection duration at a small effective distance from the injection location. The value for effective distance must be carefully selected as Equation (1) is very sensitive to radial distance when estimating pressure changes nearby the injection location, where a conservative estimate for this value would be the injection well's casing radius. Also, since the left-hand side of Equation (24) contains stochastic state variables, these stochastic constraints have to be transformed into deterministic. This is carried out using a chance-constraint approach [54] such that:

$$Prob\{p_{iw,l}(\mathbf{Q}, \tilde{\mathbf{s}}) < p_{frac_l}\} \geq S_P\ ;\ iw = 1, 2, .., M\ ; l = 1, 2, .., L \tag{25}$$

Equation (25) requires the probability that the fluid pressure at injection wells does not exceed the layer fracture pressure to be larger than or equal to a prescribed fracture safety probability, S_p.

2.3 Multi-objective GCS Optimization Algorithm

In order to solve the stochastic multi-objective optimization problem presented in Section 2.2, the semi-analytical CO_2 leakage algorithm (Section 2.1) and the Monte Carlo procedure (Section 2.2) are integrated into a NSGA-II with ε-dominance. Each trial injection strategy is encoded into a "chromosome" (i.e. a unique sequence of binary numbers representing the values of each decision variable). The first segment of the chromosome contains spatial location information for M_{max} injection

wells represented by N_{cl} predefined candidate injection well location indices, thus intrinsically satisfying the spatial location constraint defined by Equation (22). The number of digits required to represent each injection well's location is a function of the number of candidate locations, N_{cl}. For example, if N_{cl} = 16 for a potential GCS site, the locational information of each injection well for each injection strategy would require four binary digits (i.e. '0000' = 1, '0001' = 2, … , '1111'=16). In this case, the spatial data component of the chromosome has a length of $M{\cdot}4$. The last segment of the chromosome represents the injection rate index of each well. Injection rate indices represent N_{ir} prescribed discrete flow rate values within the constraints of Equation (23). For example, injection rate index values of 0, 1, 2, and 3 may represent injection rates of 0, 20, 30, and 40 kg/s, respectively (N_{ir} = 4). In this case, two binary digits would be used to encode each well's injection index ('00' = 0, '01' = 1, … , '11'=3) bringing the total chromosome length to $M{\cdot}4 + M{\cdot}2$.

The general procedure followed by the NSGA-II with ε-dominance is presented in Figure 3.2. Once input files containing domain characteristics and algorithm parameters are read, an initial population of N_{pop} trial injection scenarios, including the spatial location and flux rate for each injection well, is randomly generated. In step (b), objective function values are calculated for each population member and simulation archiving keeps a record of simulation results, preventing the NSGA-II from recalculating objective values for identical scenarios. As described in Section 2.2, an ensemble of parameter set realizations are generated for each trial injection strategy in step (c). After this, fitness values (i.e. an assessment of performance related to objective function values) are calculated for each injection strategy. The semi-analytical leakage algorithm is used to estimate $Mass_{leak}$ for each of these realizations in step (d), then objective values $Mass_{inj}$ and $\tilde{C}$ are calculated using Equations (16-20). Also in step (d), if Equation (25) is violated the injection strategy is deemed infeasible.

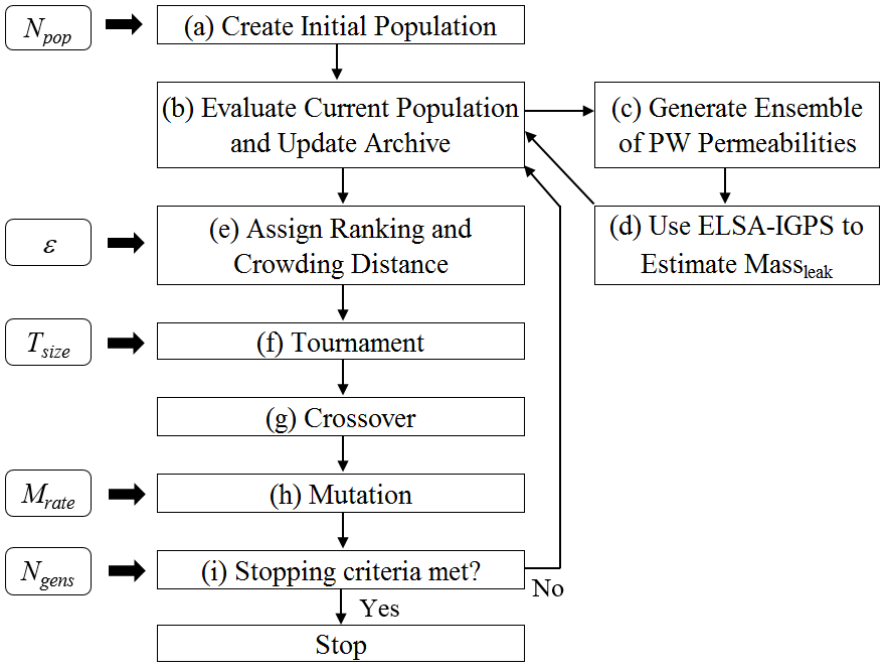

Figure 3.2. Schematic of the stochastic optimization algorithm

Next, the NSGA-II is used to generate new injection strategy populations of size N_{pop} using selection, crossover, and mutation operators. In step (e), population members are first ranked (i_{rank}) as the number of solutions dominating population member i using the fast-nondominated sorting procedure from [15] then assigned a crowding distance ($i_{distance}$) as the largest cuboid in objective space enclosing the point i without including any other point in the population [15]. A partial order is established using the crowding comparison operator, $\geq_n$ [15]. Population member i outperforms member j if the following conditions are met:

$$i \geq_n j \text{ IF } \{(i_{rank} < j_{rank}) \text{ OR } ((i_{rank} = j_{rank}) \text{ AND } (i_{distance} > j_{distance}))\} \quad (26)$$

The NSGA-II's ranking process is further improved with the concept of ε-dominance [29]. Suppose population members p_1 and p_2 have fitness values of f_1 and f_2, respectively. Using ε-dominance, p_1 is

allowed to dominate p_2 if $(1+\varepsilon)\cdot f_1$ is greater than or equal to f_2. ε-dominance allows for the inclusion of additional, well-performing population members to each rank's Pareto-optimal front.

Next, in step (f) an iterative tournament-style selection process is used to select parent injection strategies for the next generation. A subset of T_{size} population members is selected randomly and the population member with highest partial order according to Equation (26) is chosen as a parent. Once parents are selected, a crossover operator is used to create the new generation of population members in step (g). During each crossover operation, components of chromosomes from two randomly selected parents are used to build a new trial injection strategy. Crossover is repeated until the new population is filled. Finally, there is a chance, quantified as the mutation rate, M_{rate}, in which chromosome elements of this new population will be randomly altered during step (h). Steps (b-h) are repeated until the maximum prescribed number of generations, N_{gens}, is reached.

2.4 Efficient Computational Implementation

This framework utilizes parallel computing and simulation archiving to improve the computational efficiency. Due to the iterative nature of both evolutionary search and Monte Carlo analyses, large numbers of model simulations are needed for each stochastic optimization run. Without using simulation archiving, the total number of model calls required for each stochastic optimization run, N_{ct}, is equal to the product of N_{MC}, N_{pop}, and N_{gens}. CO_2 leakage estimation calculations for each trial injection strategy are independent and therefore may be processed in parallel (i.e. simultaneously) rather than sequentially by distributing processes on different computer cores.

A custom optimization program is created to apply both parallel processing and simulation archiving. An efficient, multi-tier archive lookup method is implemented. As results from new trial injection scenarios are received, the archive dataset continually remains sorted from smallest to largest based upon the sum

of each archived injection strategy's decision variable values. When the code is searching through the archive database to determine if an identical trial injection strategy had previously been evaluated, the code first looks for a match between the summations of decision variable values. If a match is found, the code checks to see if each decision variable is identical. The archive search process is stopped if either an identical set of decision variables is found or the remainder of archived injection scenarios have a larger decision variable value sum.

3 Characterization of the MB test site

The Michigan Basin (MB) is near the town of Thompsonville in northwest Michigan. Michigan Technological University's data library provides detailed subsurface data in this region. A cross-sectional schematic of the MB is provided in Figure 3.3, showing a nearly depleted hydrocarbon reservoir between depths of approximately 4660 and 5000 feet (1420-1520 meters) overlain by multiple confining and saline aquifer layers. This reservoir's only production well, Merit 1-20A, was originally drilled by the Shell Oil Company and is located between two exploration boreholes, Burch 1-20B and Stech 1-21A. This work explores the simulation and optimization of GCS into the saline Grey Niagaran formation immediately below the hydrocarbon reservoir.

The Burch 1-20B (Burch) and Stech 1-21A (Stech) boreholes have provided a wide variety of high resolution well logs that may be used to characterize subsurface domain properties such as density, porosity, electrical resistivity, compressional and shear wave velocities. For this analysis, we choose to use Neutron Porosity Hydrogen Index (NPHI) data gathered from the boreholes to estimate aquifer and caprock locations, thicknesses, and permeabilities. High NPHI values indicate relatively high permeability while regions exhibiting low NPHI values indicate low permeability caprock layers. Figure 3.4 shows NPHI versus depth for both the Burch and Stech boreholes. Aquifer (highlighted light blue) and caprock (highlighted brown) layers are then defined using this data. Derived formation thicknesses and depths shown in Figure 3.4 correspond with aggregated layer sets displayed in Figure 3.3.

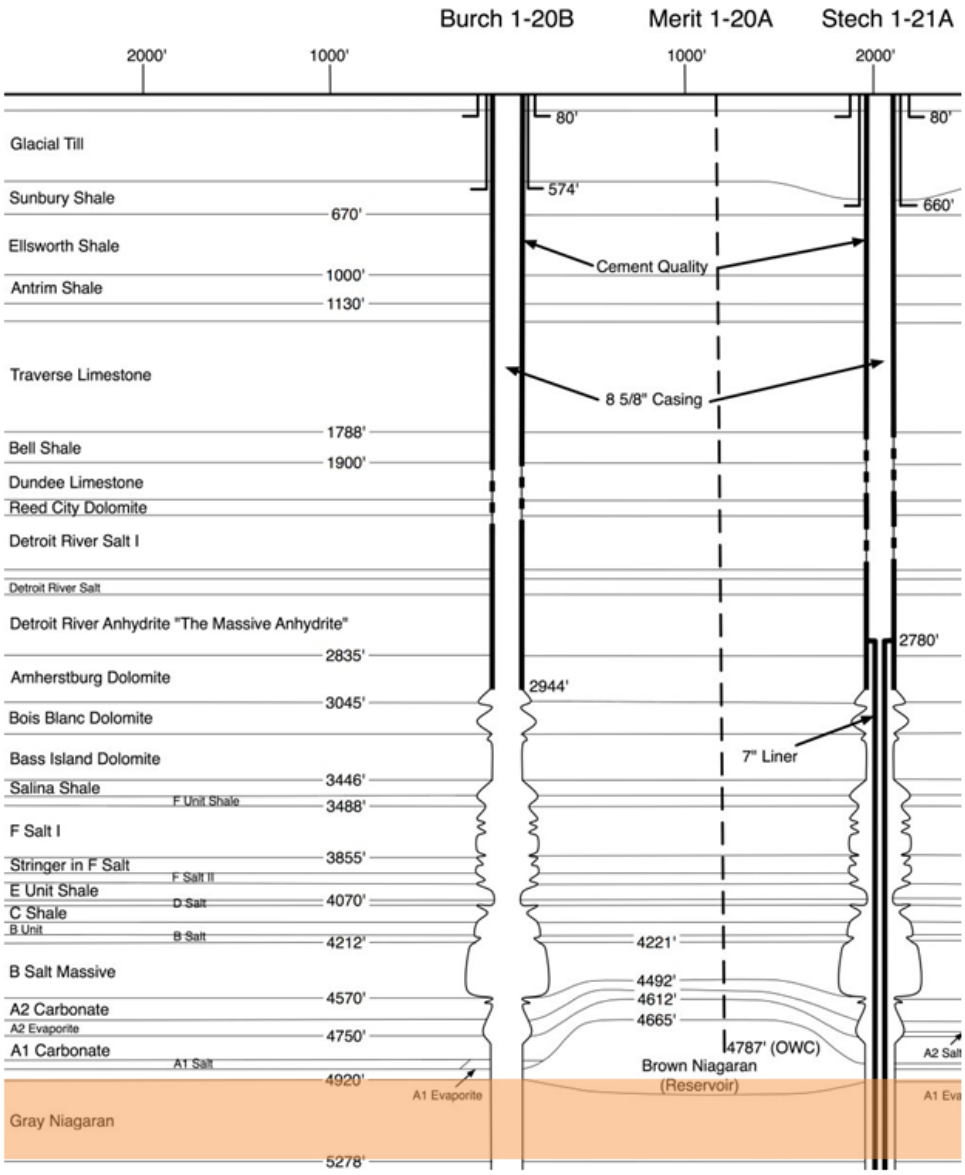

Figure 3.3. Cross-sectional schematic of the MB with the simulated injection layer highlighted orange (modified with permission from [53])

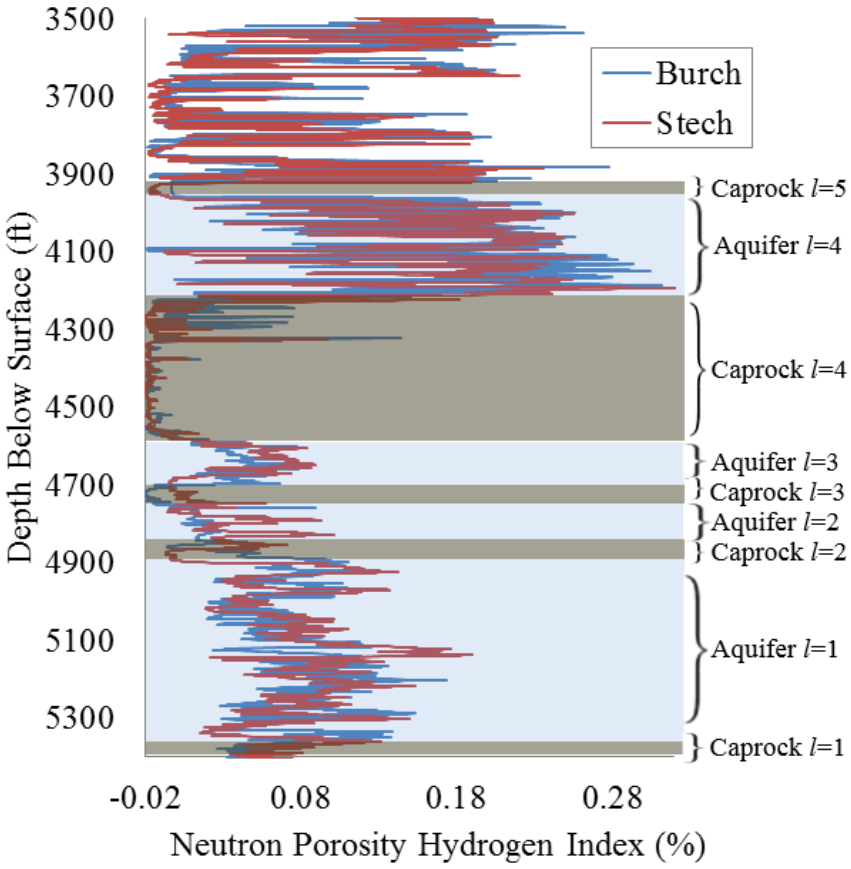

Figure 3.4. NPHI vs. Depth for the Burch 1-20B (Burch) and Stech 1-21A (Stech) boreholes. Light blue areas are defined as aquifers (A1 – A4) while brown areas are defined as confining units (C1 – C5).

Five derived aquitards and four interlaying aquifer layers (including the Grey Niagaran formation) are used in the computational model (L = 4). Caprock thicknesses are estimated to be 16.8, 18.3, and 109.1 m for layers 2, 3, and 4, respectively, while layers 1 and 5 are assumed to be completely impermeable even at passive well locations. Average aquifer permeability, k, in milliDarcys (mD; 1 mD ≅ 10^{-15} m^2) is estimated for all aquifer layers using the following from [52]:

$$k = \begin{cases} 2 \cdot e^{31.6 \cdot \phi} & if\ \phi < 0.124 \\ 4.94 \cdot 10^4 \cdot \phi^2 - 763 & if\ \phi \geq 0.124 \end{cases} \quad (27)$$

where, ϕ is assumed to equal NPHI. Table 3.1 shows the permeability, thickness, and porosity value for each aquifer layer obtained using the preceding methodology.

Table 3.1. Aquifer permeability, thickness, and porosity values used in this study

Parameter	Symbol	Value for Aquifer Layer *l*				Units
		$l = 1$	$l = 2$	$l = 3$	$l = 4$	
Permeability	k	24	4.5	6.7	655	mD
Thickness	H	119.5	35.1	36.6	75.3	m
Porosity	ϕ	0.079	0.026	0.038	0.169	/

The Michigan Department of Environmental Quality maintains a database of producing and inactive oil and gas wells in the state. Although 65,560 well records containing permit number, depth, and spatial coordinates are retrieved from the department's website [34], only 131 wells are located within 4 km of the reservoir's production well, Merit 1-20A, and intersect the four aquifer layers defined above.

A GCS test site is envisioned herein using MB data characterized above. Optimal injection rates and well locations are determined for a maximum of 3 injection wells (M_{max} = 3). Injection wells are allowed to operate at a constant injection rate of either $Q_1 = Q_{min} = 0$, $Q_2 = 20$, $Q_3 = 30$, or $Q_4 = Q_{max} = 40$ kg/s (N_{ir} = 4) over a 50-year duration (t_{inj} = 50 yrs.), thereby satisfying Equation (23). Injection well locations may be selected from 16 candidate locations uniformly distributed over a 1 km^2 square grid. Figure 3.5 provides a plan view of the MB site with candidate injection well locations (N_{cl} = 16) shown as orange circles and existing passive well locations (N = 131) shown as blue pluses. Horizontal positions are relative to the Merit 1-20 production well with $x_{min} = y_{min} = -500$ m and $x_{max} = y_{max} = 500$ m), thereby satisfying constraint Equation (22).

In Equation (19), $Mass_{leak}$ is defined as the cumulative mass of CO_2 that escapes into the top layer (l = 4) at the end of the 50-year injection duration. The radii, r_{pw}, used in Equation (12) is assumed to be 0.2 m for all 131 passive wells. A fracture safety probability of S_p = 95% is assumed for the pressure constraint

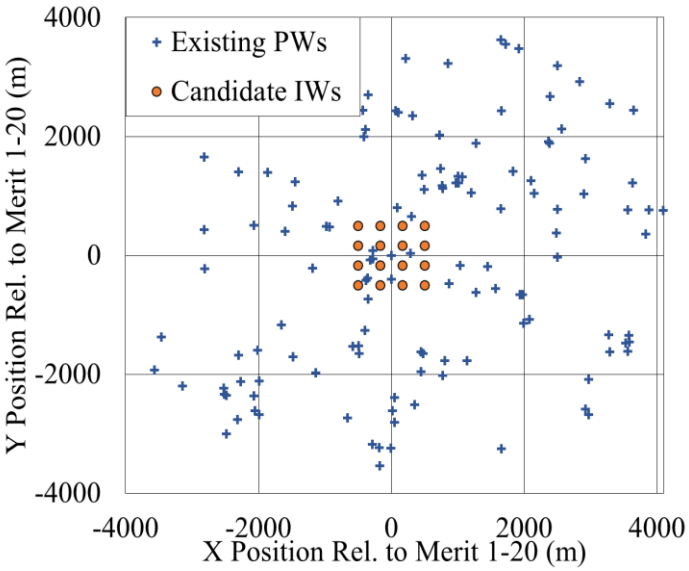

Figure 3.5. Plan view of the MB test site showing all PWs included in the study

(Equation (25)). Also a fracture gradient of 20.0 kPa/m, as used in [9] is used for the purposes of optimization and analysis, however the effects of using the more conservative fracture gradient of 14.2 kPa/m [43] are also considered. Table 3.2 lists additional deterministic hydrogeological parameter values used herein.

Table 3.2. Deterministic hydro-geological parameter symbols and values

Parameter	Symbol	Value	Units
Brine density	ρ_b	1,045	kg/m^3
CO_2 density	ρ_c	479	kg/m^3
Brine viscosity	μ_b	2.94x10^{-4}	Pa·s
CO_2 viscosity	μ_c	3.95x10^{-5}	Pa·s
Effective compressibility	c_{eff}	4.6x10^{-10}	m^2/N
Brine residual saturation	S_{res}	0.3	/

The costs associated with installation, operation, and maintenance [30] used for each candidate well location in this study are shown in Table 3.3. This preliminary analysis does not include costs involved

with site characterization, permitting, lease/purchase of land/pore space, financing, insurance, monitoring, verification, EPA financial bond requirement, post-injection site care, and long-term liabilities although these may be significant in the final financial assessment [30]. The leakage cost parameter c_L in Equation (18) is assigned a values of 0.6 $/kg.

Table 3.3. Cost parameter values for each candidate well location in Equation (17)

Capital Cost, *Cap* ($/well)	**Fixed O&M Cost, *OP* ($/day/well)**	**Surface Maintenance, *SurM* ($/yr/well)**	**Subsurface Maintenance, *SubM* ($/yr/well)**	**Variable Cost, *Var* ($/kg of CO_2)**
3,537,104	11,566	120,608	37,612	0.009

In this case study, passive well segment permeability is assumed to be the only uncertain variable. For each MC simulation, passive well segment permeabilities are randomly assigned as either 0.01 or 1000 mD, representing "intact" and "degraded" cement, respectively [8,13,36]. Table 3.4 shows the probability of each passive well segment being assigned an "intact" or "degraded" permeability value during the MC ensemble generation for each uncertainty scenario. Herein, three uncertainty scenarios are tested and compared including 1) data supporting an abundance of intact passive well segments (U1); 2) no available passive well permeability data (U2); and 3) data supporting an abundance of degraded passive well segments (U3). Passive well segment permeabilities are assumed to be fully uncorrelated (i.e. passive wells may have differing permeabilities at different depths).

4 Results and Discussion

4.1 NSGA-II Parameter Calibration

The number of Monte Carlo simulations, N_{MC}, generated and simulated for each trial injection strategy is determined from an analysis of the uncertainty scenario U3. U3 is assumed to be the worst case (i.e. most difficult to solve) optimization problem because it has the largest probability of degraded passive wells and, therefore, the greatest potential for CO_2 leakage. Both $P_{50\%}$(**Cost**) and $P_{95\%}$(**Cost**) (Equation (20))

Table 3.4. Probability of passive well segments being assigned either an "intact" or "degraded" permeability value for each uncertainty scenario.

Uncertainty Scenario	Description	Probability of being assigned an "intact" permeability value	Probability of being assigned a "degraded" permeability value
U1	Intact Passive Well Data	90%	10%
U2	No Passive Well Data	50%	50%
U3	Degraded Passive Well Data	10%	90%

are estimated for ten different injection strategies (N_{sims} = 10). For each of these simulations, the value of N_{MC} is ranged between 50 and 1000 in intervals of 50. An inspection of the results of this analysis shows that N_{MC} values of 200 and 400 produce convergence for $P_{50\%}$(**Cost**) and $P_{95\%}$(**Cost**), respectively. $P_{95\%}$(**Cost**) is further from the center of the CDF and thus requires a greater N_{MC} value for stabilization.

Optimal NSGA-II parameter values of N_{pop}, M_{rate}, T_{size}, and ε are selected from a series of preliminary tests using a deterministic optimization problem having 50% degraded and 50% intact passive well segments. A deterministic problem is used because it requires much less computational time for each simulation as there is no need for MC analysis. First, a single measure is established to quantify the performance of each NSGA-II parameter value set where the average project cost per unit mass sequestered ($/kg) over all non-dominated solutions is assumed to represent the fitness of any given Pareto set. Next, the true optimal Pareto set is found for the test deterministic optimization problem by performing three exhaustive evolutionary searches, each with 5,000 generations. Each of these arrived at the same average project cost per unit mass sequestered. Finally, the set of parameter values consistently requiring the least number of simulation calls to arrive within 0.1% of the minimal average project cost per unit mass sequestered found from exhaustive search are selected to be used by the stochastic optimization problem. Table 3.5 shows the NSGA-II parameter values and maximum number of optimization generations found using this analysis.

Table 3.5. NSGA-II parameter values and maximum number of optimization generations used for the stochastic case study

N_{pop}	M_{rate}	T_{size}	ε	N_{gens}
25	1.6%	2	0.001	200

A performance comparison between the NSGA-II and a random search algorithm is also performed to further validate the effectiveness of the NSGA-II used in this study. One hundred deterministic optimization trials having differing random number seeds are processed. The genetic algorithm is found to greatly outperform the random search algorithm. The percent of trials reaching 0.1% of the minimal project cost per unit mass sequestered in 200 generations is 100% for the NSGA-II compared to 0% for the random search algorithm. Results from this convergence test provide strong evidence that, for this problem, optimal or close-to-optimal Pareto sets are found using the algorithmic parameter set shown in Table 3.5.

4.2 Stochastic Optimization Analysis

Three goals regarding the stochastic optimization of the MB site are investigated and discussed within this section: 1) quantify the impact of DM preferences on heuristically determined Pareto-optimal objective values (i.e. mass sequestered and project cost); 2) quantify the impact of DM preferences on carbon injection strategy (i.e. the selection of injection well flow rate and location), and; 3) assess the suitability of the MB test site for GCS. To accomplish this, results from several optimization test cases having differing DM preference values, including the selection of risk adversity factor, r_A, (Equation (18)), stochastic non-exceedance cost probability, z, (Equation (20)), and passive well uncertainty scenario (Table 3.4), are compared and discussed. Twelve stochastic optimization cases are performed for the MB test site data described in Section 3. The risk adversity factor, r_A, is set to either 1.0 or 1.2 while the stochastic non-exceedance cost probability, z, is set to either 50% or 95% for each of the three possible passive well uncertainty scenarios (U1, U2, U3), hence obtaining a total of $2 \cdot 2 \cdot 3 = 12$

combinations of DM preference selections. Table 3.6 shows DM preferences for each of these stochastic optimization cases (i.e. cases C1-C12).

Table 3.6. DM preferences for each of the 12 stochastic optimization runs (C1-C12)

Stochastic Optimization Case	Risk Adversity Factor, r_A	Passive Well Uncertainty Scenario	Stochastic non-exceedance cost probability, z
C1	1.0	U1	50%
C2			95%
C3		U2	50%
C4			95%
C5		U3	50%
C6			95%
C7	1.2	U1	50%
C8			95%
C9		U2	50%
C10			95%
C11		U3	50%
C12			95%

4.2.1 Impact of DM Preferences on Objective Function Values

The first step in investigating relationships between DM preferences and objective function values is to determine Pareto-optimal (or close-to-optimal) tradeoff sets for each stochastic optimization case described in Table 3.6 using the methodology presented in Section 2. The quantity of total mass sequestered (Equation (16)) is a function of the injection duration, t_{inj}, the maximum number of injection wells, M_{max}, as well as the number, N_{ir}, and flow rates, $\mathbf{Q}$, of prescribed injection rates. Because values for these three variables are prescribed before the start of optimization, all possible values of the total mass sequestered objective function are known. Recall from Section 3 that each injection well may only assume an injection rate of either 0, 20, 30, or 40 kg/s. Because of this, there are only 11 possible non-zero, discrete values of total mass sequestered when M_{max} = 3 and t_{inj} = 50 yrs., as the total injection rate for all three wells may range between 20 and 120 kg/s in increments of 10 kg/s.

A visual representation of resulting Pareto sets is provided in Figure 3.6, where project cost versus mass of CO_2 sequestered are displayed for each of the 12 optimization cases described in Table 3.6. Subpanels in Figure 3.6 plot the objective function tradeoff curve associated each uncertainty scenario (i.e. U1, U2, and U3) for given values of r_A and z. Capital, operation and maintenance (CO&M) costs, defined herein as all project costs other than the penalties incurred from CO_2 leakage, are also plotted. Also, while all plotted Pareto-optimal solutions are valid using a fracture constraint of 20.0 kPa/m, only those solutions represented by solid markers are feasible when the fracture gradient is set to 14.2 kPa/m. Note that, due to higher project costs, a larger scale is used on the ordinate axis when r_A = 1.2.

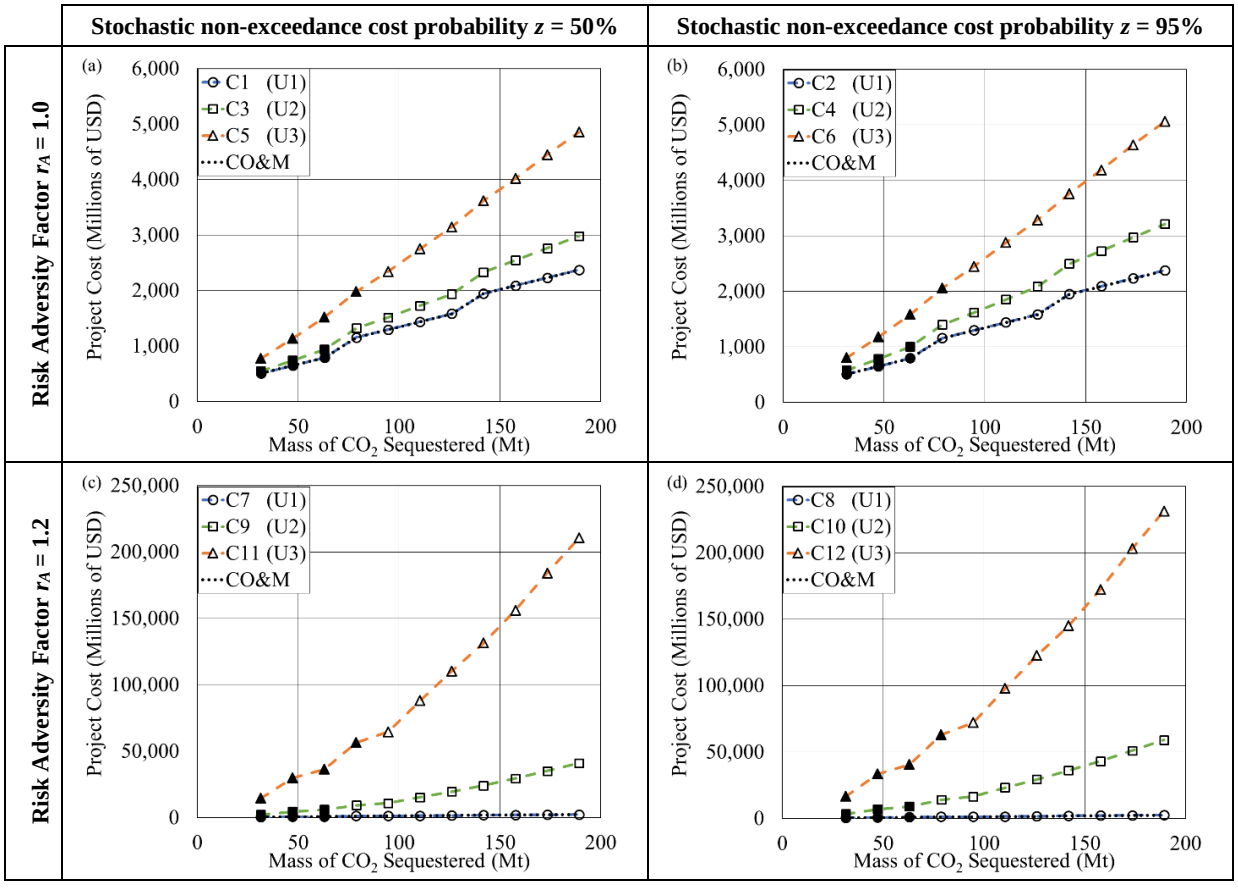

Figure 3.6. Optimal project costs in millions of USD versus mass of CO_2 sequestered for the 12 optimization runs described in Table 3.6. While all discrete solutions are valid using the 20.0 kPa/m fracture gradient, solid markers denote feasible solutions when assuming the lower fracture gradient of 14.2 kPa/m.

The choice of fracture gradient is found to significantly reduce the quantity of feasible objective tradeoff solutions shown in Figure 3.6. Only 30.3% of total tradeoff solutions for all test cases remain valid when assuming a 14.2 kPa/m fracture gradient. Tradeoff solutions for only the three lowest values of mass of CO_2 sequestered remain valid for uncertainty scenarios U1 and U2. The fourth lowest value of mass of CO_2 sequestered also remains valid for U3 because this uncertainty scenario has a greater quantity of degraded wells, thus allowing for more fluid pressure release from the injection layer. These observations indicate that the choice of fracture gradient significantly affects optimization results and should, therefore, be accurately estimated for each injection layer when applying this framework.

A general trend exhibited by these tradeoff profiles shows that project cost increases with the mass of CO_2 sequestered in all optimization runs. Two sharper increases in capital project cost are observed in CO&M costs when r_A = 1.0 (Figure 3.6, subpanels (a-b)) because, due to the maximum prescribed injection rate, additional injection wells are needed when sequestering more than 63.1 or 126.1 Mt of CO_2. While increases in injection well capital costs are also incurred when r_A = 1.2 (Figure 3.6, subpanels (c-d)), they are completely overshadowed by much larger total project costs.

In this work, DM risk adversity preference, r_A, is quantified through an exponential term when estimating leakage cost (Equation (18)) and therefore does not affect the estimated mass of CO_2 leakage. However, as seen in optimization cases C9-C12, when the estimated mass of CO_2 leakage is high, r_A is found to have a profound effect on project cost. While all optimization cases under uncertainty scenario U1 (90% probability of any passive well being assigned as intact) exhibit very little CO_2 leakage, substantial CO_2 leakage masses are estimated for test cases assigned U2 (50% probability of any passive well being assigned as intact) and U3 (10% probability of any passive well being assigned as intact) uncertainty scenarios, resulting in very large leakage costs when r_A = 1.2.

The selection of uncertainty scenario (Table 3.4) represents a DM's knowledge of the GCS site's caprock integrity. Uncertainty scenario selection directly impacts the estimated mass of CO_2 leakage and, therefore, indirectly affects the estimated cost associated with CO_2 leakage. Cases assigned uncertainty scenarios having greater percentages of intact well segments are found to exhibit less CO_2 leakage. All optimization cases assigned U1 uncertainty scenarios exhibit fairly negligible CO_2 leakage costs as their minimized total project costs are very similar to CO&M costs. In contrast, cases assigned U3 uncertainty scenarios are found to have much more leakage cost than corresponding cases with U2 uncertainty scenarios especially when $r_A = 1.2$.

Finally, the choice of stochastic non-exceedance cost probability, *z*, affects the estimated cost associated with CO_2 leakage because greater project costs are required to increase non-exceedance probability. Data shown in Figure 3.6 suggest that the value chosen for *z* has a minor impact on resulting Pareto-optimal objective function values, thus indicating that spread of each **Cost** CDF is relatively contained. Estimated project costs increase when a greater value of *z* is used. However, the project cost variability associated with stochastic non-exceedance cost probability is much smaller than the project cost variability associated with risk adversity or uncertainty scenario selection.

4.2.2 Impact of DM Preferences on Injection Strategy Selection

The impact of DM preferences upon the heuristic selection of optimal injection locations and flow rates is also investigated. Figure 3.7 displays a close-up, plan view of the MB test site showing the 16 candidate injection well location indices.

As explained in Section 4.2.1, there are 11 possible mass sequestered values for each of the 12 optimization cases. Therefore, a total of 12·11=132 Pareto optimal injection strategies are found using the NSGA-II. As a general presentation of decision variable results, Table 3.7 shows both candidate well

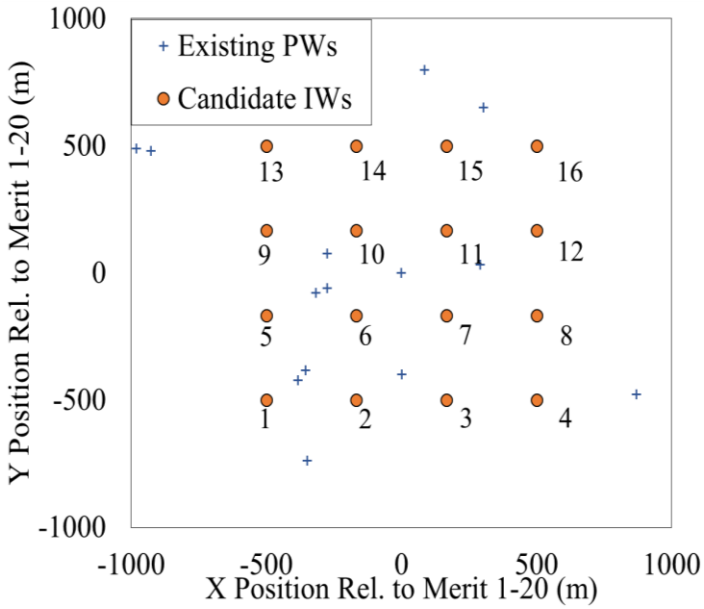

Figure 3.7. Close-up plan view of the MB test site showing candidate injection well location indices.

location indices (see Figure 3.7) and injection rates in kg/s for each injection strategy. While injection strategies eliminated when using the lower fracture gradient of 14.2 kPa/m are highlighted grey, all injection strategies shown in Table 3.7 are feasible when assuming a fracture gradient of 20.0 kPa/m and are therefore used in the following analyses. Note that injection strategies may use multiple injection wells.

Using the data presented in Table 3.7, two quantitative analyses are performed to study how DM preferences ultimately influence the heuristic selection of carbon injection strategies. First, the relative sensitivity of carbon injection strategy selection in relation to each DM parameter (i.e. r_A, z, and uncertainty scenario) is quantified as the percentage of injection well rate/location combinations that change when varying each DM preference. These percentages are calculated as the sum of differing injection well rate/location combinations divided by the total number of injection well rate/location combinations in each comparison set. Optimization cases having all but one identical DM preferences are individually compared. When contrasting r_A (r_A=1.0 with r_A =1.2) a set of six injection strategy comparisons are made; stochastic optimization cases C1-C6 are thus compared with cases C7-C12,

Table 3.7. Candidate well location indices from Figure 3.7 and injection rates for each injection. Injection strategies eliminated by using the lower fracture gradient of 14.2 kPa/m are highlighted grey.

Stochastic Optimization Run Index	*Mass Sequestered (MT)*										
	31.5	***47.3***	***63.1***	***78.8***	***94.6***	***110.4***	***126.1***	***141.9***	***157.7***	***173.4***	***189.2***
	Injection Strategy Selection [*Location(Injection Rate)*]										
C1	1(20)	1(30)	1(40)	9(20) 13(30)	9(30) 13(30)	1(40) 2(30)	1(40) 5(40)	1(30) 2(30) 5(30)	1(30) 5(40) 6(30)	1(40) 2(30) 5(40)	1(40) 2(40) 6(40)
C2	1(20)	1(30)	1(40)	1(30) 5(20)	1(30) 5(30)	1(40) 5(30)	1(40) 5(40)	1(30) 2(30) 5(30)	1(40) 2(30) 5(30)	1(40) 2(30) 5(40)	1(40) 2(40) 5(40)
C3	1(20)	1(30)	1(40)	1(30) 5(20)	1(30) 5(30)	1(40) 5(30)	1(40) 5(40)	1(30) 2(30) 5(30)	1(40) 2(30) 5(30)	1(40) 2(30) 5(40)	1(40) 5(40) 9(40)
C4	1(20)	1(30)	1(40)	1(30) 5(20)	1(30) 2(30)	1(40) 2(30)	1(40) 5(40)	1(30) 2(30) 5(30)	1(40) 2(30) 5(30)	1(40) 2(30) 5(40)	1(40) 2(40) 5(40)
C5	1(20)	1(30)	1(40)	1(30) 2(20)	1(30) 2(30)	1(40) 2(30)	1(40) 5(40)	1(30) 2(30) 5(30)	1(40) 2(30) 5(30)	1(40) 5(40) 9(30)	1(40) 2(40) 5(40)
C6	1(20)	1(30)	1(40)	1(30) 2(20)	1(30) 2(30)	1(40) 2(30)	1(40) 2(40)	1(30) 2(30) 5(30)	1(40) 2(30) 5(30)	1(40) 2(30) 5(40)	1(40) 2(40) 5(40)
C7	1(20)	1(30)	1(40)	9(20) 13(30)	9(30) 13(30)	1(40) 2(30)	1(40) 5(40)	1(30) 2(30) 5(30)	1(40) 5(30) 9(30)	5(30) 9(40) 13(40)	1(40) 2(40) 5(40)
C8	1(20)	1(30)	1(40)	9(20) 13(30)	1(30) 5(30)	1(40) 5(30)	1(40) 5(40)	1(30) 2(30) 5(30)	1(40) 2(30) 5(30)	1(40) 2(30) 5(40)	1(40) 2(40) 5(40)
C9	1(20)	1(30)	1(40)	1(30) 5(20)	1(20) 2(20) 5(20)	1(30) 2(20) 5(20)	1(30) 2(20) 5(30)	1(30) 2(30) 5(30)	1(40) 2(30) 5(30)	1(40) 2(30) 5(40)	1(40) 2(40) 5(40)
C10	1(20)	1(30)	1(40)	1(30) 5(20)	1(20) 2(20) 5(20)	1(30) 2(20) 5(20)	1(30) 2(20) 5(30)	1(30) 2(30) 5(30)	1(40) 2(30) 5(30)	1(40) 2(30) 5(40)	1(40) 2(40) 5(40)
C11	1(20)	1(30)	1(40)	1(30) 2(20)	1(20) 2(20) 5(20)	1(30) 2(20) 5(20)	1(30) 2(30) 5(20)	1(30) 2(30) 5(30)	1(40) 2(30) 5(30)	1(40) 2(30) 5(40)	1(40) 2(40) 5(40)
C12	1(20)	1(30)	1(40)	1(30) 2(20)	1(20) 2(20) 5(20)	1(30) 2(20) 5(20)	1(30) 2(20) 5(30)	1(30) 2(30) 5(30)	1(40) 2(30) 5(30)	1(40) 2(30) 5(40)	1(40) 2(40) 5(40)

respectively. Six injection strategy comparisons are also made when contrasting z (z=50% with z=95%); case C1 with case C7, case C2 with case C8, case C3 with case C9, case C4 with case C10, case C5 with case C11, and case C6 with case C12. A set of 12 injection strategy comparisons are made when

contrasting uncertainty scenario (U1 with U2, U2 with U3, and U3 with U1); cases C1-C2 are compared with cases C3-C4, respectively, cases C7-C8 are compared with cases C9-C10, respectively, cases C3-C4 are compared with cases C5-C6, respectively, cases C9-C10 are compared with cases C11-C12, respectively, cases C5-C6 are compared with cases C1-C2, respectively, and cases C11-C12 are compared with cases C7-C8, respectively. The percentage of injection strategies that remain constant in both location and injection rate when varying values of r_A, uncertainty scenario, and values of z is quantified as 72.2%, 75.5%, and 87.9%, respectively. These findings are used to augment the following discussion.

Secondly, a categorical distribution analysis is used to identify general injection strategy trends associated with DM preferences. The number of times each candidate location is selected for injection well placement is counted for all cases having each given DM preference value. For example, candidate location 1 is found to be selected for well placement 64 times when r_A=1.0 (i.e. for cases C1-C6), 38 times when assuming uncertainty scenario U1 (i.e. for cases C1, C2, C7, and C8) and 61 times when z=50% (i.e. for cases C1, C3, C5, C7, C9, and C11). Table 3.8 provides the number of selections of each candidate injection location for each DM preference value.

Table 3.8. Number selections for each candidate well location index. Indices having zero selections are not shown.

Candidate Location	***Risk Adversity Factor, r_A***		***Passive Well Uncertainty Scenario***			***Stochastic non-exceedance cost probability, z***	
	1.0	***1.2***	***U1***	***U2***	***U3***	***50%***	***95%***
1	64	62	38	44	44	61	65
2	31	39	15	23	32	32	38
5	35	44	24	32	23	38	41
6	2	0	2	0	0	2	0
9	4	5	7	1	1	8	1
13	2	4	6	0	0	5	1
Total	*138*	*154*	*92*	*100*	*100*	*146*	*146*

From the results shown in Table 3.8, the southwest corner of the candidate injection well field is heavily favored by the optimization algorithm, regardless of parameter choice, with 94.2% of all injection well placements being made at either candidate location 1, 2, or 5. This is due to the presence of a passive well cluster approximately 1000 meters northeast of the candidate injection well field (see Figure 3.5). Also, the furthest southwest candidate injection well location is found to have a substantially greater number of selections than all other individual locations. Approximately 41.2% of all injection well placements being made at candidate location 1, compared with 24.0% and 27.1% for candidate location 2 and 5, respectively.

DM risk adversity is found to have the greatest effect on injection strategy selection as only 72.2% of injection strategy selections remain constant when varying values of r_A (see second and third columns of Table 3.8). Also, increasing r_A from 1.0 to 1.2 is found to increase the total number of candidate well location selections from 138 to 154. This increased number in total candidate well location selections is caused by the optimization algorithm attempting to reduce CO_2 leakage cost by using additional injection wells to spread out and reduce the injection induced pressure distribution. For example, a total injection rate of 40 kg/s may be achieved by one well injecting at 40 kg/s or by two each injecting at 20 kg/s. This finding suggests that the leakage penalty savings from diversifying the injection well field are greater in certain cases than the additional CO&M costs incurred from installing, operating, and maintaining more injection wells.

Passive well uncertainty scenario selection, also having a low percentage (75.5%) of injection strategy selections remaining constant, is found to significant affect injection strategy selection (see fourth to sixth columns of Table 3.8). The total number of candidate well location selections is found to increase from 92 for uncertainty scenario U1 to 100 for the more expensive uncertainty scenario U2, further validating the trend found when studying risk adversity. Also, greater estimated CO_2 leakage, as in the case of uncertainty scenarios U2 and U3, is clearly observed to drive candidate injection well location selections

further southwest. The likelihood of selecting the three furthest southwest candidate locations (i.e. locational indices 1, 2, and 5) increases from 83.7% in cases assigned uncertainty scenario U1 to 99.0% in cases assigned either uncertainty scenario U2 or U3.

While stochastic non-exceedance cost probability, *z*, is found to have the highest percentage (87.9%) of injection strategy selections remaining constant and, therefore, has the least effect on injection strategy selection, trends are still observed when examining results shown in the seventh and eighth columns of Table 3.8. As with uncertainty scenario selection, increases in estimated CO_2 leakage (e.g. increasing *z* from 50% to 95%) are also found to drive candidate injection well location selections further southwest when studying the stochastic non-exceedance cost probability. The likelihood of selecting candidate locations 1, 2, and 5 increased from 89.7% in cases assigned $z = 50\%$ to 98.6% in cases assigned $z = 95\%$.

4.2.3 GCS Suitability Assessment for the MB test site

The final decision of whether or not to proceed with GCS project planning will be made by the DM. This choice will ultimately be made by assessing a large number of political and financial indicators. However, the preliminary stochastic cost assessment presented above suggests that GCS feasibility at the MB test site is highly dependent upon the DM's risk adversity preference. Figure 3.6 shows that all three uncertainty scenarios produce feasible project cost results if the DM selects $r_A = 1.0$, although a U3 uncertainty scenario is predicted to be about twice as expensive as the U1 uncertainty scenario due to its higher CO_2 leakage cost penalties from a greater percentage of degraded passive well segments. If the DM decides to select $r_A = 1.2$, U1 is the only uncertainty scenario providing feasible project cost results due to high CO_2 leakage costs resulting from the exponential leakage cost term, r_A.

4.3 Computational Efficiency

It is interesting to note that the complete enumeration of this problem when using N_{MC} = 400 would require 17,817,600 simulation calls:

$$N_{MC} \cdot N_{ir}^{M_{max}} \cdot \sum_{i=1}^{M_{max}} \binom{N_{cl}}{i} = 400 \cdot 4^3 \cdot \left[\frac{16!}{1! \cdot 15!} + \frac{16!}{2! \cdot 14!} + \frac{16!}{3! \cdot 13!}\right] = 17{,}817{,}600 \quad (28)$$

Assuming that a numerical model would require two hours per simulation, the CPU time required to sequentially process 17,817,600 CO_2 leakage evaluations without archiving would be approximately 4,068 years. However, a semi-analytical algorithm and an NSGA-II optimization approach is used for this problem. For the NSGA-II optimization parameters provided in Table 3.5, each optimization run requires either 1,000,000 or 2,000,000 simulation model calls, N_{ct}, to estimate CO_2 leakage without archiving, depending if N_{MC} = 200 or 400, respectively (e.g. $N_{ct} = N_{MC} \cdot N_{pop} \cdot N_{gens}$ = 400·25·200 = 2,000,000). Assuming that each semi-analytical simulation requires 1 second, the CPU time required to sequentially process 2 million CO_2 leakage evaluations without archiving would be 23.2 days. The computational time required for this problem may also be reduced using parallel processing and archiving. For example, if 25 computer processor cores are available, setting the number of parallel processes to N_{pop} will reduce this theoretical simulation evaluation time by 96% to 0.93 days. The actual CPU time required for a single optimization run with N_{MC} = 400, N_{pop} = 25, and N_{gens} = 200 using 12 processor cores and employing both parallel processing and simulation archiving is approximately 1.04 days, or about six orders of magnitude less than the theoretical time required for the complete enumeration of this problem using a numerical model.

5 Conclusions

A stochastic methodology for determining optimal GCS injection strategies has been presented, where a semi-analytical CO_2 leakage algorithm and a Monte Carlo procedure were integrated into a NSGA-II with ε-dominance. In an effort to show the applicability of this method to real world potential injection sites,

the stochastic optimization framework has been used to assess a hypothetical GCS project at a MB test site in northern Michigan, USA. The following three goals were investigated regarding the stochastic optimization of the MB site: 1) quantify the impact of DM preferences on heuristically determined Pareto-optimal objective values (i.e. mass sequestered and project cost); 2) quantify the impact of DM preferences on carbon injection strategy (i.e. the selection of injection well flow rate and location), and; 3) assess the suitability of the MB test site for GCS. This was accomplished by analyzing twelve MB test site stochastic optimization cases having differing DM preferences. DM preferences were varied as follows: the risk adversity factor, r_A, was set to either 1.0 or 1.2 while the stochastic non-exceedance cost probability, z, was set to either 50% or 95% for each of three possible passive well uncertainty scenarios (i.e. U1 where any passive well had a 90% probability of being assigned as intact, U2 where any passive well had a 50% probability of being assigned as intact, and U3 where any passive well had a 10% probability of being assigned as intact).

The choice of fracture gradient was found to significantly impact optimization results, with only 30.3% of the total tradeoff solutions remaining valid when assuming a 14.2 kPa/m (as opposed to 20.0 kPa/m) fracture gradient. Also, DM risk adversity preference, r_A was found to have a profound effect on project cost when the estimated mass of CO_2 leakage was high. While all optimization cases assigned a U1 uncertainty scenario exhibited very little CO_2 leakage, substantial CO_2 leakage masses were estimated for test cases assigned U2 and U3 uncertainty scenarios, resulting in very large leakage costs when $r_A = 1.2$. Uncertainty scenarios having greater percentages of intact well segments were found to exhibit less CO_2 leakage. All optimization cases assigned a U1 uncertainty scenario exhibited fairly negligible CO_2 leakage costs, as their minimized total project costs were found to be very similar to CO&M costs. Cases assigned U3 uncertainty scenarios were found to have much more leakage cost than corresponding cases assigned U2 uncertainty scenarios especially when $r_A = 1.2$. The choice of stochastic non-exceedance cost probability, z, had only a minor impact on resulting Pareto-optimal objective function values, thus indicating that **Cost** vectors were typically relatively uniform.

The southwest corner of the candidate injection well field was heavily favored by the optimization algorithm, regardless of parameter choice, with 94.2% of all injection well placements being made at the three furthest southwest candidate locations. DM risk adversity was found to have the greatest effect on injection strategy selection. Increasing r_A from 1.0 to 1.2 was found to increase the total number of candidate well location selections from 138 to 154. This finding suggests that the leakage penalty savings from diversifying the injection well field were greater in certain cases than the additional project costs incurred from installing, operating, and maintaining more injection wells. Passive well uncertainty scenario selection was also found to significant affect injection strategy selection where greater estimated CO_2 leakage, as in the case of uncertainty scenarios U2 and U3, was clearly observed to drive candidate injection well location selections further southwest. Stochastic non-exceedance cost probability, *z*, was estimated to have the least effect on injection strategy selection. However, as with uncertainty scenario selection, increases in estimated CO_2 leakage from a greater values of *z* were found to drive candidate injection well location selections further southwest.

This work also discussed large gains in computational efficiency using semi-analytical modeling, NSGA-II optimization, parallel computing, and simulation archiving. The actual CPU time required for a single optimization run with N_{MC} = 400, N_{pop} = 25, and N_{gens} = 200 using 12 processor cores and employing both parallel processing and simulation archiving was approximately 1.04 days, or about six orders of magnitude less than the theoretical time required for the complete enumeration of this problem using a numerical model. In addition, further gains in computational efficiency may also be obtained by processing each trial injection strategy's MC ensemble in parallel using large processing core clusters. This may lead to the ability to use a more computational expensive, thus more accurate, leakage algorithm, increase the number of model calls per optimization run, or process greater quantities of potential injection sites.

The final decision of whether or not to proceed with GCS project planning within the MB will be made by the decision maker (DM). While this choice should ultimately be made by assessing a large number of political and financial indicators, the preliminary stochastic cost assessment presented herein suggested that GCS feasibility at the MB test site is highly dependent on the DM's risk adversity preference. All three uncertainty scenarios produce feasible project cost results if the DM selects $r_A = 1.0$, while U1 was the only uncertainty scenario providing feasible project cost results when selecting $r_A = 1.2$ due to high CO_2 leakage costs resulting from this exponential leakage cost term.

Because of the large set of assumptions made by the semi-analytical CO_2 leakage algorithm, this framework may only be used for initial site planning and characterization. After 'coarse scale' project planning has been completed using this stochastic optimization framework, more rigorous, although slower, numerical models should be used for final project development of individual potential injection sites. However, this tool has potential for initial carbon sequestration project planning and performing initial screening and ranking of large sets of potential carbon sequestration sites.

REFERENCES

1. Alzraiee, A.H., Bau, D.A., Garcia, L.A.: Multiobjective design of aquifer monitoring networks for optimal spatial prediction and geostatistical parameter estimation. Water Resour. Res. 49, 3670–3684 (2013).
2. Baú, D.A.: Planning of Groundwater Supply Systems Subject to Uncertainty Using Stochastic Flow Reduced Models and Multi-Objective Evolutionary Optimization. Water Resour. Manag. 26, 2513–2536 (2012).
3. Birkholzer, J.T., Cihan, A., Zhou, Q.: Impact-driven pressure management via targeted brine extraction—Conceptual studies of CO2 storage in saline formations. Int. J. Greenh. Gas Control. 7, 168–180 (2012).
4. Bossie-Codreanu, D., Le Gallo, Y.: A simulation method for the rapid screening of potential depleted oil reservoirs for CO2 sequestration. Energy. 29, 1347–1359 (2004).
5. Box, G., Draper, N.: Response surfaces, mixtures, and ridge analyses. (2007).
6. Buscheck, T.A., Sun, Y., Chen, M., Hao, Y., Wolery, T.J., Bourcier, W.L., Court, B., Celia, M.A., Julio Friedmann, S., Aines, R.D.: Active CO2 reservoir management for carbon storage: Analysis of operational strategies to relieve pressure buildup and improve injectivity. Int. J. Greenh. Gas Control. 6, 230–245 (2012).
7. Celia, M.A., Nordbotten, J.M., Bachu, S., Dobossy, M., Court, B.: Risk of Leakage versus Depth of Injection in Geological Storage. Energy Procedia. 1, 2573–2580 (2009).
8. Celia, M.A., Nordbotten, J.M., Court, B., Dobossy, M., Bachu, S.: Field-scale application of a semi-analytical model for estimation of CO2 and brine leakage along old wells. Int. J. Greenh. Gas Control. 5, 257–269 (2011).
9. Chen, L., McPhee, J., Yeh, W.W.-G.: A diversified multiobjective GA for optimizing reservoir rule curves. Adv. Water Resour. 30, 1082–1093 (2007).
10. Cheng, Y., Jin, Y., Hu, J.: Adaptive epsilon non-dominated sorting multi-objective evolutionary optimization and its application in shortest path problem. ICCAS-SICE, 2009. 2545–2549 (2009).
11. Cihan, A., Birkholzer, J.T., Zhou, Q.: Pressure buildup and brine migration during CO2 storage in multilayered aquifers. Ground Water. 51, 252–67 (2013).
12. Cody, B.M., Baú, D.A., González-Nicolás, A.: Improved Semi-Analytical Simulation of Geological Carbon Sequestration. *In press* (2014)
13. Court, B., Bandilla, K.W., Celia, M.A., Janzen, A., Dobossy, M., Nordbotten, J.M.: Applicability of vertical-equilibrium and sharp-interface assumptions in CO2 sequestration modeling. Int. J. Greenh. Gas Control. 10, 134–147 (2012).

14. Crow, W., Brian Williams, D., William Carey, J., Celia, M., Gasda, S.: Wellbore integrity analysis of a natural CO2 producer. Energy Procedia. 1, 3561–3569 (2009).
15. Deb, K., Agrawal, S.: A fast elitist non-dominated sorting genetic algorithm for multi-objective optimization: NSGA-II. Proc. Parallel Probl. Solving from Nat. VI. 849–858 (2000).
16. Doster, F., Nordbotten, J.M., Celia, M.A.: Impact of capillary hysteresis and trapping on vertically integrated models for CO2 storage. Adv. Water Resour. 62, 465–474 (2013).
17. Eccles, J.K., Pratson, L., Newell, R.G., Jackson, R.B.: The impact of geologic variability on capacity and cost estimates for storing CO2 in deep-saline aquifers. Energy Econ. 34, 1569–1579 (2012).
18. Espinet, A.J., Shoemaker, C.A.: Comparison of optimization algorithms for parameter estimation of multi-phase flow models with application to geological carbon sequestration. Adv. Water Resour. 54, 133–148 (2013).
19. Gasda, S.E., Nordbotten, J.M., Celia, M.A.: Vertical equilibrium with sub-scale analytical methods for geological CO2 sequestration. Comput. Geosci. 13, 469–481 (2009).
20. Gasda, S.E., Nordbotten, J.M., Celia, M.A.: The impact of local-scale processes on large-scale CO2 migration and immobilization. Energy Procedia. 4, 3896–3903 (2011).
21. Gasda, S.E., Nordbotten, J.M., Celia, M.A.: Application of simplified models to CO2 migration and immobilization in large-scale geological systems. Int. J. Greenh. Gas Control. 9, 72–84 (2012).
22. Goda, T., Sato, K.: Optimization of well placement for geological sequestration of carbon dioxide using adaptive evolutionary Monte Carlo algorithm. Energy Procedia. 4, 4275–4282 (2011).
23. Hahn, G.J., and Shapiro, S.S.: Statistical Models in Engineering. John Wiley, New York (1967).
24. Hansen, A.K., Hendricks Franssen, H.-J., Bauer-Gottwein, P., Madsen, H., Rosbjerg, D., Kaiser, H.-P.: Well Field Management Using Multi-Objective Optimization. Water Resour. Manag. 27, 629–648 (2013).
25. Heße, F., Prykhodko, V., Attinger, S.: Assessing the validity of a lower-dimensional representation of fractures for numerical and analytical investigations. Adv. Water Resour. 56, 35–48 (2013).
26. Huang, X., Bandilla, K.W., Celia, M.A., Bachu, S.: Basin-scale modeling of CO2 storage using models of varying complexity. Int. J. Greenh. Gas Control. 20, 73–86 (2014).
27. Juanes, R., MacMinn, C.W., Szulczewski, M.L.: The Footprint of the CO2 Plume during Carbon Dioxide Storage in Saline Aquifers: Storage Efficiency for Capillary Trapping at the Basin Scale. Transp. Porous Media. 82, 19–30 (2009).

28. Kumphon, B.: Genetic Algorithms for Multi-objective Optimization: Application to a Multi-reservoir System in the Chi River Basin, Thailand. Water Resour. Manag. 27, 4369–4378 (2013).
29. Laumanns, M., Thiele, L., Deb, K., Zitzler, E.: Combining convergence and diversity in evolutionary multiobjective optimization. Evol. Comput. 10, 263–82 (2002).
30. Lepinski, J.: RE: Questions regarding geological sequestration costs. Message to author. 25 September 2012. Email. (2012)
31. Mantoglou, A., Kourakos, G.: Optimal Groundwater Remediation Under Uncertainty Using Multi-objective Optimization. Water Resour. Manag. 21, 835–847 (2006).
32. The MathWorks, Inc.: MATLAB and Statistics Toolbox Release 2012b. Natick, Massachusetts, United States (2012).
33. McPhee, J., Yeh, W.W.-G.: Multiobjective Optimization for Sustainable Groundwater Management in Semiarid Regions. J. Water Resour. Plan. Manag. 130, 490–497 (2004).
34. Michigan Department of Environmental Quality Oil and Gas Database. http://www.michigan.gov/deq/0,4561,7-135-6132_6828-98518--,00.html (2014) Accessed 08 March 2014
35. Nicklow, J., Reed, P., Savic, D.: State of the art for genetic algorithms and beyond in water resources planning and management. J. Water Resour. Plan. Manag. 412–432 (2010).
36. Nogues, J., Dobossy, M.: A methodology to estimate maximum probable leakage along old wells in a geological sequestration operation. Int. J. Greenh. Gas Control. 7, 39–47 (2012).
37. Nordbotten, J., Celia M., Geological Storage of CO2, Wiley, 2012.
38. Nordbotten, J., Celia, M.: Semianalytical solution for CO2 leakage through an abandoned well. Environ. Sci. Technol. 39, 602–611 (2005).
39. Nordbotten, J., Celia, M., Bachu, S.: Analytical solutions for leakage rates through abandoned wells. Water Resour. Res. 40, 1–10 (2004).
40. Nordbotten, J., Flemisch, B.: Uncertainties in practical simulation of CO2 storage. Int. J. Greenh. Gas Control. 9, 234–242 (2012).
41. Nordbotten, J., Kavetski, D., Celia, M., Bachu, S.: Model for CO2 leakage including multiple geological layers and multiple leaky wells. Environ. Sci. Technol. 43, 743–749 (2009).

42. Oladyshkin, S., Class, H., Helmig, R., Nowak, W.: An integrative approach to robust design and probabilistic risk assessment for CO2 storage in geological formations. Comput. Geosci. 15, 565–577 (2011).
43. Oldenburg, C.M., Jordan, P.D., Nicot, J.-P., Mazzoldi, A., Gupta, A.K., Bryant, S.L.: Leakage risk assessment of the In Salah CO2 storage project: Applying the certification framework in a dynamic context. Energy Procedia. 4, 4154–4161 (2011).
44. Pacala, S., Socolow, R.: Stabilization wedges: solving the climate problem for the next 50 years with current technologies. Science. 305, 968–972 (2004).
45. Peralta, R.C., Forghani, A., Fayad, H.: Multiobjective genetic algorithm conjunctive use optimization for production, cost, and energy with dynamic return flow. J. Hydrol. (2014).
46. Reed, P.M., Hadka, D., Herman, J.D., Kasprzyk, J.R., Kollat, J.B.: Evolutionary multiobjective optimization in water resources: The past, present, and future. Adv. Water Resour. 51, 438–456 (2013).
47. Reed, P.M., Kollat, J.B.: Visual analytics clarify the scalability and effectiveness of massively parallel many-objective optimization: A groundwater monitoring design example. Adv. Water Resour. 56, 1–13 (2013).
48. Singh, A.: Simulation and optimization modeling for the management of groundwater resources. I: Distinct applications. J. Irrig. Drain. Eng. 1–10 (2013).
49. Singh, A.: Simulation and Optimization Modeling for the Management of Groundwater Resources. II: Combined Applications. J. Irrig. Drain. Eng. 1–9 (2014).
50. Singh, T.S., Chakrabarty, D.: Multi-objective optimization for optimal groundwater remediation design and management systems. Geosci. J. 14, 87–97 (2010).
51. Tabari, M.M.R., Soltani, J.: Multi-Objective Optimal Model for Conjunctive Use Management Using SGAs and NSGA-II Models. Water Resour. Manag. 27, 37–53 (2012).
52. Trebin, F.A.: Oil Permeability of Sandstone Reservoirs. Gostoptekhizdat, Moscow (1945).
53. Turpening, R.M., Toksöz, M.N., Born, A.E., et al.: Reservoir Delineation Consortium Annual Report, Massachusetts Institute of Technology, Cambridge (1992).
54. Wagner, B., Gorelick, S.: Optimal groundwater quality management under parameter uncertainty. Water Resour. Res. 23, 1162–1174 (1987).

55. Walter, L., Binning, P., Oladyshkin, S.: Brine migration resulting from CO2 injection into saline aquifers–An approach to risk estimation including various levels of uncertainty. Int. J. Greenh. Gas Control. 9, 495–506 (2012).
56. Watson, T., Bachu, S.: Identification of wells with high CO2-leakage potential in mature oil fields developed for CO2-enhanced oil recovery. SPE Symp. Improv. Oil Recover. SPE, (2008).
57. Watson, T., Bachu, S.: Evaluation of the potential for gas and CO2 leakage along wellbores. SPE Drill. Complet. SPE, (2009).
58. Wriedt, J., Deo, M., Han, W.S., Lepinski, J.: A methodology for quantifying risk and likelihood of failure for carbon dioxide injection into deep saline reservoirs. Int. J. Greenh. Gas Control. 20, 196–211 (2014).
59. Zheng, F., Zecchin, A.: An efficient decomposition and dual-stage multi-objective optimization method for water distribution systems with multiple supply sources. Environ. Model. Softw. 55, 143–155 (2014).

CHAPTER IV: PERFORMANCE COMPARISON BETWEEN A MULTI-OBJECTIVE GRAVITATIONAL SEARCH ALGORITHM AND NSGA-II FOR INJECTION STRATEGY OPTIMIZATION OF GEOLOGICAL CO_2 SEQUESTRATION

Summary Geological carbon sequestration (GCS) has been proposed as a technology to mitigate CO_2 emissions from fossil fuels while cleaner, more sustainable energy production methods are developed. However, the global trend of increasing atmospheric concentrations of carbon dioxide (CO_2) will only be addressed through large scale, international efforts. Hence, it is important to select the most efficient optimization algorithm available to address the immense scale of the GCS problem. This work presents a performance comparison between a recently proposed multi-objective gravitational search algorithm (MOGSA) and the well-established fast non-dominated sorting genetic algorithm (NSGA-II) for the optimization of GCS. Both techniques are used to heuristically determine Pareto-optimal solutions by minimizing project cost and maximizing mass of CO_2 sequestered for nine test cases in the Michigan Basin (MB). Two performance measures are explored for each algorithm, including 1) objective solution diversity and 2) objective solution convergence rate. Substantially faster convergence rates by the MOGSA were observed early in the majority of test optimization runs, while the NSGA-II was found to provide a better search of objective function space as well as lower average project cost per unit mass sequestered solutions.

1 Introduction

The global trend of increasing atmospheric concentrations of carbon dioxide (CO_2) will only be addressed through large scale, international efforts [34,38]. Geological carbon sequestration (GCS) has been proposed as a technology to mitigate CO_2 emissions from fossil fuels while cleaner, more sustainable energy production methods are developed. With total annual global anthropogenic carbon emissions measured in mass of CO_2 at approximately 30,000 million tonnes (Mt) in 2008 [34], the success of GCS will be dependent upon the scale at which it is applied. Hence, it is important to select an efficient optimization algorithm to sufficiently address the immense scale of the GCS problem.

In multi-objective problems, a Pareto-optimal, or non-dominated, solution outperforms all other solutions with respect to all objectives [41]. Multi-objective evolutionary algorithms (MOEAs) have been shown to effectively find optimal or close-to-optimal Pareto-optimal solution sets for a large number of subsurface flow applications possessing several decision variables [1,2,6,21,27,31,33,39,42,44,45,46,47,50]. Reference [41] presents a comprehensive review of state-of-the-art MOEAs highlighting key algorithm advances, which may be used to identify critical tradeoffs in water resources problems.

A stochastic optimization method using a fast non-dominated sorting genetic algorithm (NSGA-II) for the purposes of preliminary GCS site assessment has been presented by [10] where mass of CO_2 sequestered is maximized while project cost is minimized by selecting optimal injection well locations and injection rates. The NSGA-II [12] with ε-dominance [28] was selected as the computational optimization tool in [10] because it was found by [7] to be among the best performing multi-objective optimization evolutionary algorithms. While the current literature does not contain any other examples of NSGA-II being used for GCS optimization, a large amount of research has been performed using the NSGA-II to assist water resources management. The optimization of conjunctive management of surface and groundwater resources using both a NSGA-II and sequential genetic algorithms (SGA) was performed by [47] where the NSGA-II was found to considerably reduce the computational burden in comparison to the SGA. Also, [19] used an NSGA-II for a multi-objective cost analysis for the removal of VOCs from water by pervaporation. Finally, uncertainty analysis of water supply networks was studied by [20] where the NSGA-II was found to improve the process of network fuzzy analysis.

Reference [40] recently proposed a novel heuristic optimization method, namely the gravitational search algorithm (GSA), inspired by Newtonian laws of gravity. Reference [40] also compared the GSA to particle swarm optimization (PSO), a real genetic algorithm (RGA), and central force optimization (CFO), finding that the GSA provided superior results in most cases and comparable results in all other

cases. While the GSA has not been applied to subsurface optimization problems, it has been applied to a number of non-linear engineering applications, with several studies reporting favorable results when comparing the GSA to other heuristic search algorithms. Reference [4] found the GSA to exhibit better performance in terms of final fitness values and computational efficiency when compared against a modified PSO algorithm to minimize sidelobe levels in concentric ring array antenna design. Reference [30] studied parameter identification of a hydraulic turbine governing system finding their improved GSA to be more accurate and efficient than both genetic and particle swarm algorithms. References [14] and [15] used the GSA to solve large scale electrical power control problems while a slope stability analysis was performed using a modified GSA by [26].

In addition, several versions of multi-objective GSAs (MOGSA) have been presented. Reference [22] proposed and compared a MOGSA with a multi-objective genetic algorithm (MOGA), Pareto-archived evolution strategy (PAES), and multi-objective particle swarm optimization (MOPSO) finding the MOGSA to outperform all the other methods. A MOGSA has also been proposed and tested by [43] and was found to outperform almost 20 other heuristic algorithms when optimizing a routing and wavelength assignment problem.

This work compares the performance of the NSGA-II to the MOGSA using a deterministic version of the GCS optimization framework presented by [10]. We begin with an explanation of the multi-objective GCS problem followed by a description of the methodology of the optimization framework, including an overview of the semi-analytical CO_2 leakage algorithm, NSGA-II, and MOGSA. Next, a characterization of the Michigan Basin (MB) test site and the formulation of nine hypothetical GCS test cases are described. Finally, we compare performance results for each algorithm and conclude with a discussion of advantages and limitations of each heuristic optimization method.

2 Methodology

The GCS injection strategy optimization framework is an assembly of an optimization algorithm (i.e. either an NSGA-II or MOGSA) linked to a semi-analytical CO_2 leakage algorithm. New sets of trial injection strategies are generated by either the NSGA-II or MOGSA to heuristically determine Pareto-optimal solutions between two competing objectives where both optimization algorithms call on the semi-analytical CO_2 leakage algorithm to quantify CO_2 leakage mass for each trial injection strategy during the ranking process.

2.1 Semi-Analytical CO_2 Leakage Estimation

A modified version of the Estimating Leakage Semi-Analytically (ELSA) Algorithm [5,9,37] is chosen to estimate the mass of CO_2 leakage resulting from each injection strategy since it is the only semi-analytical model able to simulate multiphase flow in domains having multiple layers, injection wells, and weak caprock areas (i.e. passive wells). Figure 4.1 shows a schematic of the semi-analytical leakage model's computational domain. The subsurface domain is structured as a horizontal stack of aquifer/aquitard layers perforated by injection and passive wells. Users of this algorithm are able to specify the number and spatial location of injection wells, passive wells, and aquifer/aquitard layers. Passive wells are the only pathways for fluid flux between aquifer layers and are represented by cylindrical portions of the aquitard layers having non-negligible permeability values.

This CO_2 leakage simulator is highly efficient, capable of simulating 50 years of CO_2 injection into a domain having 100 passive wells and 4 aquifer layers in less than 1 second on a standard laptop. However, several assumptions must be made to achieve this level of computational efficiency. Aquifers are assumed to be horizontally level, homogenous, and isotropic. Aquitards are assumed to be impermeable, except where perforated by passive wells. Injection wells are able to inject into any layer.

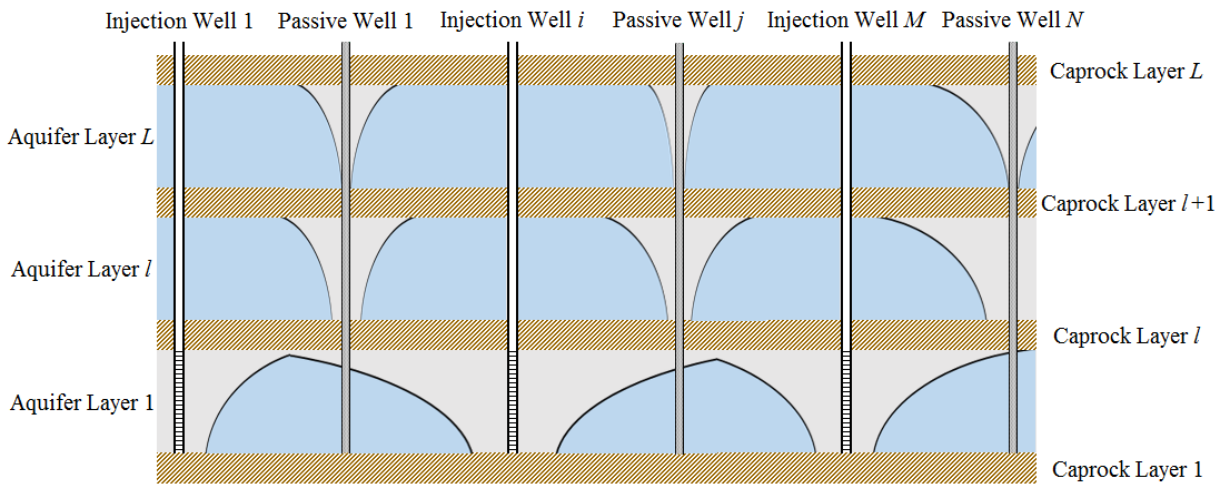

Figure 4.1. Schematic of the semi-analytical leakage model's computational domain from [10]

Initially, fluid is not flowing through any of the passive wells because the entire domain is assumed to be saturated with brine at hydrostatic pressure. Additional assumptions made by this model include: 1) Aquifers exhibit horizontal flow; 2) Capillary pressure is negligible resulting in a sharp fluid interface; 3) CO_2 plume thickness at any given location is assumed to be the maximum plume thickness from all sources and sinks in the aquifer; 4) Pressure response from sources and sinks are superimposed in each aquifer; and 5) the injectivity of the formation remains constant. The radial pressure response p [$ML^{-1}T^{-2}$] at the bottom of the aquifer where a single well injects CO_2 is expressed as [5]:

$$p = p_0 + (\rho_b - \rho_c) \cdot g \cdot H \cdot \Delta p' \quad (1)$$

where p_0 is the initial fluid pressures at the bottom of the aquifer, ρ_α is fluid density [ML^{-3}] (α denotes the phase type, b for brine and c for CO_2), g is gravitational acceleration [LT^{-2}] and H is aquifer thickness [T] and $\Delta p'$ (/) is defined by:

$$\Delta p'(\chi) = \begin{cases} 0 & \text{for } \chi \geq \psi \\ -\frac{1}{2\Gamma}\ln\left(\frac{\chi}{\psi}\right) + \Delta p'(\psi) & \text{for } \psi > \chi \geq 2\lambda \\ \frac{1}{\Gamma} - \frac{\sqrt{\chi}}{\Gamma\sqrt{2\lambda}} + \Delta p'(2\lambda) + F(h') & \text{for } 2\lambda > \chi \geq \frac{2}{\lambda} \\ -\frac{1}{2\lambda\Gamma}\ln\left(\frac{\chi\lambda}{2}\right) + \Delta p'\left(\frac{2}{\lambda}\right) & \text{for } \frac{2}{\lambda} > \chi \end{cases} \quad (2)$$

where,

$$\chi = \frac{2\pi H\phi(1 - S_b^{res})r^2}{Q \cdot t} \quad (3)$$

$$\Gamma = \frac{2\pi(\rho_b - \rho_c)gkH^2}{\mu_b Q} \quad (4)$$

$$\psi = \frac{4.5\pi H\phi k(1 - S_b^{res})}{\mu_b c_{eff} Q} \quad (5)$$

$$h' = \frac{h(\chi)}{H} = \frac{1}{\lambda - 1}\left(\frac{\sqrt{2\lambda}}{\sqrt{\chi}} - 1\right) \quad (6)$$

$$F(h') = \frac{-\lambda}{\lambda - 1}\left[\mathrm{h}' - \frac{ln[(\lambda - 1)h' + 1]}{\lambda - 1}\right] \quad (7)$$

where B is aquitard thickness [/]; h is CO_2 plume thickness [L]; h' [/] is the CO_2 plume thickness relative to the aquifer thickness H; S_b^{res} is the residual saturation of the brine [/]; t is time [T]; k is the aquifer permeability [L^2]; μ is the dynamic viscosity [$ML^{-1}T^{-1}$]; ϕ is the aquifer porosity [/]; Q is the total volumetric well flux [L^3T^{-1}]; c_{eff} is the effective compressibility of the fluid and solid matrix [$M^{-1}LT^2$]; and r is the radial distance [L]. Also, $F(h')$ is an offset term related to the vertical pressure distribution [5]

and the mobility ratio is defined as $\lambda = \lambda_c/\lambda_b$, where $\lambda_\alpha = k_{r,\alpha}/\mu_\alpha$ and $k_{r,\alpha}$ is the relative permeability of phase α ($\alpha = b$ for brine or $\alpha = c$ for CO_2).

Superposition is applied to determine the fluid overpressure throughout the aquifer system resulting in the following definition of fluid pressure at any given time *t*, at the bottom of the generic aquifer *l* (*l*=1,2,..,*L*) and for each passive well *j* (*j*=1,2,..,*N*):

$$p_{j,l} = p_{0_l} + (\rho_b - \rho_c) \cdot g \cdot H_l \cdot \left[\sum_{iw=1}^{M} \Delta p'(\chi_{iw,j,l}) + \sum_{i=1}^{N} \Delta p'(\chi_{i,j,l}) \right] \quad (8)$$

where $\chi_{iw,j,l} = 2\pi H_l \phi_l (1 - S_{b,l}^{res}) r_{iw,j}^2 / (Q_{iw,l} \cdot t)$ and $\chi_{i,j,l} = 2\pi H_l \phi_l (1 - S_{b,l}^{res}) r_{i,j}^2 / \int_o^t (Q_{j,l} - Q_{j,l+1}) \cdot d\tau$. A vector, **p,** of the fluid pressures at the bottom of each aquifer with size *N*×*L* may then be assembled:

$$\mathbf{p}(t) = \mathbf{p}[\mathbf{P_1}, \mathbf{M}(t)] \quad (9)$$

Also, **p**(t) is a function of the array:

$$\mathbf{P}_1 \equiv \left[\mathbf{H}, \boldsymbol{\phi}, \mathbf{k}, \boldsymbol{S}_b^{res}, \mathbf{r}, \mathbf{Q}_{iw}, \rho_c, \rho_b, g, \lambda, \pi, \mu_b, c_{eff} \right] \quad (10)$$

where, the *L*×*1* vectors **H**, $\boldsymbol{\phi}$, $\boldsymbol{S}_b^{res}$ and **k** include the thicknesses, porosities, brine residual saturations and permeabilities of all aquifers; $\mathbf{Q}_{iw}$ is *M*×*L* vector including the CO_2 inflow rates for each aquifer *l* (*l*=1,2,..,*L*) for injection well *iw* (*iw*=1,2,..,*M*); and the (*M*+*N*)×(*M*+*N*) **r** matrix includes the relative

distances between injection and passive wells. The generic component of the $N \times L$ vector $\mathbf{M}(t)$ is net cumulative fluid mass transferred into aquifer l through passive well j, $M_{j,l}(t)$ and is defined as:

$$M_{j,l}(t) = \int_0^t \rho_{eff,j,l}(\tau) \cdot \left[Q_{j,l}(\tau) - Q_{j,l+1}(\tau)\right] \cdot d\tau \tag{11}$$

In Equation (11), $\rho_{eff,j,l}(\tau)$ is the effective fluid density in aquifer l, at passive well j and effective fluid density is estimated as $\rho_{eff,j,l} = \rho_c \cdot S_{c\,j,l} + \rho_b \cdot \left(1 - S_{c\,j,l}\right)$. The temporal evolution of leakage rates through passive wells $Q_{j,l}$, is then calculated using the multiphase version of Darcy's law across each confining layer l for each passive well j:

$$Q_{j,l} = \sum_{\alpha=b,c} \left[\pi r_{pw\,j,l}^2 \frac{k_{r,\alpha\,j,l} k_{pw\,j,l}}{\mu_\alpha B_l} \left(p_{j,l-1} - \rho_\alpha g B_l - g\rho_\alpha H_{l-1} - p_{j,l}\right) \right] \tag{12}$$

where, $r_{pw\,j,l}$ is the passive well radius and $k_{pw\,j,l}$ is the single phase passive well permeability for passive well j (j=1,2,..,N) and aquitard layer l. The $N \times L$ vector $\mathbf{Q}$ contains flow rates across each aquitard l (l=1,2,..,L) for each passive well j (j=1,2,..,N):

$$\mathbf{Q}(t) = \mathbf{Q}[\mathbf{P_2}, \mathbf{p}(t)] \tag{13}$$

where:

$$\mathbf{P}_2 \equiv \left[\mathbf{B}, \mathbf{H}, \mathbf{r}_{pw}, \mathbf{k}_{pw}, \mathbf{k}_{r,c}, \mathbf{k}_{r,b}, \rho_c, \rho_b, \mu_c, \mu_b, g\right] \tag{14}$$

The $(L+1)\times 1$ vector **B** includes the aquitard thicknesses, the $N\times(L+1)$ matrices $\mathbf{r}_{pw}$ and $\mathbf{k}_{pw}$ contain the passive well radii and permeabilities, and the $N\times(L+1)$ matrices $\mathbf{k}_{r,c}$ and $\mathbf{k}_{r,b}$ include the relative permeabilities of CO_2 and brine at passive wells. A set of $N{\cdot}L$ non-linear equations in $N{\cdot}L$ unknowns is obtained by combining Equations (9) and (13) are combined and solved to determine fluid pressures at the bottom of each aquifer and at each passive well (Equation 8). Fluid pressures are then used to estimate flow rates (Equation 12) across each aquitard for each passive well.

Also, as in [10], this work has chosen to neglect effects from upconing and apply the IGPS modification from [9] to further increase computational efficiency. Several assumptions made by this algorithm are important [8,11,13,17,18,23,25] and should be included [3,16,24,36] when accurate is more important that efficiency (e.g. final project design). Additional information regarding the implementation of the leakage model, as well as modifications made to the original work presented by [5,35,37], are discussed in detail in [9].

2.2 Multi-objective GCS Problem

The multi-objective GCS problem presented in this section is a deterministic version of the problem set forth by [10]. The goal herein is to determine the Pareto-optimal set of injection scenarios which minimize the project cost, C, while maximizing the mass of CO_2 injected, $Mass_{inj}$.

$$\begin{aligned} &\min\{C(\mathbf{x},\mathbf{Q},\mathbf{s})\} \\ &\max\{Mass_{inj}(\mathbf{Q})\} \end{aligned} \tag{15}$$

In Equation (15), spatial position, **x**, and flow rate, **Q**, are the two decision variables comprising each injection strategy and **s** is the set of state variables (i.e. aquifer fluid pressures at injection wells and passive well flow rates) dependent on each simulation's injection strategy and parameter set.

Several components comprise the cost, *C*, associated with each trial injection strategy, including the summation of each injection well's (*iw*) capital cost, *Cap*, operational cost, *OP*, surface maintenance cost, *SurM*, subsurface maintenance cost, *SubM*, and variable cost, *Var*, added to the cost associated with CO_2 leakage, *LC*:

$$C(\mathbf{Q}, Mass_{leak}) = \sum_{iw=1}^{M} \left[Cap_{iw} + OP_{iw}(t_{inj}) + SurM_{iw}(t_{inj}) + SubM_{iw}(t_{inj}) + Var_{iw}(Q_{iw}, t_{inj}) \right] + LC[Mass_{leak}(\mathbf{Q}, \mathbf{s})] \tag{16}$$

In the following analyses *LC* is estimated as:

$$LC[Mass_{leak}(\mathbf{Q}, \mathbf{s})] = c_L \cdot Mass_{leak}(\mathbf{Q}, \mathbf{s})^{r_A} \tag{17}$$

where, c_L is a coefficient representing penalty cost per unit of CO_2 leakage ($/kg) and r_A is a risk adversity factor reflecting the adversity of the DM to injection strategies that cause leakage. The effect of this coefficient is to significantly increase *LC* in relation to the mass of CO_2 leakage. The mass of CO_2 leakage (kg), $Mass_{leak}$, associated with each trial injection strategy is quantified numerically using the semi-analytical leakage algorithm Equation (11) as the mass of CO_2 that has escaped into the top layer by the end of simulation.

$Mass_{inj}$ is the total mass of CO_2 injected into the domain at the end of the injection duration, t_{inj}, is calculated as:

$$Mass_{inj} = \sum_{iw=1}^{M} Q_{c_{iw}} * t_{inj} \tag{18}$$

where M is the number of injection wells, and $Q_{c_{iw}}$ is the CO_2 mass injection rate for injection well *iw*. The fluid pressure at each injection well in each layer, $p_{iw,l}$, must remain less than each layer's fracture pressure, p_{frac_l}.

$$p_{i,l}(\mathbf{Q}, \mathbf{s}) < p_{frac_l}\ ;\ i = 1, 2, .., M; l = 1, 2, .., L \tag{19}$$

where, p_{frac_l} is calculated by multiplying a specified fracture gradient [5] by layer depth and $p_{i,l}$ is estimated for each injection well *i* at the end of the injection duration at a small effective distance (e.g. the borehole radius) from the injection location using Equation (8). In addition, the number of injection wells is limited to a maximum integer value, M_{max}:

$$0 \leq M \leq M_{max} \tag{20}$$

Also, the prescribed areal extent selected for the construction of GCS faculties will limit the minimum and maximum spatial bounds of candidate injection wells:

$$x_{min} \leq x_{iw} \leq x_{max}\ ;\ y_{min} \leq y_{iw} \leq y_{max}\ ;\ iw = 1, 2, .., M \tag{21}$$

Finally, each injection well's flow rate must be between prescribed minimum and maximum flow rates Q_{min} and Q_{max}:

$$Q_{min} \leq Q_{iw} \leq Q_{max}\ ;\ iw = 1, 2, .., M \tag{22}$$

In Equation (22), Q_{min} and Q_{max} represent physical constraints related to the technical capacity of injection pumps and wells.

2.3 Multi-objective GCS Optimization using the NSGA-II with ε-dominance

The NSGA-II is implemented in the same manner as in [10]. Trial injection strategies are encoded into a unique sequence (i.e. "chromosome") of binary numbers representing the values of each decision variable, where the first part of the chromosome contains spatial location information represented by N_{cl} predefined candidate injection well location indices for each of the M_{max} injection wells. This intrinsically satisfies the locational constraint defined by Equation (21) because each candidate injection well location is previously defined within minimum and maximum spatial bounds. The last segment of the chromosome represents the injection rate index of each well. There are N_{ir} injection rate indices to represent prescribed discrete flow rate values within the constraints of Equation (22).

The number of digits required to identify each injection well's location is a function of the number of candidate locations, N_{cl}. As an example, if N_{cl} = 16 for a potential GCS site, the locational information of each injection well for each injection strategy would require four binary digits (i.e. '0000' = 1, '0001' = 2, … , '1111'=16). In this case, the spatial data component of the chromosome has a length of $M{\cdot}4$. The number of digits required to represent each well's injection rate is a function of the number of injection rate indices, N_{ir}. If injection rate index values of 0, 1, 2, and 3 represent injection rates of 0, 20, 30, and 40 kg/s, respectively (N_{ir} = 4), two binary digits would be used to encode each well's injection index ('00' = 0, '01' = 1, … , '11'=3) bringing the total chromosome length to $M{\cdot}4 + M{\cdot}2$.

Figure 4.2 shows a schematic of the NSGA-II's procedure. An initial population of N_{pop} trial injection scenarios, each typically having unique spatial location and injection rate data, is randomly generated after first reading domain characteristics and algorithm parameters. Next, objective function values are

calculated for each population member in step (b) by first using the semi-analytical leakage algorithm described in Section 2.1 to estimate $Mass_{leak}$ for each population member in step (c) then using Equations (16) and (18) to calculate objective values C and $Mass_{inj}$, respectively. The semi-analytical algorithm is also used to check if the fracture pressure defined by Equation (19) is exceeded. If the fracture pressure constraint is violated the injection strategy is deemed infeasible. Finally, simulation archiving is used to prevent the NSGA-II from recalculating objective values for identical scenarios by keeping a record of simulation results.

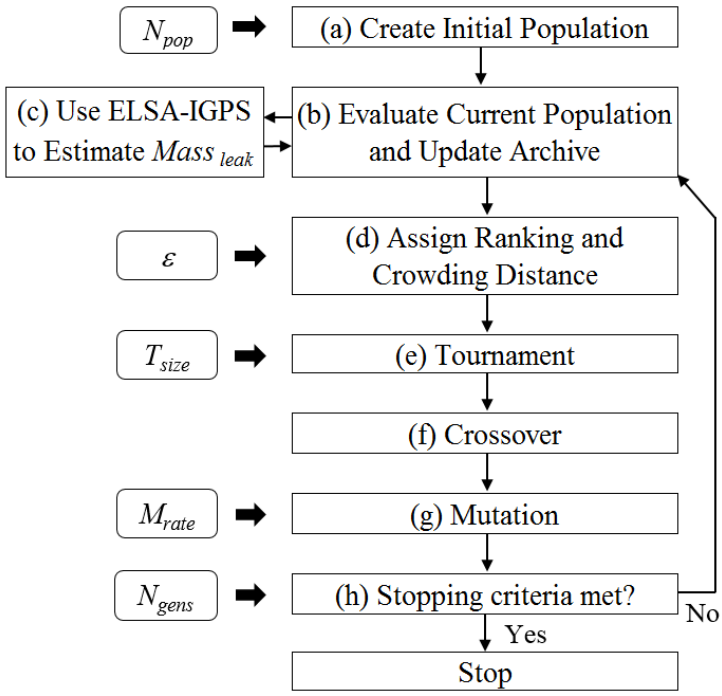

Figure 4.2. Schematic of the NSGA-II optimization algorithm

After this, a partial order is established using crowding comparison operator, $\geq_n$ [15] where population member *i* outperforms member *j* if the following conditions are met:

$$i \geq_n j \quad \text{IF} \left\{ (i_{rank} < j_{rank}) \text{ OR } \left((i_{rank} = j_{rank}) \text{ AND } (i_{distance} > j_{distance}) \right) \right\} \tag{23}$$

where population members are ranked (i_{rank}) as the number of solutions dominating population member i using the fast-nondominated sorting procedure from [15] and assigned a crowding distance ($i_{distance}$) as the largest cuboid in objective space enclosing the point i without including any other point in the population [15]. In addition, NSGA-II's ranking procedure is improved with concept of ε-dominance [28] by allowing for the inclusion of additional, well-performing population members to each rank's Pareto-optimal front. For example, if population members p_1 and p_2 have fitness values of f_1 and f_2, respectively, using ε-dominance, p_1 is allowed to dominate p_2 if $(1+\varepsilon)\cdot f_1$ is greater than or equal to f_2.

A subset, T_{size}, of population members is selected randomly and, through an iterative tournament-style selection process, are used to choose parents for the next generation. The population member with highest partial order out of this subset using Equation (23) is chosen as a parent. Following the selection of N_{pop} parents, a crossover operator is used to create a new generation of population members in step (f) until the new population is filled. During each crossover operation, components of chromosomes from two randomly selected parents are used to build a new trial injection strategy. In step (g), there is a chance, quantified as the mutation rate, M_{rate}, in which chromosome elements of this new population will be randomly altered. Steps (b-g) are repeated until the maximum prescribed number of generations, N_{gens}, is reached. This work uses NSGA-II parameter values found by the convergence analysis in [10]. Table 4.1 lists the parameter values used for the NSGA-II.

Table 4.1. NSGA-II parameter values

N_{pop}	M_{rate}	T_{size}	ε	N_{gens}
25	1.6%	2	0.001	200

2.4 Multi-objective GCS Optimization using the Gravitational Search Algorithm

When applying a MOGSA, the decision space is encoded into a set of vectors containing the injection well location and flow rate values for each search agent (i.e. population member). The first and second

sets of M_{max} values in each vector contain X and Y horizontal injection well positions, respectively, while the third set of M_{max} values contain each injection well's flow rate. The number of values, hence the number of dimensions, in each vector is $3 \cdot M_{max}$. All values within each vector are normalized as real numbers ranging between 0 and 1 where 0 represents the minimum injection rate (Q_{min}) or locational (x_{min}, y_{min}) constraint value and 1 represents the maximum injection rate (Q_{max}) or locational (x_{max}, y_{max}) constraint value.

Due to the bi-objective nature of this problem, the MOGSA proposed and tested by [43] is used to generate new injection strategy populations. This MOGSA's general procedure is presented below in Figure 4.3. Once input files containing domain characteristics and algorithm parameters are read, an initial population of N_{pop} trial injection scenarios, including the spatial location and flux rate for each injection well, is randomly generated. In step (b), objective function values are calculated for each population member. The semi-analytical leakage algorithm described in Section 2.1 is used to estimate $Mass_{leak}$ for each of these realizations in step (c) then objective values C and $Mass_{inj}$ are calculated using Equations (16) and (18). Once again, simulation archiving is used to keep a record of simulation results, therefore preventing the MOGSA from recalculating objective values for identical scenarios and if the fracture pressure defined by Equation (19) is exceeded the injection strategy is deemed infeasible.

In step (d), fitness values, fit_i, are assigned to each search agent i using:

$$fit_i(k) = \left(i_{rank} + \frac{1}{1 + i_{distance}} \right)^{-1} \tag{24}$$

where k is the generation iteration index and i_{rank} and $i_{distance}$ are defined in Section 2.3. Here, better performing search agents are assigned lower fitness values. Because i_{rank} must be an integer and both i_{rank}

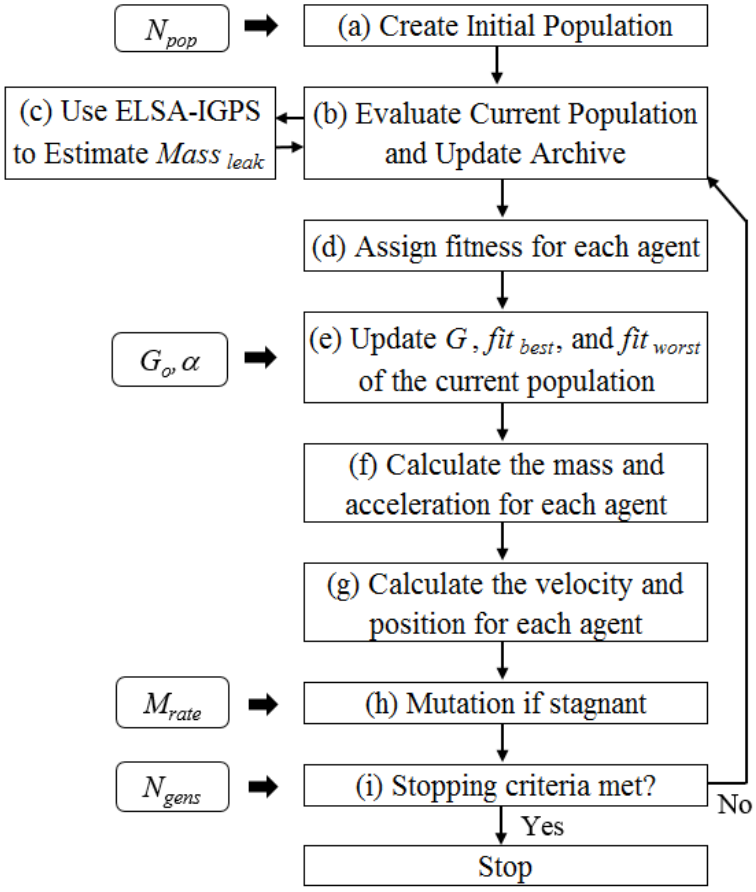

Figure 4.3. Schematic of the MOGSA optimization algorithm

and $i_{distance}$ must be greater than or equal to zero, significant preference is given to ranking versus crowding distance in Equation (24). Next, in step (e) a gravitational constant used for determining each search agent's acceleration in decision space, $G(k)$, is updated as:

$$G(k) = G_0 e^{-\alpha \frac{k}{N_{gen}}} \tag{25}$$

where G_0 is an initial gravitational constant value, α is a reduction factor, and N_{gen} is the total number of generations. In addition, $fit_{best}(k)$ and $fit_{worst}(k)$ are assigned as the best and worst fitness values for the current population.

The MOGSA conceptualizes the search agent population as a collection of masses in the decision space. In step (f) the relative fitness of each search agent, q_i, calculated as:

$$q_i(k) = \frac{fit_i(k) - fit_{worst}(k)}{fit_{best}(k) - fit_{worst}(k)} \tag{26}$$

Once relative fitness's are calculated, the mass of each search agent, M_i, is assigned as:

$$M_i(k) = \frac{q_i(k)}{\sum_{j=1}^{N_{pop}} q_j(k)} \tag{27}$$

where, N_{pop} is the number of search agents and is analogous to the NSGA-II's population size variable. In each dimension, d, new velocities, $v_i^d(k)$, and positions, $x_i^d(k)$, of each search agent i are determined at step (g) using both old velocities from the preceding iteration, $v_i^d(k-1)$, and the cumulative acceleration, $a_i^d(k)$, resulting from the gravitational forces induced by a number of the best performing search agents:

$$a_i^d(k) = \frac{F_i^d(k)}{M_i(k)} = \sum_{j \in kbest, j \neq i} rand_j^d G(k) \frac{M_j(k)}{R_{ij}(k-1) + \xi} (x_j^d(k-1) - x_i^d(k-1)) \tag{28}$$

$$v_i^d(k) = rand_i^d \cdot v_i^d(k-1) + a_i^d(k)\Delta t \tag{29}$$

$$x_i^d(k) = x_i^d(k-1) + v_i^d(k)\Delta t \tag{30}$$

where, $F_i^d(k)$ is the total gravitational force acting upon search agent i along dimension d, $rand_j^d$ and $rand_i^d$ are uniform random numbers between 0 and 1, $R_{ij}(k-1)$ is the Euclidian distance in decision

variable space between the two agents *i* and *j*, ξ is a very small number, and **kbest** is the set of *K* agents with the best fitness values in the current generation. *K* decreases linearly to 1 in the final iteration. Finally, a mutation operation is applied at a rate of M_{rate} if the Pareto-front is determined to be stagnant at step (h). New positions within the normalized decision space, $x_i^d(k+1)$, are then converted back to the nearest discrete injection well locations and flow rates. Steps b-h are repeated until the maximum prescribed number of generations, N_{gens}, is reached.

The value of M_{rate} used by the MOGSA is identical that is used by the NSGA-II while N_{pop}, N_{gens}, G_0 and α are found through a trial and error analysis similar to the analysis used by [10]. Optimal parameter values are selected from a series of preliminary tests using an optimization problem having 50% degraded and 50% intact passive well segments. First, a single measure is established to quantify the performance of each NSGA-II parameter value set where the average project cost per unit mass sequestered ($/kg) over all non-dominated solutions is assumed to represent the fitness of any given Pareto set. Next, the true optimal Pareto set is found for the test optimization problem by performing three exhaustive evolutionary searches, each with 5,000 generations where each arrived at the same average project cost per unit mass sequestered. Finally, the set of parameter values consistently requiring the least number of simulation calls to arrive within 0.1% of the minimal average project cost per unit mass sequestered found from exhaustive search are selected to be used by the stochastic optimization problem. Table 4.2 provides the resulting MOGSA parameter values and maximum number of optimization generations.

Table 4.2. MOGSA parameter values

N_{pop}	M_{rate}	G_0	α	N_{gens}
100	1.6%	2	0.001	50

2.5 Efficient Computational Implementation

Due to the iterative nature of each optimization method, large numbers of model simulations are needed for each optimization run. Without using simulation archiving, the total number of model calls, required for each optimization run will be equal to $N_{pop} \cdot N_{gens}$. However, this framework utilizes parallel computing and, as described in the previous two sections, simulation archiving to improve computational efficiency. CO_2 leakage estimation calculations for each trial injection strategy are independent and therefore may be processed in parallel (i.e. simultaneously) rather than sequentially.

3 Characterization of the MB test site

Michigan Technological University's data library provides detailed subsurface data for the Michigan Basin (MB) located near the town of Thompsonville in northwest Michigan. A nearly depleted hydrocarbon reservoir exists between depths of approximately 4660 and 5000 feet (1420-1520 meters) and is overlain by multiple confining and saline aquifer layers. Located between two exploration boreholes, Burch 1-20B and Stech 1-21A, this reservoir's only production well, Merit 1-20A, was originally drilled in by the Shell Oil Company. Figure 4.4 shows a cross-sectional schematic of the MB site.

This work uses the site characterization methodology presented in [10] to conceptualize the simulation and optimization of GCS into the saline Grey Niagaran formation immediately below the hydrocarbon reservoir (highlighted orange in Figure 4.4). Five derived aquitards and three interlaying aquifer layers in addition to the Grey Niagaran formation are used in the computational model (L = 4). From Neutron Porosity Hydrogen Index (NPHI) data [48] gathered from the Burch 1-20B and Stech 1-21A boreholes caprock thicknesses are estimated to be 16.8, 18.3, and 109.1 m for layers 2, 3, and 4, respectively, while layers 1 and 5 are assumed to be completely impermeable even at passive well locations. Table 4.3 shows aquifer permeability, thickness, and porosity values used in this study.

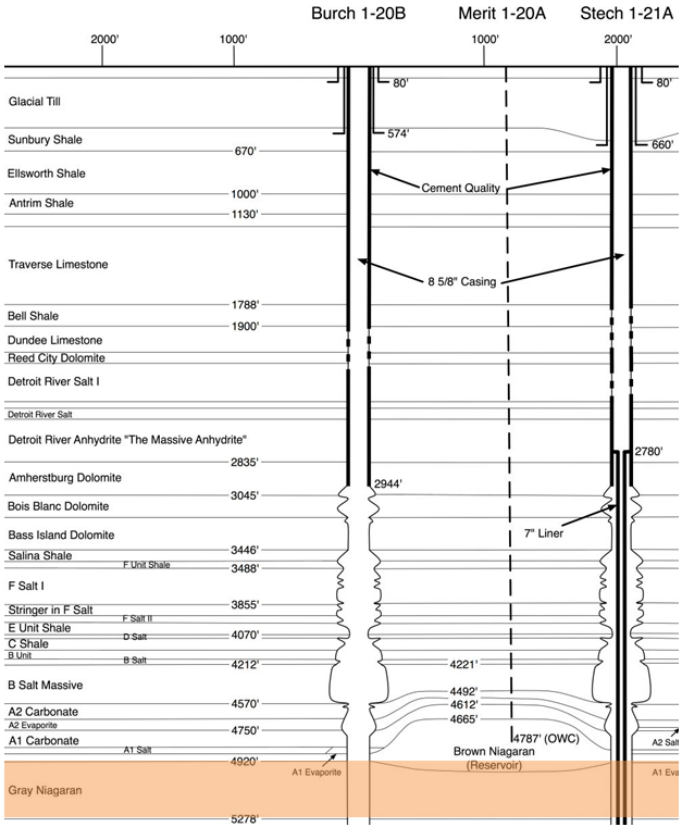

Figure 4.4. Cross-sectional schematic of the MB with the simulated injection layer highlighted orange (modified with permission from [49])

Table 4.3. Aquifer permeability, thickness, and porosity values used in this study

Parameter	Symbol	Value for Aquifer Layer *l*				Units
		$l = 1$	$l = 2$	$l = 3$	$l = 4$	
Permeability	k	24	4.5	6.7	655	mD
Thickness	H	119.5	35.1	36.6	75.3	m
Porosity	ϕ	0.079	0.026	0.038	0.169	/

As in [10], this work includes a small subset of the 65,560 producing and inactive oil and gas well records from the Michigan Department of Environmental Quality database [32]. Only the 131 passive wells (N = 131) found within 4 km of the reservoir's production well, Merit 1-20A, and intersect the 4 aquifer layers defined above are included in the computational domain.

Domain data characterized above are used to create a GCS test site in the MB. Injection well locations may be selected from 16 (N_{cl} = 16) candidate locations uniformly distributed over a 4 km^2 square grid where horizontal positions are relative to the Merit 1-20 production well with $x_{min} = y_{min}$ = -1000 m and $x_{max} = y_{max}$ = 1000 m where injection wells assumed to operate at a constant injection rate of either $Q_1 = Q_{min} = 0$, $Q_2 = 20$, $Q_3 = 30$, or $Q_4 = Q_{max} = 40$ kg/s ($N_{ir} = 4$) over a 50-year duration (t_{inj} = 50 yrs.), thereby satisfying Equation (22). Table 4.4 lists additional hydrogeological and cost parameter [29] values used herein.

Table 4.4. Hydro-geological and cost parameter symbols and values used herein

Parameter	Symbol	Value	Units
Brine density	ρ_b	1,045	kg/m^3
CO_2 density	ρ_c	479	kg/m^3
Brine viscosity	μ_b	2.94x10^{-4}	Pa·s
CO_2 viscosity	μ_c	3.95x10^{-5}	Pa·s
Effective compressibility	c_{eff}	4.6x10^{-10}	m^2/N
Brine residual saturation	S_{res}	0.3	/
Fracture Gradient	-	20	kPa/m
Capital Cost	*Cap*	3,537,104	($/well)
Fixed O&M Costs	*OP*	11,566	($/day/well)
Surface Maintenance Costs	*SurM*	120,608	($/yr/well)
Subsurface Maintenance Costs	*SubM*	37,612	($/yr/well)
Variable Costs	*Var*	0.009	($/kg of CO_2)
Penalty Cost Coefficient	c_L	0.6	($/kg of CO_2)
Risk Adversity Factor	r_A	1.1	/

This analysis does not include costs involved with site characterization, permitting, lease/purchase of land/pore space, financing, insurance, monitoring, verification, EPA financial bond requirement, post-injection site care, and long-term liabilities though these may be significant in the final financial assessment [29].

4 Results and Discussion

In this section a performance comparison is made between the MOGSA and the NSGA-II to determine the best algorithm for injection strategy optimization at potential GCS sites. It is important that multi-objective optimization algorithms perform the following: 1) fully explore the objective space providing diverse Pareto-optimal tradeoff sets and 2) find the best or close-to-best Pareto-optimal solutions with minimal computational expense. Appropriate measures are applied herein to evaluate how well each algorithm accomplishes these tasks. First, to measure objective space diversity, the percentage of optimization runs reaching full Pareto-optimal sets of solutions (defined further in Section 4.1) is calculated for each test case. Secondly, convergence rates are graphically and quantitatively compared by calculating the average project cost per unit mass sequestered versus number of model calls for the average of the top two best performing optimization runs of each test case.

A total of 360 optimization runs are processed where 20 different random seed optimization runs are performed for each of nine GCS test cases using each algorithm. Redundancy is needed as heuristic algorithms may occasionally produce abnormal results which are not representative of typically performance. Hypothetical GCS test cases are generated for the MB test site by varying both the maximum allowable number of injection wells and passive well permeability. The maximum allowable number of injection wells is ranged between 2 and 4. Passive well segment permeabilities are assumed to be either 0.01 or 1000 mD (mD; 1 mD = $\sim 10^{-15}$ m^2), representing "intact" and "degraded" cement, respectively [5,11]. Three uncertainty scenarios are assumed, including 1) data supporting an abundance of intact passive well segments (75% intact/25% degraded); 2) no passive well permeability data available (50% intact/50% degraded); and 3) data supporting an abundance of degraded passive well segments (25% intact/75% degraded). To provide an element of structure to the optimization problem, degraded wells are concentrated in specific quadrants of the domain for each uncertainty scenario. Passive well segment permeabilities are assumed to be fully correlated, therefore all caprock segments for any given

passive well are given the same permeability value. Figure 4.5 shows locations for both candidate injection wells as well as intact and degraded passive wells for each uncertainty scenario.

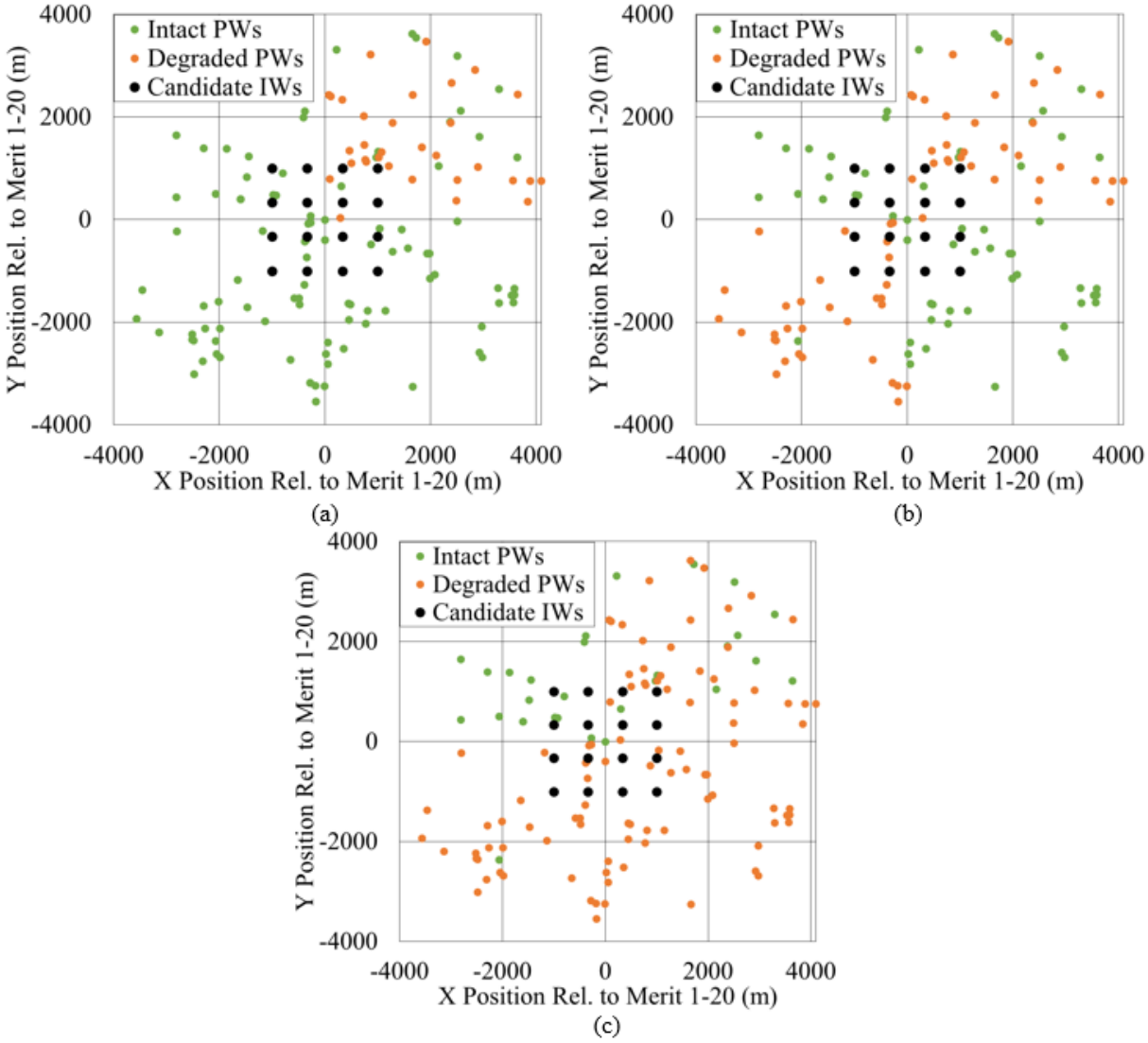

Figure 4.5. Spatial locations of both candidate injection wells and intact and degraded passive wells for the (a) 75% intact/25% degraded, (b) 50% intact/50% degraded, and (c) 25% intact/75% degraded uncertainty scenarios.

Also, Table 4.5 shows both the maximum allowable number of injection wells and the probability of passive well segments being assigned either an "intact" or “degraded” permeability value for each of the nine test optimization cases. It should be noted that increasing the maximum allowable number of

injection wells adds to the optimization problem's complexity by significantly expanding both objective function and decision variable search space.

Table 4.5. Maximum allowable injection wells and the percent likelihood of passive well segments being assigned either an "intact" or "degraded" permeability value for each test case

Test Case	Maximum Number of Injection Wells	Percentage of passive wells being assigned an "intact" permeability value	Percentage of passive wells being assigned a "degraded" permeability value
I	2	75%	25%
II	2	50%	50%
III	2	25%	75%
IV	3	75%	25%
V	3	50%	50%
VI	3	25%	75%
VII	4	75%	25%
VIII	4	50%	50%
IX	4	25%	75%

4.1 Objective Solution Diversity

Objective solution diversity may be evaluated using either the Spacing metric [22] to find how well objective solutions are uniformly distributed or the Hyper-volume metric [43,51] to compare how well objection solution sets are "spread-out". However, our problem is more finely structured than most multi-objective optimization problems, thus enabling a more rigorous evaluation of objective solution diversity. Before processing each optimization run, all possible values of the total mass sequestered objective function are known. This is because values for the variables composing the quantity of total mass sequestered (i.e. injection duration, t_{inj}, maximum number of injection wells, M_{max}, and the number N_{ir} and allowable injection rates, Q_{iw}) are prescribed before the start of optimization. Recall from Section 3 that each injection well may only assume an injection rate of either 0, 20, 30, or 40 kg/s. Hence, the total injection rate may range between 20 and M_{max}·40 kg/s in increments of 10 kg/s. Table 4.6 shows all possible injection rates and mass sequestered quantities for up to 4 injection wells. Cases with 2, 3, and 4 injection wells have 7, 11, and 15 non-zero, discrete values of total mass sequestered, respectively.

Table 4.6. Injection rates and mass sequestered quantities for up to 4 injection wells

Max Number of IWs	Total Flow Rate (kg/s)	Mass of CO_2 Sequestered after 50 years (Mt)
2	20	31.5
2	30	47.3
2	40	63.1
2	50	78.8
2	60	94.6
2	70	110.4
2	80	126.1
3	90	141.9
3	100	157.7
3	110	173.4
3	120	189.2
4	130	205.0
4	140	220.8
4	150	236.5
4	160	252.3

Therefore, it is possible to define a single measure of objective solution diversity that takes into account both the Spacing and Hyper-volume measures. Optimization runs providing project cost solutions for each possible discrete mass sequestered value are defined as having full objective function solution sets. The percentage of optimization runs arriving at full solution sets out of the 20 runs processed for each test case is used herein as the objective solution diversity measure. Table 4.7 shows the percentage of optimization runs arriving at a full solution set for each trial case.

The results provided by Table 4.7 show the NSGA-II to outperform the MOGSA when evaluating objective solution diversity. The average percentage of full solutions sets over all 9 simulations is 94% and 78% for the NSGA-II and the MOGSA, respectively. Both algorithms typically provide full solutions sets for test cases having either two or three injection wells. However, the MOGSA has difficulty filling the objective function space when optimizing cases allowing for four injection wells. It should also be noted that a lower percentage of full solutions sets is typically observed in both algorithms when

Table 4.7. Percentage of optimization runs arriving at full solution set for each trial case

Test Case	Percentage of full solution sets	
	NSGA	MOGSA
I	100%	100%
II	100%	100%
III	100%	100%
IV	100%	90%
V	85%	80%
VI	100%	100%
VII	100%	15%
VIII	65%	20%
IX	100%	95%
Average	*94%*	*78%*

optimizing the 50%-intact/50%-degraded uncertainty scenario, indicating a more difficult optimization problem.

4.2 Objective Solution Convergence

The rate at which each algorithm converges (i.e. progresses) toward the true Pareto-optimal solution is also investigated using the nine test cases described by Table 4.5. To obtain a general understanding of the convergence performance, the average project cost per unit mass sequestered ($/kg) over the non-dominated objective trade-off set is calculated at each generation using averages from the two best performing optimization runs for each test case. Figure 4.6 contains plots of the average project cost per unit mass sequestered versus number of model (i.e. CO_2 leakage simulator) calls made by each optimization algorithm.

Several convergence rate trends are observed through both the qualitative and quantitative inspection of Figure 4.6. The NSGA-II is found to have a more consistent improvement of the average project cost per unit mass sequestered as the generation index (thus, the total number of model calls) progresses while the MOGSA tends to display large but infrequent reductions in average project cost per unit mass

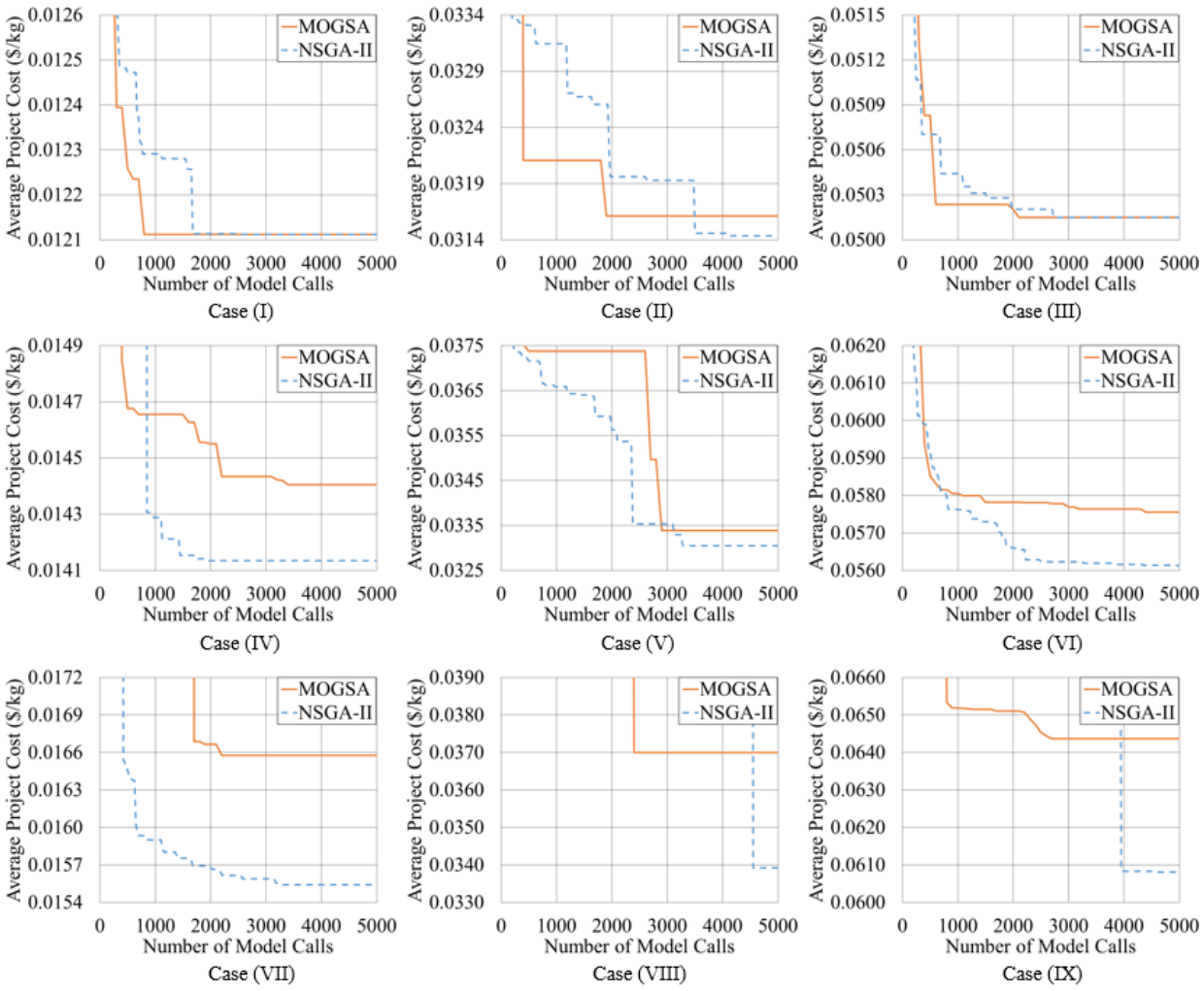

Figure 4.6. Average project cost per unit mass sequestered versus number of model calls for Cases (I-IX)

sequestered. Also related to the previous observation, in 78% of cases studied the MOGSA finds better average project cost per unit mass sequestered values early in the optimization run only to be overtaken by the NSGA-II. This is especially obvious in test cases I, II, VIII, and IX. These trends are caused by a fundamental methodology difference between the two optimization algorithms. In comparison to the NSGA-II, the MOGSA takes a significantly more direct approach related to fitness weighting when generating new sets of trial injection strategies. With the MOGSA, new trial injection strategies are directly driven toward well-performing trial injection strategy positions in decision space using Equations (26-30). The NSGA-II uses a much more convoluted method to generate each new trial population

member. Two trial injection strategies are chosen as parents through tournament selection then encoded into a chromosome of binary numbers. Using the crossover operator, these chromosomes are then split at a random length then merged into a unique chromosome representing a new trial injection strategy. In addition, the mutation operator (i.e. the random altering of trial injection strategy components) is only used in the MOGSA if the Pareto-set is found to be stagnant after several generations where it performed at every generation using the NSGA-II.

Both algorithms are shown to arrive at relatively similar final average objective function tradeoff solutions in all trial cases. At first glance, the NSGA-II is found to outperform the MOGSA when comparing solution accuracy. Although and the NSGA-II and the MOGSA arrive at the same final average project cost per unit mass sequestered in test cases I and III, the NSGA-II found better final solutions in all 7 other trial cases. In addition, the NSGA-II's outperformance of the MOGSA in the area of objective solution accuracy is accentuated in cases having greater optimization problem difficulty. The solution diversity results presented in Table 4.7 suggest that cases with either M_{max} set to 4 (i.e. cases VII, VIII, IX) or a 50% intact/50% degraded uncertainty scenario (i.e. cases II, V, VIII) are the most difficult to optimize. The NSGA-II is found to provide more accurate solutions in all 5 of these cases. However, a further investigation of the data presented in Figure 4.6 shows the relative accuracy differences between the two algorithms to be fairly small. Table 4.8 shows the relative differences in the MOGSA's final Pareto set solution compared to the NSGA-II's solution.

Although the MOGSA provides less accurate solutions in seven out of nine of the test cases, the average relative difference in solution accuracy is found to be only -3.1%. In test cases having only two or three injection wells (i.e. Cases I-VI) the average absolute relative difference between the two algorithms is only 1.0%. The largest absolute relative differences are found in test cases having four injection wells (i.e. Cases VII-IX) where the average absolute relative difference is found to be approximately 7.2%.

Table 4.8. Relative differences in the MOGSA's final Pareto set solution compared to the NSGA-II solutions.

Test Case	MOGSA Relative Difference in Solution Accuracy
I	0.0%
II	-0.6%
III	0.0%
IV	-1.9%
V	-1.0%
VI	-2.5%
VII	-6.7%
VIII	-9.1%
IX	-5.9%
Average	*-3.1%*

Even with slightly less accurate final objective solutions, the MOGSA may still be preferable over the NSGA-II due to its fast early convergence rates. Figure 4.7 shows project cost versus mass sequestered for Case (IX) where objective function tradeoffs are shown at 1000 model calls for the MOGSA and 4000 model calls for the NSGA-II to demonstrate the effectiveness of the MOGSA's faster early convergence.

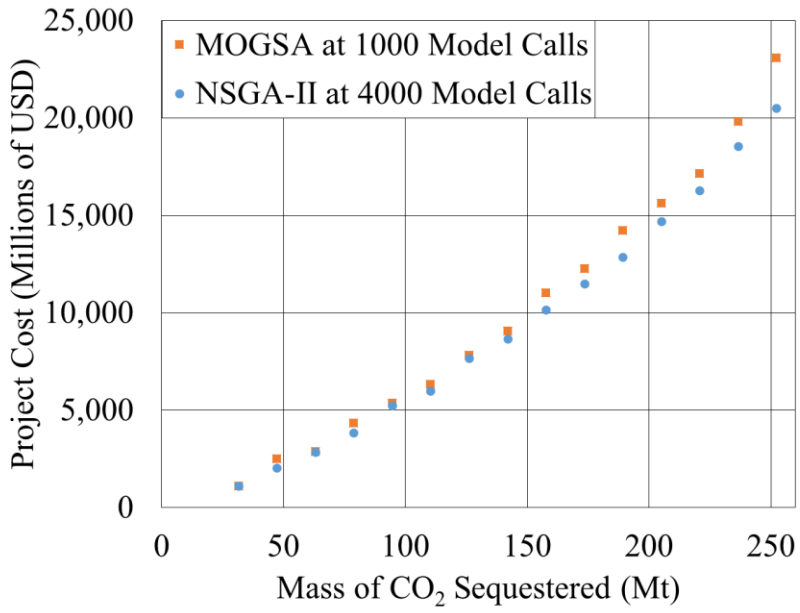

Figure 4.7. Project cost versus mass sequestered for Case (IX). Objective function tradeoffs are shown at 1000 model calls for the MOGSA and 4000 model calls for the NSGA-II.

As shown by Figures 4.6 and 4.7, when optimizing Case (IX) the MOGSA found a comparable tradeoff solution using about one-quarter of the computational cost spent by the NSGA-II. The MOGSA and NSGA-II provided very similar project cost values when injecting less that 150 Mt of CO_2 but began to differ with greater quantities of mass sequestered. These trends suggest that the best method may be to use a hybrid approach where the MOGSA performs an initial optimization then the NSGA-II is used to "fine-tune" injection strategy selection.

5 Conclusions

Two heuristic algorithms, the NSGA-II and MOGSA, have been applied to nine different injection strategy optimization test cases at the MB test site. Two performance measures, included 1) objective solution diversity and 2) objective solution convergence rate were compared for each optimization algorithm. The NSGA-II provided a better search of objective function space and slightly more accurate objective function solutions. The average percentage of full solutions sets over all 9 test cases was 94% and 78% for the NSGA-II and the MOGSA, respectively. In addition, the MOGSA had difficulty filling the objective function space when optimizing cases allowing for four injection wells. The NSGA-II provided slightly better average project cost per unit mass sequestered solutions in 7 of the 9 test cases while each algorithm provided equal average project cost per unit mass sequestered in the other two test cases. The average relative difference in solution accuracy was found to be only 3.1% between the two algorithms.

Perhaps the most significant finding of this work was that, faster convergence rates by the MOGSA were observed early in the majority optimization runs. The MOGSA found a comparable tradeoff solution using about one-quarter of the computational cost spent by the NSGA-II for Case (IX). It may be possible to exploit this trend by creating a multi-stage hybrid method between the two algorithms where the MOGSA is first used to quickly perform an initial optimization then the NSGA-II is used complete the final stage of injection strategy selection.

REFERENCES

1. Alzraiee, A.H., Bau, D.A., Garcia, L.A.: Multiobjective design of aquifer monitoring networks for optimal spatial prediction and geostatistical parameter estimation. Water Resour. Res. 49, 3670–3684 (2013).
2. Baú, D.A.: Planning of Groundwater Supply Systems Subject to Uncertainty Using Stochastic Flow Reduced Models and Multi-Objective Evolutionary Optimization. Water Resour. Manag. 26, 2513–2536 (2012).
3. Buscheck, T.A., Sun, Y., Chen, M., Hao, Y., Wolery, T.J., Bourcier, W.L., Court, B., Celia, M.A., Julio Friedmann, S., Aines, R.D.: Active CO2 reservoir management for carbon storage: Analysis of operational strategies to relieve pressure buildup and improve injectivity. Int. J. Greenh. Gas Control. 6, 230–245 (2012).
4. Chatterjee, A., Mahanti, G., Pathak, N.: Comparative performance of gravitational search algorithm and modified particle swarm optimization algorithm for synthesis of thinned scanned concentric ring array. Prog. Electromagn. Res. B. 25, 331–348 (2010).
5. Celia, M.A., Nordbotten, J.M., Court, B., Dobossy, M., Bachu, S.: Field-scale application of a semi-analytical model for estimation of CO2 and brine leakage along old wells. Int. J. Greenh. Gas Control. 5, 257–269 (2011).
6. Chen, L., McPhee, J., Yeh, W.W.-G.: A diversified multiobjective GA for optimizing reservoir rule curves. Adv. Water Resour. 30, 1082–1093 (2007).
7. Cheng, Y., Jin, Y., Hu, J.: Adaptive epsilon non-dominated sorting multi-objective evolutionary optimization and its application in shortest path problem. ICCAS-SICE, 2009. 2545–2549 (2009).
8. Cihan, A., Birkholzer, J.T., Zhou, Q.: Pressure buildup and brine migration during CO2 storage in multilayered aquifers. Ground Water. 51, 252–67 (2013).
9. Cody, B.M., Baú, D.A., González-Nicolás, A.: Improved Semi-Analytical Simulation of Geological Carbon Sequestration. *In press* (2014)
10. Cody, B.M., Baú, D.A., González-Nicolás, A.: Stochastic Injection strategy Optimization for the Preliminary Assessment of Candidate Geological Storage Sites. In press (2014)
11. Court, B., Bandilla, K.W., Celia, M.A., Janzen, A., Dobossy, M., Nordbotten, J.M.: Applicability of vertical-equilibrium and sharp-interface assumptions in CO2 sequestration modeling. Int. J. Greenh. Gas Control. 10, 134–147 (2012).
12. Deb, K., Agrawal, S.: A fast elitist non-dominated sorting genetic algorithm for multi-objective optimization: NSGA-II. Proc. Parallel Probl. Solving from Nat. VI. 849–858 (2000).

13. Doster, F., Nordbotten, J.M., Celia, M.A.: Impact of capillary hysteresis and trapping on vertically integrated models for CO2 storage. Adv. Water Resour. 62, 465–474 (2013).
14. Duman, S., Güvenç, U., Sönmez, Y., Yörükeren, N.: Optimal power flow using gravitational search algorithm. Energy Convers. Manag. 59, 86–95 (2012).
15. Duman, S., Guvenc, U., Yorkukeren, N.: Gravitational search algorithm for economic dispatch with valve-point effects. Int. J. Electr. Eng. 5, 2890–2895 (2010).
16. Gasda, S.E., Nordbotten, J.M., Celia, M.A.: Vertical equilibrium with sub-scale analytical methods for geological CO2 sequestration. Comput. Geosci. 13, 469–481 (2009).
17. Gasda, S.E., Nordbotten, J.M., Celia, M.A.: The impact of local-scale processes on large-scale CO2 migration and immobilization. Energy Procedia. 4, 3896–3903 (2011).
18. Gasda, S.E., Nordbotten, J.M., Celia, M.A.: Application of simplified models to CO2 migration and immobilization in large-scale geological systems. Int. J. Greenh. Gas Control. 9, 72–84 (2012).
19. Gopal, N.R., Satyanarayana, S.V.: Cost analysis for removal of VOCs from water by pervaporation using NSGA-II. Desalination. 274, 212–219 (2011).
20. Haghighi, A., Asl, A.Z.: Uncertainty analysis of water supply networks using the fuzzy set theory and NSGA-II. Eng. Appl. Artif. Intell. 1–13 (2014).
21. Hansen, A.K., Hendricks Franssen, H.-J., Bauer-Gottwein, P., Madsen, H., Rosbjerg, D., Kaiser, H.-P.: Well Field Management Using Multi-Objective Optimization. Water Resour. Manag. 27, 629–648 (2013).
22. Hassanzadeh, H.R., Rouhani, M.: A Multi-objective Gravitational Search Algorithm. 2010 2nd Int. Conf. Comput. Intell. Commun. Syst. Networks. 1, 7–12 (2010).
23. Heße, F., Prykhodko, V., Attinger, S.: Assessing the validity of a lower-dimensional representation of fractures for numerical and analytical investigations. Adv. Water Resour. 56, 35–48 (2013).
24. Huang, X., Bandilla, K.W., Celia, M.A., Bachu, S.: Basin-scale modeling of CO2 storage using models of varying complexity. Int. J. Greenh. Gas Control. 20, 73–86 (2014).
25. Juanes, R., MacMinn, C.W., Szulczewski, M.L.: The Footprint of the CO2 Plume during Carbon Dioxide Storage in Saline Aquifers: Storage Efficiency for Capillary Trapping at the Basin Scale. Transp. Porous Media. 82, 19–30 (2009).

26. Khajehzadeh, M., Taha, M.R., El-Shafie, A., Eslami, M.: A modified gravitational search algorithm for slope stability analysis. Eng. Appl. Artif. Intell. 25, 1589–1597 (2012).
27. Kumphon, B.: Genetic Algorithms for Multi-objective Optimization: Application to a Multi-reservoir System in the Chi River Basin, Thailand. Water Resour. Manag. 27, 4369–4378 (2013).
28. Laumanns, M., Thiele, L., Deb, K., Zitzler, E.: Combining convergence and diversity in evolutionary multiobjective optimization. Evol. Comput. 10, 263–82 (2002).
29. Lepinski, J.: RE: Questions regarding geological sequestration costs. Message to author. 25 September 2012. Email. (2012)
30. Li, C., Zhou, J.: Parameters identification of hydraulic turbine governing system using improved gravitational search algorithm. Energy Convers. Manag. 52, 374–381 (2011).
31. Mantoglou, A., Kourakos, G.: Optimal Groundwater Remediation Under Uncertainty Using Multi-objective Optimization. Water Resour. Manag. 21, 835–847 (2006).
32. Michigan Department of Environmental Quality Oil and Gas Database. http://www.michigan.gov/deq/0,4561,7-135-6132_6828-98518--,00.html Accessed 08 March 2014 (2014)
33. Nicklow, J., Reed, P., Savic, D.: State of the art for genetic algorithms and beyond in water resources planning and management. J. Water Resour. Plan. Manag. 412–432 (2010).
34. Nordbotten, J., Celia M., Geological Storage of CO2, Wiley, (2012)
35. Nordbotten, J., Celia, M., Bachu, S.: Analytical solutions for leakage rates through abandoned wells. Water Resour. Res. 40, 1–10 (2004).
36. Nordbotten, J., Flemisch, B.: Uncertainties in practical simulation of CO2 storage. Int. J. Greenh. Gas Control. 9, 234–242 (2012).
37. Nordbotten, J., Kavetski, D., Celia, M., Bachu, S.: Model for CO2 leakage including multiple geological layers and multiple leaky wells. Environ. Sci. Technol. 43, 743–749 (2009).
38. Pacala, S., Socolow, R.: Stabilization wedges: solving the climate problem for the next 50 years with current technologies. Science. 305, 968–972 (2004).
39. Peralta, R.C., Forghani, A., Fayad, H.: Multiobjective genetic algorithm conjunctive use optimization for production, cost, and energy with dynamic return flow. J. Hydrol. (2014).

40. Rashedi, E., Nezamabadi-Pour, H., Saryazdi, S.: GSA: a gravitational search algorithm. Inf. Sci. (Ny). 179, 2232–2248 (2009).
41. Reed, P.M., Hadka, D., Herman, J.D., Kasprzyk, J.R., Kollat, J.B.: Evolutionary multiobjective optimization in water resources: The past, present, and future. Adv. Water Resour. 51, 438–456 (2013).
42. Reed, P.M., Kollat, J.B.: Visual analytics clarify the scalability and effectiveness of massively parallel many-objective optimization: A groundwater monitoring design example. Adv. Water Resour. 56, 1–13 (2013).
43. Rubio-Largo, A., Vega-Rodriquez, M.., Gomez-Pulido, J.A., Sanchez-Perez, J.M.: A Multiobjective Gravitational Search Algorithm Applied to the Static Routing and. Appl. Evol. Comput. Lect. Notes Comput. Sci. 6625, 41–50 (2011).
44. Singh, A.: Simulation and optimization modeling for the management of groundwater resources. I: Distinct applications. J. Irrig. Drain. Eng. 1–10 (2013).
45. Singh, A.: Simulation and Optimization Modeling for the Management of Groundwater Resources. II: Combined Applications. J. Irrig. Drain. Eng. 1–9 (2014).
46. Singh, T.S., Chakrabarty, D.: Multi-objective optimization for optimal groundwater remediation design and management systems. Geosci. J. 14, 87–97 (2010).
47. Tabari, M.M.R., Soltani, J.: Multi-Objective Optimal Model for Conjunctive Use Management Using SGAs and NSGA-II Models. Water Resour. Manag. 27, 37–53 (2012).
48. Trebin, F.A.: Oil Permeability of Sandstone Reservoirs. Gostoptekhizdat, Moscow (1945).
49. Turpening, R.M., Toksöz, M.N., Born, A.E., et al.: Reservoir Delineation Consortium Annual Report, Massachusetts Institute of Technology, Cambridge (1992).
50. Zheng, F., Zecchin, A.: An efficient decomposition and dual-stage multi-objective optimization method for water distribution systems with multiple supply sources. Environ. Model. Softw. 55, 143–155 (2014).
51. Zitzler, E., Thiele, L.: Multiobjective Optimization Using Evolutionary Algorithms - A Comparative Case Study, 292–301. Springer, Heidelberg (1998)